Laser Welded Steel Sandwich Panel Bridge Deck Development: Finite Element Analysis and Stake Weld Strength Tests

Final Report
September 2009

MaineDOT

A Publication from the Maine Department of Transportation's Research Division

Technical Report Documentation Page

1. Report No. 09-09	2.	3. Recipient's Accession No.
4. Title and Subtitle LASER WELDED STEEL SANDWICH PANEL BRIDGE DECK DEVELOPMENT: FINITE ELEMENT ANALYSIS AND STAKE WELD STRENGTH TESTS		5. Report Date September 2009 6.
7. Author(s) Vincent Caccese, Ph.D., P.E., Professor Serdar Yorulmaz, Graduate Research Asst.		8. Performing Organization Report No.
9. Performing Organization Name and Address University of Maine Department of Mechanical Engineering 5711 Boardman Hall 212 Orono, ME, 04469-5711		10. Project/Task/Work Unit No. 11. Contract © or Grant (G) No.
12. Sponsoring Organization Name and Address Maine DOT 16 State House Station Augusta, ME 04333-0016		13. Type of Report and Period Covered 14. Sponsoring Agency Code

15. Supplementary Notes

16. Abstract (Limit 200 words)

This report summarizes the analysis of laser welded steel sandwich panels for use in bridge structures and static testing of laser stake welded lap shear coupons. Steel sandwich panels consist of two face sheets connected by a relatively low-density core resulting in high strength and stiffness, which leads to promising design advantages. Steel sandwich panels offer substantial resistance to static and dynamic loads due to their high stiffness and substantial energy absorbing capacity. Panels of this kind are of interest for potential use in bridges for deck replacement. They are especially efficient in resisting dynamic events such as fatigue, impact or shock loading.

A verification study is performed comparing finite element analysis and an analytical model to an experimental study documented in the literature. Results demonstrate good agreement between the approaches. Modeling techniques are developed from the verification study. Finite element analyses are subsequently employed to study the response of a laser welded steel sandwich panel case study of a deck replacement for a steel bridge located in Gardiner, Maine. The deck design results in a stiff structure that has a deflection of 1/1500 of the span at a depth of 7.25 inches. Structural response of stake welds was also investigated experimentally in a single lap shear configuration. Multiple pass welds consisting of 2 and 4 stake weld passes were fabricated and tested to assess the process of using multi-passes to increase weld resistance.

17. Document Analysis/Descriptors Light weight bridge decks, steel sandwich panels, laser welded		18. Availability Statement	
19. Security Class (this report)	20. Security Class (this page)	21. No. of Pages 106	22. Price

LASER WELDED STEEL SANDWICH PANEL BRIDGE DECK DEVELOPMENT: FINITE ELEMENT ANALYSIS AND STAKE WELD STRENGTH TESTS

Final Report:
Submitted to:
Applied Thermal Sciences
c/o Lawrence Thompson
(207) 459-7777

by:

Vincent Caccese, Ph.D., P.E., Professor
and
Serdar Yorulmaz, Graduate Research Asst.

Project Funding Under MDOT
(IBRC) program under agreement No 1018

Dale Peabody, Program Officer

Department of Mechanical Engineering
5711 Boardman Hall 212
Orono, ME, 04469-5711
Tel: 207-581-2131
Fax: 207-581-2379.
E-mail: vince_caccese@umit.maine.edu

September 22, 2009

Project No. C2006-014-RPT-01

ABSTRACT

This report summarizes the analysis of laser welded steel sandwich panels for use in bridge structures and static testing of laser stake welded lap shear coupons. Steel sandwich panels consist of two face sheets connected by a relatively low-density core resulting in high strength and stiffness, which leads to promising design advantages. Steel sandwich panels offer substantial resistance to static and dynamic loads due to their high stiffness and substantial energy absorbing capacity. Panels of this kind are of interest for potential use in bridges for deck replacement. They are especially efficient in resisting dynamic events such as fatigue, impact or shock loading.

A verification study is performed comparing finite element analysis and an analytical model to an experimental study documented in the literature. Results demonstrate good agreement between the approaches. Modeling techniques are developed from the verification study. Finite element analyses are subsequently employed to study the response of a laser welded steel sandwich panel case study of a deck replacement for a steel bridge located in Gardiner, Maine. The deck design results in a stiff structure that has a deflection of 1/1500 of the span at a depth of 7.25 inches. Structural response of stake welds was also investigated experimentally in a single lap shear configuration. Multiple pass welds consisting of 2 and 4 stake weld passes were fabricated and tested to assess the process of using multi-passes to increase weld resistance.

ACKNOWLEDGEMENTS

Funding provided by the Maine Department of Transportation (MDOT) Innovative Bridge Research and Construction (IBRC) program under agreement No 1018 is gratefully acknowledged. Special thanks go to MDOT program officer Dale Peabody. In addition project direction provided by PLSystem, and Applied Thermal Sciences (ATS) is gratefully appreciated, in particular PLSystem project manager Steven Abbott and project engineer Larry Thompson of ATS. The assistance of UMaine students Anthony Fessenden, Radek Glaser and Douglas Dow is greatly appreciated along with the assistance Alan Treadwell of the Advanced Manufacturing Center in preparation of the lap shear test specimens.

TABLE OF CONTENTS

Page

1. INTRODUCTION

Sandwich structures composed of stiff outer layers connected by a relatively low-density core result in high specific strength and stiffness, which may lead toward substantial design advantages. Properly designed steel sandwich panels offer substantial resistance to static and dynamic loads due to their high relative stiffness and inherent energy absorbing capacity. To that end, steel sandwich construction has great potential for use in bridges, buildings, ships and other structures. Laser welded steel sandwich panels perform especially well in situations of hazard reduction due to their high energy absorbing potential. Steel sandwich construction also has other advantages. Lok and Cheng (2000) listed several including simplification of traditional connection processes (since stiffeners or joist members can be eliminated), accurate construction, less surface distortion, rapid construction practices, better retention of pressure and water leakage, greater flexibility for designers to create elegant curves, and ease of material transportation. They also noted that difficulty in fabrication and reliability of the face-sheet/core connection has been a continual problem. Laser welding of the face sheet to the core using a stake weld overcomes this problem. Assessment of the strength and fatigue resistance of the weld and connection details is essential to the implementation of laser welded steel sandwich panels.

1.1 Objectives and Current Study

The focus of this research is to assist in the further development of laser welded steel sandwich panels for use in bridges. A finite element, numerical study and experimental lap-shear testing are performed. The steel sandwich panel is based upon a design that consists of discontinuous corrugated prismatic stiffeners attached to the top and bottom of the panel with laser stake welds along the length. Experimental analysis is performed on laser welded lap-shear sections in the Hybrid Structure Laboratory (HSL), University of Maine, Orono.

Finite element analysis, comparison to theoretical models and experimental verification of mechanical behavior of the steel sandwich panels under quasi-static loading was undertaken. Specific studies performed under this effort include:

1. A verification study was performed based on Tan's et. al. (1989) work. Finite element analysis technique for simply supported boundary conditions are standardized for both continuously and discontinuously corrugated steel sandwich panels.
2. A theoretical analysis program was implemented using MATLAB, which can be easily modified order to analyze prismatic sandwich panels with different corrugation configurations.
3. Finite element analysis techniques were developed for sandwich panel bridge deck replacement case study.
4. Experimental techniques were used to investigate the strength of laser stake welds in single lap-shear.

1.2 Literature Review

Laser welding is a relatively new technique for structures, which has potential to achieve excellent static and dynamic load resistance as well as good fatigue life. Dimensional accuracies far superior to those describe in ASTM A6 (2005) have been realized in laser welded beam fabrication as a natural outcome of the process. Laser welding occurs at much greater speeds than conventional welding. In plate fabricated beam production speeds of 5-10 times that of conventional welding has been attained with the goal to develop automated systems capable of welding up to 600 in/min. (Blomquist et al., 2004). Good control over weld quality and profile is demonstrated along with greatly reduced residual stresses when compared to conventional welding (Caccese et al., 2003). Laser welding is a high energy density process that can be used on a wide variety of metals and alloys. Some of the advantages that can be achieved through laser welding are ease of process automation, high welding speed, high productivity, increased process reliability, low distortion of the finished part, low residual stresses and no requirement for filler metal. With current laser welding techniques it is possible, for example to achieve full penetration welds in one pass on materials up to 1-inch thick, depending on laser power and weld speed, with no filler and preparation as simple as precision cutting of the edges (Duhamel, 1996). The automotive industry has used laser welding in production since the 1980's. Recently, the ship building industry has looked toward laser welding to provide fabricated components in ship production due to improvements and cost benefits that can be achieved compared to hot rolled stripped-T or split-I stiffeners. Laser welded sandwich panels for ship structures are currently being developed in Finland, where a significant focus is on

replacement of ship deck panels (Klanac and Kujala, 2004). Efforts to develop laser welded sandwich panels (LASCOR) were initiated by the U.S. Navy in 1988 and ultimately resulted in the use of stake welds to attach the face-sheets to the core. LASCOR panels were produced using a 14-kW CO_2 industrial laser. The prototype panels were installed on the USS Mt. Whitney in 1994 and have performed well in the marine environment. The steel sandwich panel design provided a weight savings of over 20,000 pounds compared to the conventional stiffened-plate design. The use of the CO_2 laser and stainless steel corrugated core design of LASCOR results in a product that is economically unfeasible for building structures, where price competitive square-foot product cost is essential. The significantly more efficient fiber laser facility at ATS in Sanford ME, and the increased flexibility in core design may yield a product that has the proper economics for building construction. Laser welded sandwich construction has the potential to be a widely used structural form in ship, building and bridge construction. This type of system offers high strength-to-weight and stiffness-to-weight ratios compared to other types of construction methods. In sandwich construction, two face-sheets are separated by a core giving high flexural rigidity in both directions compared to an unstiffened plate of the same weight.

The Federal Highway Association (FHWA) also has recognized the potential advantage that weight reduction using steel sandwich panels might have for bridge deck rehabilitation and they have recently funded a project on HLAW sandwich panels for bridge decks. This Innovative Bridge Research and Construction (IBRC) project was awarded to PLSystems, ATS, and UMaine through the Maine DOT to study the use of HLAW panels in the deck rehabilitation of a steel truss bridge located in Gardiner, Maine. The research team performed a preliminary V-core sandwich panel deck design along with MDOT engineers. This effort will add to the general knowledge of the structural response of the HLAW steel sandwich panel system.

Original choice of material for use in bridge deck replacements was a ferritic stainless steel with the tradename of DURACORR. This steel is a relative inexpensive corrosion resistant stainless steel with 12% Cr content. Initial welding trials uncovered a difficulty in creating the laser stake welds in this material due to its lack of ability to achieve a good quality weld when the material is fused to itself. Subsequently, the use of the DURACORR was abandoned and the investigation processed with testing of lap shear specimens made using a HSLA-65 steel.

Core designs for sandwich panels can take on many forms and shapes depending upon the end use. Some of the basic core designs ideal for laser stake welding (Kujala et al., 2004) is presented in Figure 1.1. Prismatic cores, such as shown in Fig. 1.1, are preferred in sandwich construction because they are simple to manufacture and because their high longitudinal stiffness makes them ideal in cases where orthotropic plate action is preferred. The core is an essential element, resists predominately shear force much like the web in an I-beam, and can be used to mitigate severe dynamic effects. Some core geometries, such as the X-core, inherently have more capacity for energy absorption than others. The connection between the core and face-sheets is a key element in the long-term performance and has historically been accomplished by spot welding, rivets, self-tapping screws or adhesive (Fung et al., 1996). Laser welding adds a new dimension to steel sandwich construction.

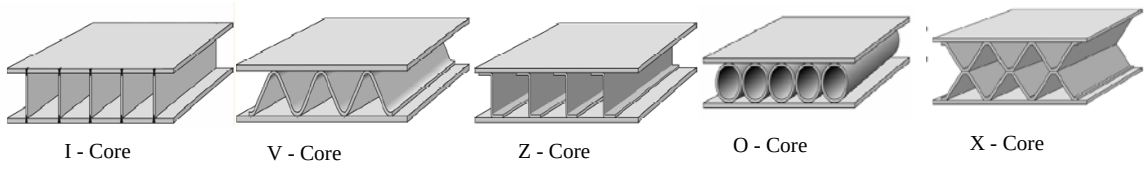

Figure 1.1 Some Examples of Prismatic Core Designs Ideal for Laser Stake Welding

Using a stake weld, the core material is metallically bonded directly through the face-sheet, resulting in a continuous and reliable attachment that can be created at much higher rates than typical in conventional welding. The effect of the relatively low core transverse shear rigidity on overall response of sandwich panels as presented by Plantema (1966), Allen (1969), Zenkert (1995), and others has been intensely studied. Vel et al. (2005) discussed the couplings that occur between axial, bending and shear resistances for tapered connections and unsymmetrical sandwich panels. The configuration used in steel sandwich panels typically results in a highly orthotropic structure where it is absolutely necessary to consider effects of shear deformations even at large length to depth ratios. The same is true in truss type sandwich panels as indicated by Chang et al. (2005) and Cheng et al. (2006).

Tan et al. (1989) performed experiments and analysis on a V-core type sandwich panel system and found good correlation between experimental results and analytical models. The effect of a discrete face-sheet/core connection in a C-core type sandwich panel was studied by Fung and Tan (1996) for use in building structures. The C shaped core material they analyzed was connected to the face-sheets using screws. They modeled this connection as a line of contact and developed a mathematical formulation for the panel response including the weak axis shear stiffness, which considers the local response of the core and the face-sheet/core connection. A stake weld can be treated mathematically in much the same manner, although, the non-linear response to ultimate capacity of a stake welded connection will be substantially different than a screw connection. Lok and Cheng (2000) developed a mathematical formulation for truss-core type sandwich panels. They developed expression to predict the orthotropic stiffness and quantified the effect of the core angle on the response. Their work was analytical and they expressed a need to have reliable fabrication methods. More recently, Kennedy and Murray (2004) discussed the design of the Shenley bridge in Quebec CA that uses steel/foam sandwich construction with two steel plates adhesively bonded to an elastomer core. This system relies upon the long-term durability of the adhesive bond between the foam core and the facings.

Shock and impact resistance of sandwich construction has also been studied intensely. Sandwich structures offer significant advantages in terms of higher flexural rigidity and flexural strength, for a given weight, in comparison to single skin structures (Zenkert, 1995). Under a blast load, the core typically absorbs more than a half of the total kinetic energy of the blast (Hutchinson and Xue, 2005). Xue and Hutchinson (2004 a,b), Hutchinson and Xue (2005) and Fleck and Deshpande (2004) have shown that prismatic geometries are nearly optimal for shock resistant sandwich construction. Fleck and Deshpande (2004) also indicated that sandwich construction is more effective in resisting dynamic shock loading than conventional construction. This is especially true for fluid loading where fluid-structure interaction has more of an influence and is an additional benefit in structures where an abnormal event such as blast, hurricane, wave surge or earthquake, might place higher energy demands on the structure than foreseen in design under normal loads.

Qiao et al., (2004) demonstrated the effectiveness of sandwich construction for mitigating the effect of impact due to foreign objects and focused mostly on collision of over-height trucks

against bridge girders. The I-Lam sandwich panels they analyzed have been shown to be effective in protecting bridge structures against vehicle impact. They were able to achieve a good correlation between their analytical model and experimental results. Furthering this work, Yang and Qiao (2005) developed a higher order impact model for sandwich structures with flexible cores. Theoretical and numerical techniques developed using their models are useful in predicting the impact response of sandwich structures.

1.3 Steel Sandwich Bridge Decks

An effort in the U.S. to investigate the use of steel sandwich panel for bridge decks was recently undertaken by the Maine Department of Transportation (MaineDOT) under a Federal Highway Administration (FHWA) grant. Abbott et al. (2008) describes this program. The project includes numerical analysis, structural connection detail development, and laboratory testing of LWSS panel stake weld subcomponents. The MaineDOT IBRC steel sandwich panel project demonstrates a lightweight, laser welded, structural steel sandwich panel deck. The panels have the potential to be cost effective alternative to conventional decking. Many of the existing engineering data, design procedures and steel design methodologies can be used in the design of a steel sandwich panel structure. Well established practices exist for design, manufacturing, repair, maintenance, quality assurance, and safety inspection of steel structures. This program initiates an engineering study of the HLAW sandwich panel performance to address any concerns with this new technology including strength of the laser stake welds.

The fatigue performance of steel sandwich panels fabricated with laser stake welds for use in bridge decks was studied by Bright & Smith (2004) in the UK. They used a 25kW CO2 laser source that operated at about 10% efficiency and a mirror beam delivery system that focused the laser light down to a 0.6-mm diameter spot. Helium was used as the shielding gas. For a stake weld they noted that penetration is dependent on welding speed with slower welds penetrating deeper. However, a weld performed too slowly would cause burn through. They noted that there are no standards for the amount of penetration required and they suggested that the maximum penetration possible without burn through should be used. Their sandwich panel concept welded HPE 240 steel beams spaced at 300-mm between 8-mm and 12-mm face plates. Deck bending and joggle type fatigue tests were conducted on cut sections with 2, 4 or

sinusoidal shaped stake welds per flange. Deck bending tests with 2 welds per flange showed the most favorable fatigue response and fell under class C with the four welds per flange falling between class D and E and a sinusoidal weld detail near class F2. In the joggle tests failure occurred in the I-beam web at the root fillet with no weld failures observed.

1.4 Laser Welding for Steel Sandwich Construction

Hybrid laser arc welding (HLAW) holds many advantages over current conventional welding technologies in steel fabrication and construction that are ideal for innovative bridge construction. Hybrid laser arc welding is automated as shown in Figure 1.2. Abbott et al (2008) described that fabricators have the ability to control the power input intensity, geometry, and accuracy of welds. Automated control allows minimum part distortion and welding near heat sensitive components due to small heat affected zones (HAZ). Non-contact operation permits welding in hard to reach areas and repeatable weld placement. By adjusting various parameters such as the laser energy and focal point position, HLAW permits geometric ratio control of the welds and consistent weld depth and width control. Although there are limitations on maximum width, that can be achieved with a single pass laser stake weld, multiple passes are possible to improve connection performance. Automated systems as shown in Figure 1.2 are also cost competitive due to minimum set-up time, low fixturing costs, and high feed rates.

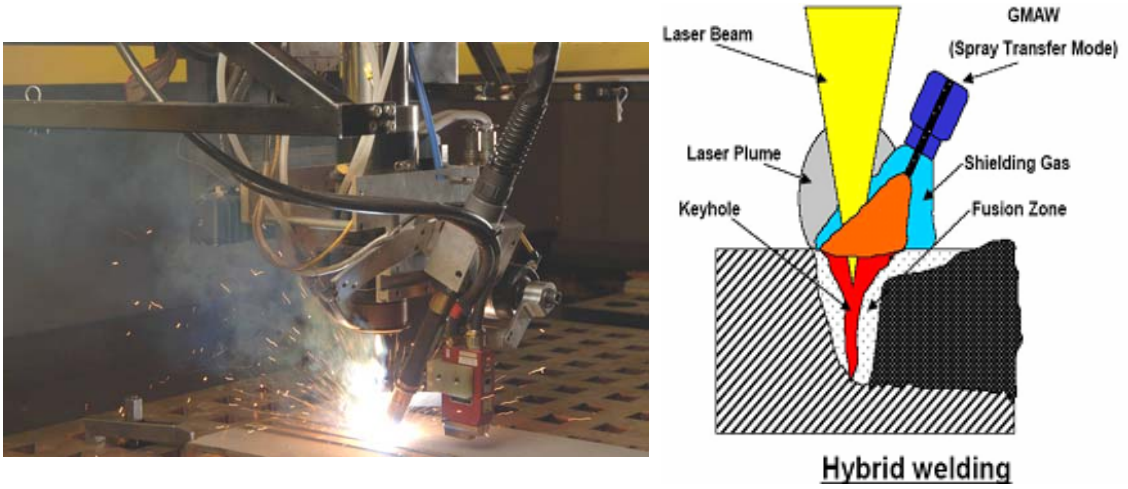

Figure 1.2 Hybrid Laser Arc Welding (HLAW) (Abbot et al. 2008)

Speed is a major advantage HLAW possesses over conventional welding technologies. It is five to ten faster than conventional methods saving time and money. Meanwhile, HLAW produces oxide free welds to improve weld quality and to enhance safety conditions. Also, HLAW can be applied to carbon steels, HSLA steels, stainless steel, aluminum, and titanium, and have little influence on the material properties or physical state of the material. Contained weld joints have no flash or particulate outside the joint to cause problems, and the assembly sees no heat or vibration because the parts do not move relative to one another in the laser welding process. More importantly, HLAW reduces the residual stresses (Abbott et al. 2008) induced upon the material, which can improve the overall stability and nonlinear dynamic response.

All things considered, HLAW is ideal for connecting the core to the face-sheets. Figure 1.3 shows hybrid laser arc welding on a section of a sandwich panel. Laser welding of the core to the face-sheets, in a steel sandwich panel system, results in a robust reliable connection. In terms of bridge construction, this improves methods for manufacturing high strength welded girders, plate-to-stiffener welding for orthotropic bridge decks, and the development of lightweight sandwich panel decks. Also, the use of thinner steel plates may be achievable, thus reducing material and installation costs, and facilitating the use of higher cost stainless steels.

Figure 1.3 Hybrid Laser Welding on Sandwich Panel (Abbot et al. 2008)

One major barrier to the advancement of laser welding is the small amount of published technical welding guidance for designers, welding engineers, and fabricators. According to Abbot et al. (2008), the American Welding Society has developed a draft specification available for qualification of laser welding, but it is not yet available to fabricators. The ASME addresses laser processes in Section IX of the Boiler and Pressure Vessel Code, but this is highly restrictive in nature, and not necessarily applicable to other types of fabrication. Additional development is needed in this area of welding codes, procedures, and specifications, especially as applied to steel bridge components, if laser welded steel sandwich panels are to become viable in this arena.

2. ANALYSIS OF TRUSS CORE SANDWICH PANELS

This section describes the analysis of structural sandwich panels that was carried out using the commercially available finite element package ABAQUS. Theoretical calculations are also performed using orthotropic plate analysis that includes shear deformation using the MATLAB software. Sandwich panel models are created using CAD modules of the finite element software. In complicated cases SOLIDWORKS, which is a dedicated computer aided design (CAD) program, is utilized. Modeling methods are verified using work performed by Tan et al. (1989). A case study is presented consisting of the analysis of a bridge deck panel subjected to patch loading.

2.1 Verification of Finite Element Model

The verification model used in this study is based upon testing and analysis performed by Tan et al. (1989). Figure 2.1 shows the panel geometry used in the study. The sandwich panel was detailed with a continuous corrugated steel core attached with spot welding to the top and bottom sheets in their verification study. Their model was a 6 m long and 2.12 m wide truss core panel at a total depth of 107.5 mm. It consists of 4 corrugations in the long direction. A boundary plate of 12 mm thick and entirely made of 2.5 mm structural steel was welded to close the specimen.

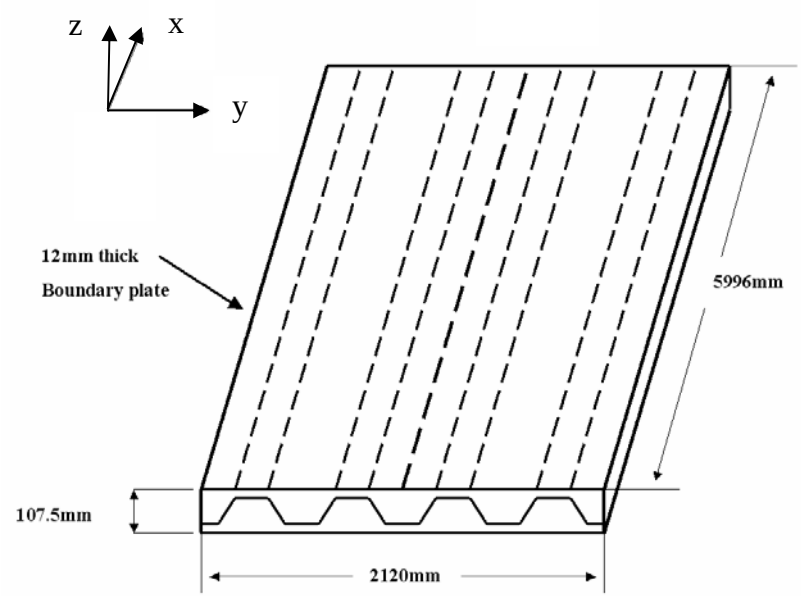

Figure 2.1 Panel Overview

In this current effort Tan's case is verified with an independent finite element analysis using the ABAQUS computer program. Once verified, the same process will be used to analyze the

sandwich panel case studies presented in the remainder of this section. Cross section of a single core cell modeling Tan's case is presented in the Figure 2.2, which shows the welding locations, side boundary plate, top and bottom sheets. Dimensions are shown in Figure 2.2 as they are used to create the quarter part of the sandwich panel in ABAQUS.

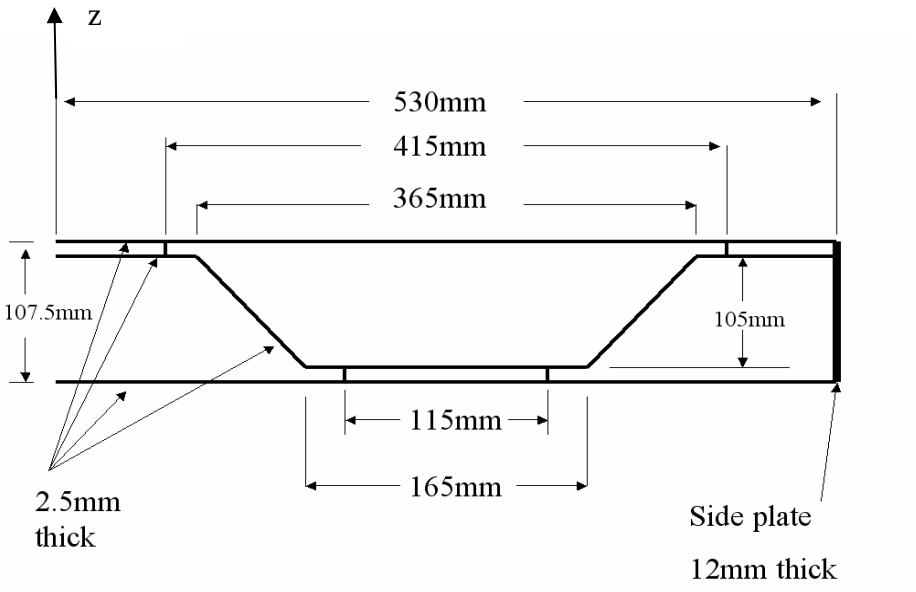

Figure 2.2- Core Section with Boundary Plate on right

The sandwich panel studied is made of a linear elastic steel material, with a Young modulus of $209{,}000 N/mm^2$ and Poisson's ratio of 0.3 (Tan et al. 1989). In this three dimensional static analysis a general-purpose conventional stress and displacement element, ABAQUS S8R6 is used. S8R6 is a quadrilateral shell element, which offers a total of 8 nodes along the edges of the element boundary with 6 degrees of freedom at each node. In the analysis a reduced integration option is selected.

2.1.1 Model of the Laser Welded Connection

In this study, the spot welding of the panel is assumed to be continuous along the length of the corrugation at the weld locations. Modeling of the weld uses a connecting plate with the same

element type (S8R6) as the corrugation, top and bottom face sheets. This was done due to the difficulties and complexity in high fidelity modeling of spot welding. The model's cross-section with the continuous stake weld is shown in Figure 2.3. The plate thickness of the representative weld element was taken as 2.5mm; equivalent to the minimum thickness of the structural panel. This value was based upon a study of the effect of weld thickness presented in Section 2.1.4. A continuous welding, which joins the corrugation to the bottom and the top plate through the length of the panel is also modeled with using shell elements. These elements are also of the same type as the ones that the sandwich panel is meshed.

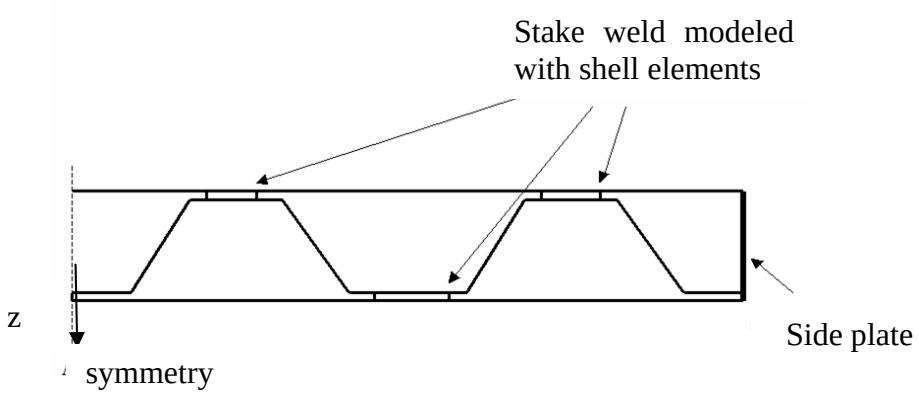

Figure 2.3 Stake Weld and Web-Core Configuration

In the final analysis, approximately 13,000 plate elements shown in Figure 2.4 are used to mesh the quarter of the sandwich panel. This model also assures achievement of appropriate element aspect ratio and convergence. Proper aspect ratio of plate element is essential in order to obtain reliability of the results in finite element analysis. This is accomplished by performing a mesh convergence study presented in the next section.

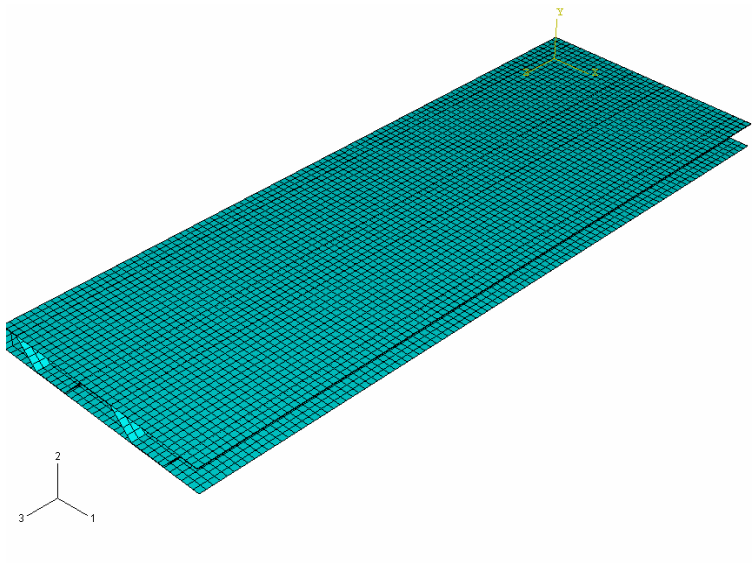

Figure 2.4 Meshed Panel

2.1.2 Convergence Study

In finite element analysis, a finer mesh generally results in a more accurate solution. However, as the mesh gets finer, the computation time and the memory requirements increase. In this sense it is important to satisfactorily balance the accuracy and computing resources. As part of the verification effort, a mesh convergence study was performed by first analyzing the structure using a coarse mesh. Subsequently, the mesh is recreated with a denser element distribution and the analysis results compared to the previous mesh. This procedure is followed by another finer mesh density and the model analyzed once again until the results converged. This approach enables one to obtain a converged solution with a mesh that is sufficiently dense and not overly demanding of computing resources. The convergence of the results is checked by plotting the maximum displacement of the bottom facing versus the number of elements as shown in Figure 2.5. This figure shows that a mesh with over 10,000 elements results in adequate convergence with regard to displacement. In Tan's case, particular attention given to the meshing of the corrugation, which is the critical structural component in the sandwich panel. After meshing the sandwich panel and running the analysis for different mesh densities, an element size of 25 mm was found to be sufficient to have converged results. Ultimately, the sandwich panel is meshed with approximately 17000 elements.

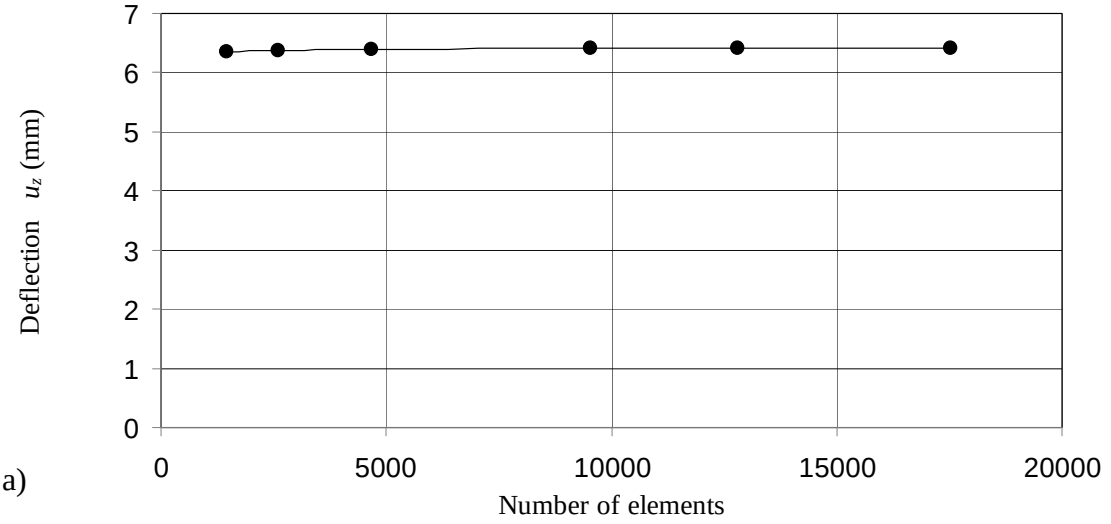

a)

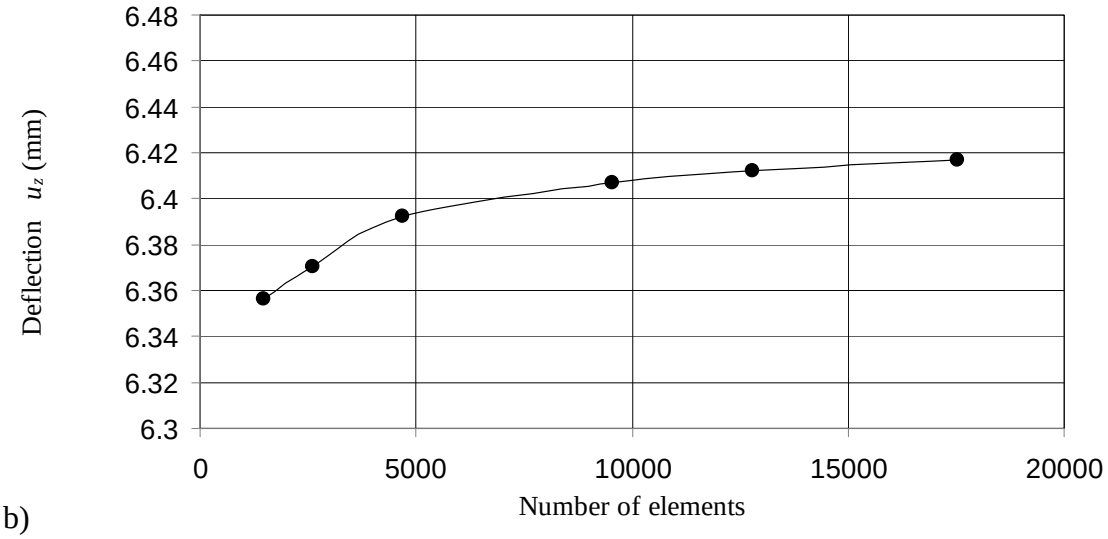

b)

Figure 2.6 Convergence Study a) Convergence Rate of Tan's Current Study
b) Magnified View of Convergence Study

2.1.3 Modeling: Load and Boundary Conditions

The distributed load is applied as a pressure of 5.5 kN/m^2 acting normal to the surface of the panel as shown in Figure 2.7. Symmetry of a quarter model was used for simplification and reduction of analysis time. Cross-section of web-core and continuous stake weld configuration of quarter model symmetry is also shown in Figure 2.7. The boundary plate on the front and the backside was modeled by forcing the U2 displacements to zero along this boundary.

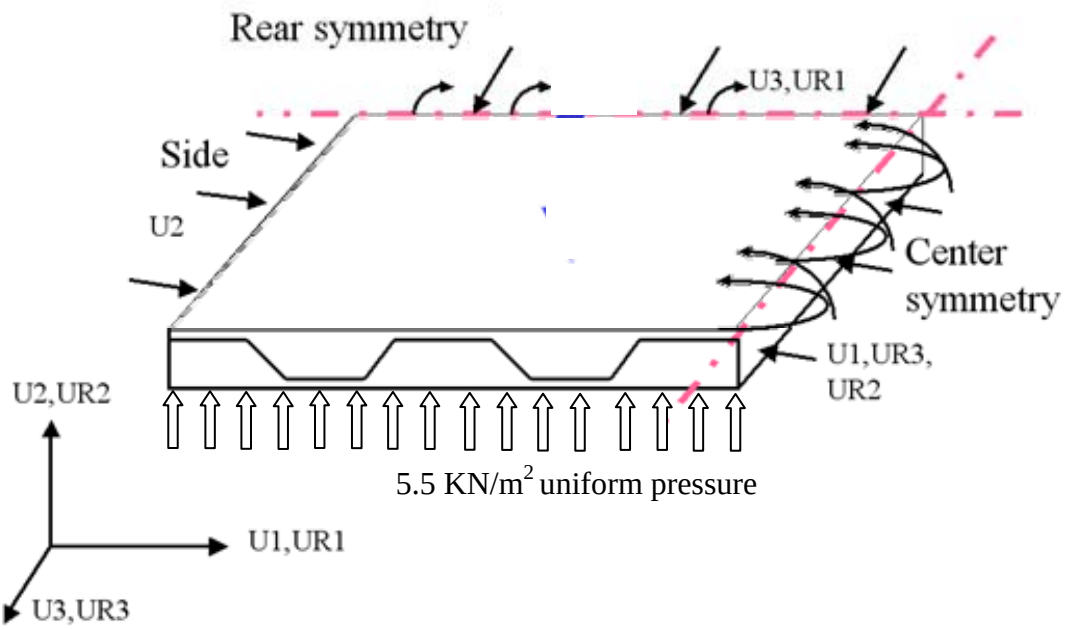

Figure 2.7 Applied Boundary Conditions to the Quarter Model

The boundary conditions and applied distributed load are shown in Figure 2.8 along with the panel modeled in ABAQUS. In the quarter model simply supported boundary conditions (BC) applied to the entire front face by fixing U2, which sufficiently simulates the existence of such boundary plate. However, this approach does not restrict the rotation of the front face due to the moment created at the center of the panel by the uniform load. That being emphasized, the

boundary condition applied in the U2 direction is on the entire face including the top plate, bottom plate and core elements.

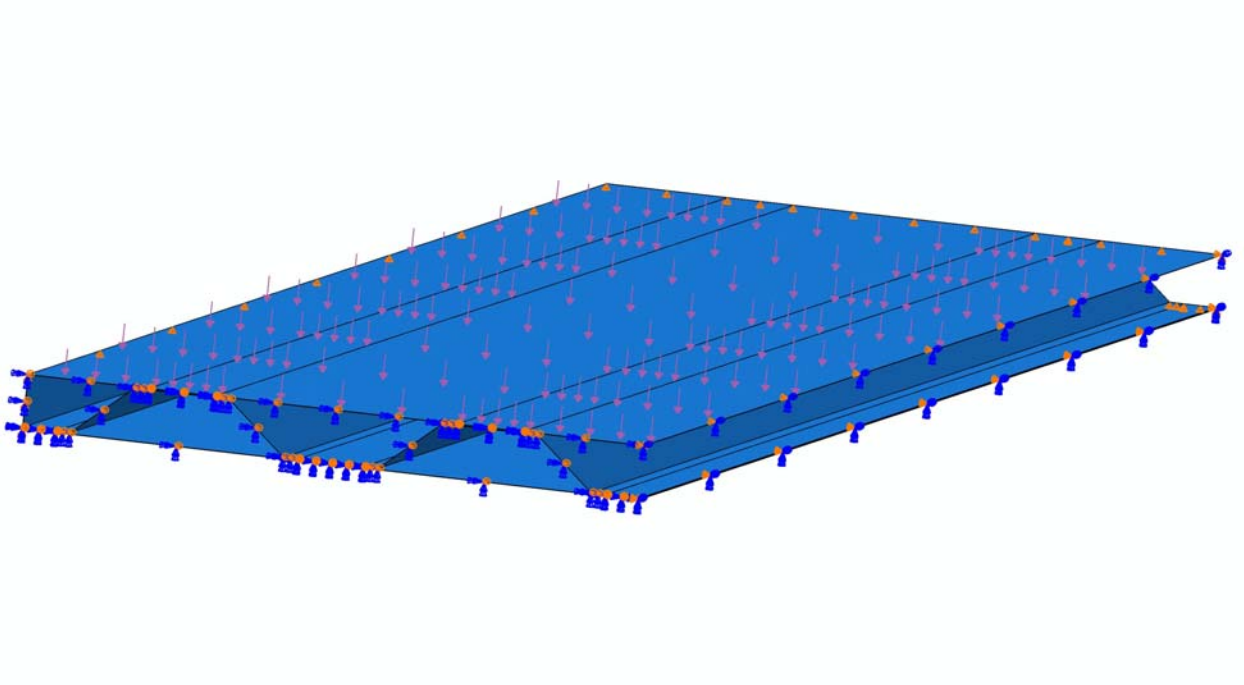

Figure 2.8 Finite Element Model BCs and Load

On the left hand side of the panel where the boundary plate exists, the boundary condition is applied again to the entire face of the plate in the U2 direction. On the rear symmetric face, while taking the advantage of symmetry, the boundary condition applied to restrain the rotation, UR2, to eliminate the drilling effect. Also fixity is applied in the U3 direction to restrain the motion in the longitudinal direction and the fixed rotation UR1 will result in zero slope along this face. On the right hand side, the center symmetry axis along the length of the panel used, all edges are restrained against drilling rotation UR2, horizontal motion along the U1 and rotation UR3 about the U3 axis.

2.1.4 Effect of Weld Link Thickness

A study was performed to investigate the effects of the weld link thickness on the overall results. It is important to understand the effect of this parameter on the response of the panel. The investigation was conducted by varying effective weld link thickness assigned to the link section in the finite element model. It is desired to have weld link stiffness high enough to have continuity but not too high to influence results by over stiffening the model. The results of the weld thickness study are presented in the Figure 2.9, which plots the normalized centerline deflection versus the non-dimensional weld link element thickness t_w/t_p, where t_p is the minimum plate thickness of 2.5 mm. This study performed for only one case with weld link at the center of the core landing. If the weld link stiffness is chosen to be equal to the plate thickness it is seen that increasing or decreasing weld link thickness by an order of magnitude does not have significant contribution to the overall stiffness of the sandwich panel.

In summary, the weld thickness does not have significant contribution to the overall stiffness of the sandwich panel when it is selected in a range between 0.1 t_p to 50 t_p. Accordingly, a weld link thickness equal to the plate thickness was chosen for this study.

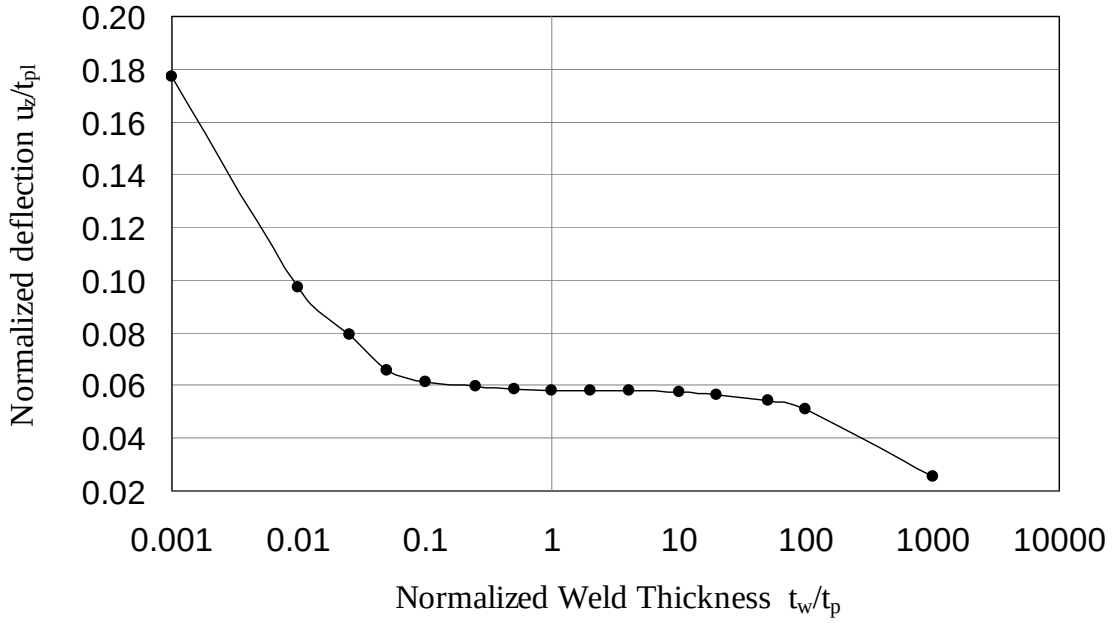

Figure 2.9 Weld Link Thickness Effect

2.1.5 Tan's Finite Element Analysis Displacement Results

Resulting displacements for Tan's case are obtained at the center of the panel, which corresponds to the front right hand side corner of the quarter model as shown in Figure 2.10. This shows that the maximum local deflection occurs in the top plate at the centerline.

A summary of deflections along with Tan et al. (1989) experimental results and Lok and Cheng (2000) results by FEM are summarized in Table 2.1. Disagreement between the current finite element analysis and Tan's experimental result is 8.3%. This verification process was necessary to take further steps in the analysis of sandwich panels with different corrugation and weld configuration.

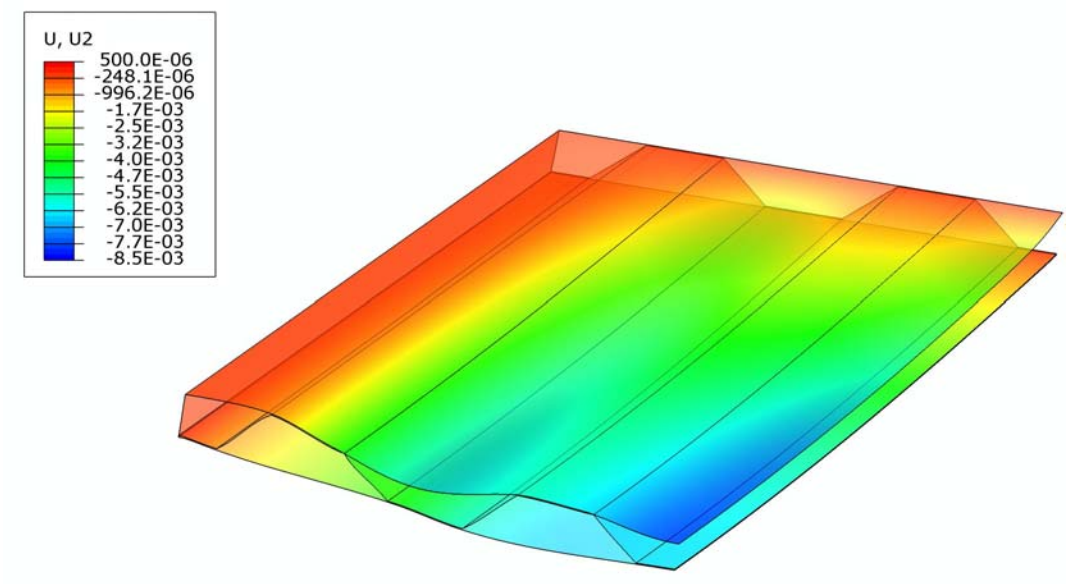

Figure 2.10 Displacement Contour Results

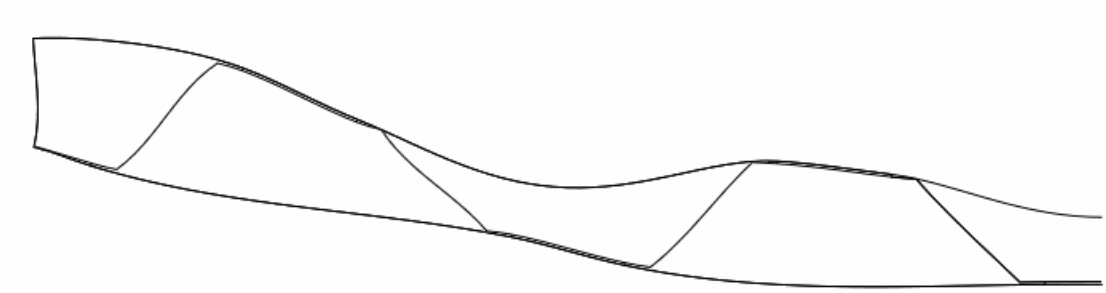

Figure 2.11 Displacement Profile Across Centerline

Table 2.1 Magnitude of Deflection

Weld Configuration	Bottom CL	Top CL	Average
Current FEM of Tan's case	6.42 mm	8.48 mm	7.45 mm
Lok and Cheng (2000) FEM study	6.78 mm	unknown	unknown
Tan et al. (1989) FEM study	5.82 mm	unknown	unknown
Tan et al. (1989) experimental study	7.39 mm	unknown	unknown

2.1.6 Tan's Finite Element Stress Results

Shown in Figure 2.12 are contours of the Von Mises stress results through the thickness of the plate elements. The peak Von Mises stress is shown to be 349.2 MPa. Top and bottom views of the Von Mises stress are shown in Figure 2.13. The location of the peak Von Mises stress is localized and occurs at the support as show in Figure 2.14.

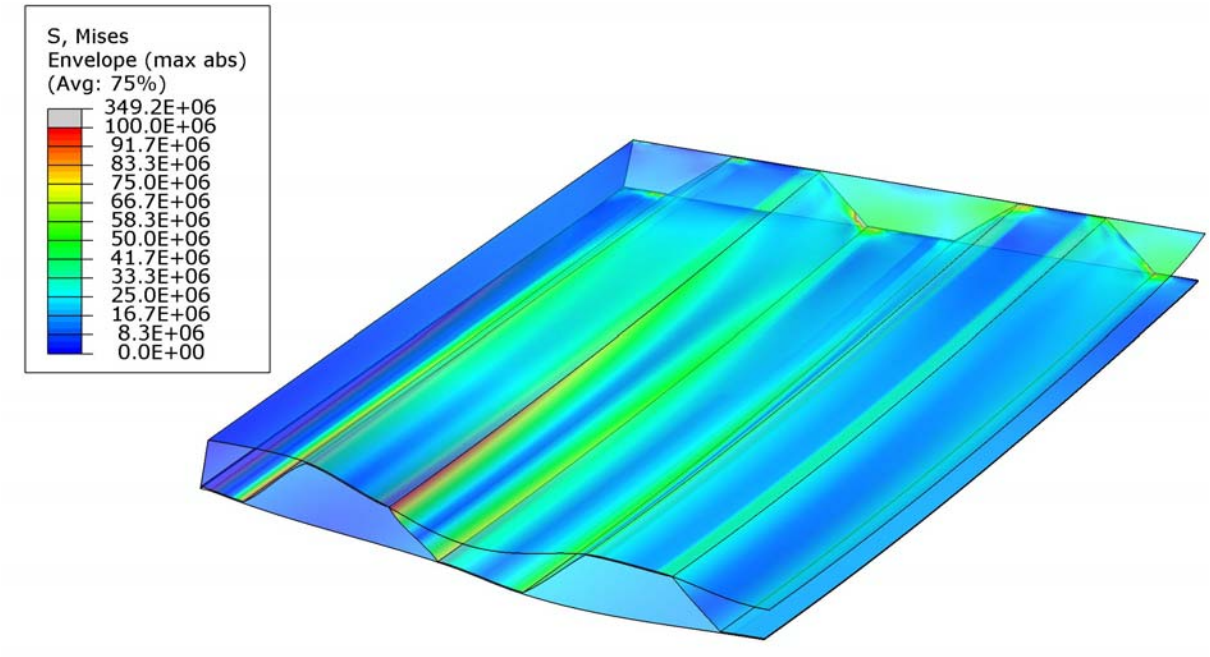

Figure 2.12 Von Mises Stress Contour

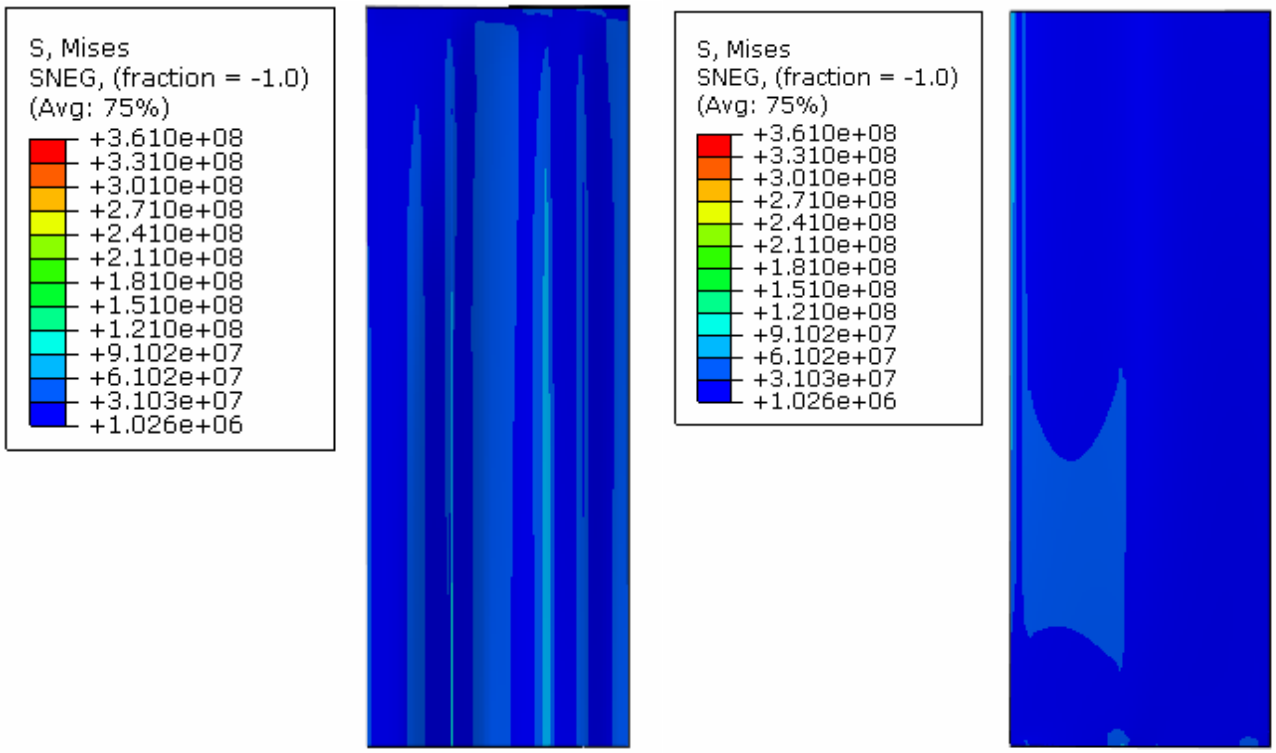

a) top view b) bottom view

Figure 2.13 – Von Mises Stress Contour

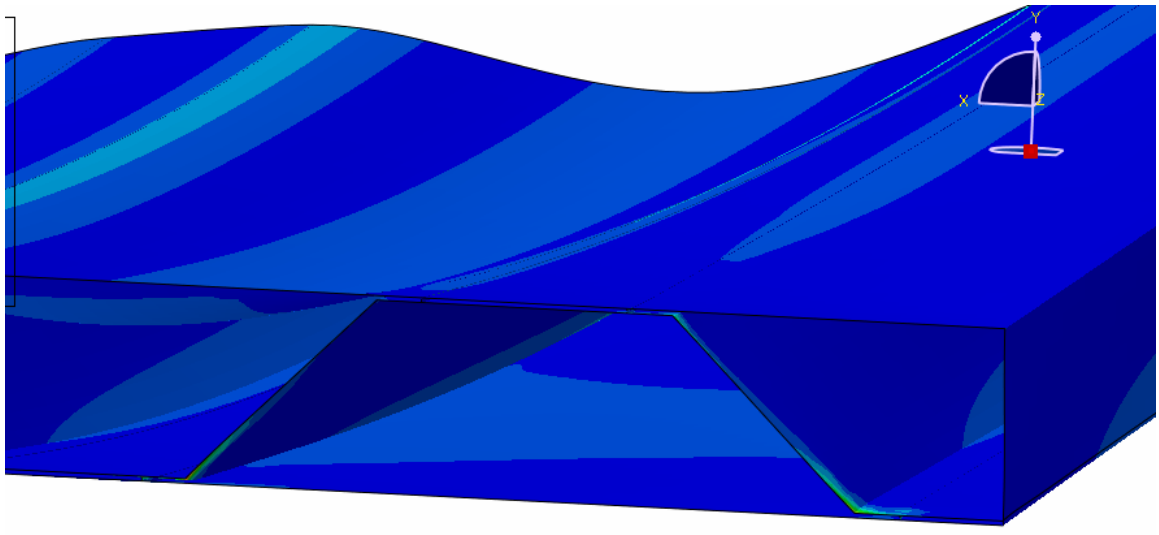

Figure 2.14 – Von Mises Stress Contour-Location of Peak Stress

2.1.7 Effect of Weld Placement

In addition to the Tan's sandwich panel configuration, the effect of weld placement for a model with the geometry the same as Tan's was also studied. Three other configurations were used as shown in Figure 2.15 also having continuous welds like Tan's model. These configurations are designated as; 1) Center - where the weld is placed at the centerline of each corrugation flat; 2) Corner - where two continuous welds are placed at the corners of the web-core and at the corner along with the center point; and 3) Center plus Corner - a combination of the previous 2 cases. In this analysis, the sandwich panel's dimensions were not modified and the weld thickness was taken as 2.5mm same as the plate thickness of the sandwich panel. The boundary conditions are applied the same as applied on Tan's model and the magnitude of the load was also identical.

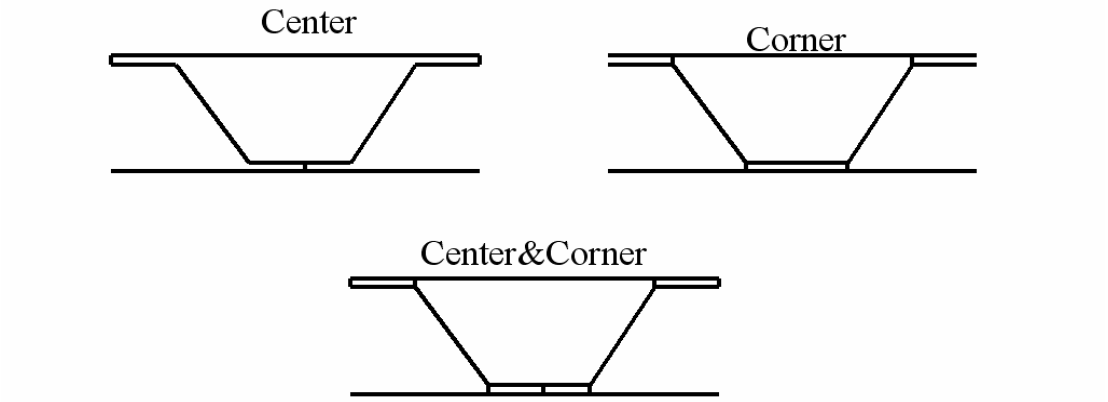

Figure 2.15 Welding Configurations

Deflection values are taken at the same location as explained in the Section 2.1.5. The maximum deflection, top and bottom deflection with the average deflection are given in the Table 2.2 along with the result from Tan's weld configuration. It is important to see that these most common welding configurations can have a significant effect on the overall response. This is predominately due to the influence that the weld location has on the shear rigidity.

This study comes to the conclusion that using one weld link at the center results in a 62% higher displacement at the centerline compared to the case with welds at the center and corners. Using two weld links at the corners instead of 1-weld increases the stiffness by 32% and using three weld links instead of two weld links improves the stiffness by 9%. On the other hand using one

weld link instead of two or three weld links will save manufacturing time by two or three times and still may offer a more economical design, especially in cases where displacement does not control.

Table 2.2 - Weld Configuration Results

Weld Configuration	BottomCL(mm)	Top CL(mm)
Tan's weld configuration	6.42	8.48
Center weld	6.92	11.01
Corner weld	6.10	7.48
Corner&center weld	5.37	6.80

2.2 Orthotropic Model Using MATLAB

This section discusses the use of an orthotropic model of the sandwich panel system computed on a theoretical basis. The application of general small deflection theory for flat sandwich panels or curved sandwich panels to any sandwich structure requires knowledge of elastic constants pertaining to that sandwich structure. These elastic constants consists of two transverse shear stiffness D_{Qx} and D_{Qy}, two bending stiffness D_{xx} and D_{yy}, one twisting stiffness D_{xy}, two elastic modulus and Poisson's rations in x and y directions describe the deformations associated with the applied load. In order to calculate these elastic constants for the corrugated sandwich panel of Tan's a series of MATLAB routines are created and used for calculation.

2.2.1 Closed Form Solution of Governing Equation

Mathematical series sum solutions used in the optimization routine are based upon the Mindlin-Reissner plate theory. This theory is for static analysis and includes the influence of shear deformations. The equation of equilibrium for plate bending can be written in terms of the shear forces, Q_x and Q_y, bending moments, M_x, M_y and M_{xy}, and applied load, q, as follows:

$$\frac{\partial M_x}{\partial x}+\frac{\partial M_{xy}}{\partial y}-Q_x=0 \quad , \quad \frac{\partial M_{xy}}{\partial x}+\frac{\partial M_y}{\partial y}-Q_y=0 \quad , \quad \frac{\partial Q_x}{\partial x}+\frac{\partial Q_y}{\partial y}+q=0 \qquad (2.1)$$

The shear forces and moments are related to the transverse displacement, w, and the mid-plane slopes, θ_x and θ_y, as follows.

$$M_x = D_{xx}\left(\frac{\partial \theta_x}{\partial x} + \nu_y \frac{\partial \theta_y}{\partial y}\right) \quad , \quad M_y = D_{yy}\left(\nu_x \frac{\partial \theta_x}{\partial x} + \frac{\partial \theta_y}{\partial y}\right) \quad ,$$

$$M_{xy} = \frac{D_{xy}}{2}\left(\frac{\partial \theta_x}{\partial y} + \frac{\partial \theta_y}{\partial x}\right) \quad , \tag{2.2}$$

$$Q_x = D_{Qx}\left(\theta_x + \frac{\partial w}{\partial x}\right) \quad , \quad Q_y = D_{Qy}\left(\theta_y + \frac{\partial w}{\partial y}\right)$$

The governing equations are then solved with respect to the orthotropic flexural and shear stiffness', D_{xx}, D_{yy}, D_{xy}, and D_{Qx}, D_{Qy}. The solution for the displacement and slopes in a simply supported plate can be cast into a double harmonic series form in terms of a set of unknown coefficients, w_{mn}, A_{mn} and B_{mn}.

$$w = \sum_{m=1}^{\infty}\sum_{n=1}^{\infty} w_{mn} \sin\left(\frac{m\pi x}{a}\right)\sin\left(\frac{n\pi y}{b}\right),$$

$$\theta_x = \sum_{m=1}^{\infty}\sum_{n=1}^{\infty} A_{mn} \cos\left(\frac{m\pi x}{a}\right)\sin\left(\frac{n\pi y}{b}\right), \tag{2.3}$$

$$\theta_y = \sum_{m=1}^{\infty}\sum_{n=1}^{\infty} B_{mn} \sin\left(\frac{m\pi x}{a}\right)\cos\left(\frac{n\pi y}{b}\right)$$

To simply the solution these expressions can be written in matrix form for each term m and n. Plugging into the equilibrium equations results in a system of equations as follows:

$$\begin{bmatrix} L_{11} & L_{12} & L_{13} \\ L_{21} & L_{22} & L_{23} \\ L_{31} & L_{32} & L_{33} \end{bmatrix}_{mn} \begin{Bmatrix} A \\ B \\ w \end{Bmatrix}_{mn} = \begin{Bmatrix} 0 \\ 0 \\ q \end{Bmatrix}_{mn} \tag{2.4}$$

which can be solved by matrix operations as follows:

$$L_{mn}U_{mn} = P_{mn} \quad , \quad U_{mn} = L_{mn}^{-1}P_{mn} \tag{2.5}$$

setting

$$\alpha_m = \frac{m\pi}{a} \quad , \quad \beta_n = \frac{n\pi}{b} \tag{2.6}$$

The components of the L matrix are computed as:

$$L_{11} = D_{xx}\alpha_m{}^2 + \frac{D_{xy}}{2}\beta_n{}^2 + D_{Qx} \ ,$$

$$L_{22} = \frac{D_{xy}}{2}\alpha_m{}^2 + D_{yy}\beta_n{}^2 + D_{Qy} \ ,$$

$$L_{33} = D_{Qx}\alpha_m{}^2 + D_{Qy}\beta_m{}^2 \ ,$$

$$L_{12} = \left[\nu_y D_{xx} + \frac{D_{xy}}{2}\right]\alpha_m\beta_n \quad , \tag{2.7}$$

$$L_{13} = D_{Qx}\alpha_m \ ,$$

$$L_{23} = D_{Qy}\beta_n \ ,$$

$$L_{21} = L_{12} \quad , \quad L_{31} = L_{13} \quad , \quad L_{32} = L_{23}$$

The load coefficient q_{mn} depends upon the load distribution and can be determined using a Fourier series. For the case of uniform load q_{mn} is written as:

$$q_{mn} = \frac{4p_o}{\pi^2 mn}\left[(1-\cos(m\pi)\cdot(1-\cos(n\pi)\right] \tag{2.8}$$

Once the load and stiffness coefficients are known the system of equations can be solved for the resulting displacement, w and slopes, θ_x and θ_y.

2.2.2 Computation of Elastic Stiffness

Computation of elastic stiffness properties is performed using a combination of closed form solutions and simple frame finite element analyses used to determine properties. Expressions for closed form computation of elastic stiffness properties are implemented for all but the transverse shear stiffness, $D_{Qy,}$ where frame finite element analysis is used.

Analysis is based upon the methodology set forth by Libove and Hubuka (1951) where several simplifying assumptions are made as follows:

1) Thickness of the core remains essentially constant
2) Cross section of the sandwich panel is undistorted
3) Local buckling of the top is not considered
4) Loading remains perpendicular to the midplane of the loading area.

2.2.3 Computation of D_{xx}, D_{yy}, D_{xy}, and D_{Qx}

Expressions for the orthotropic plate rigidities, D_{xx}, D_{yy}, D_{xy}, and D_{Qx}, are given in Equation (2.9). D_{xx} is computed by a conventional strength of materials approach. It includes the combined effect of the moment of inertia of the facesheets, I_f, and core, I_c, both computed about the centroid of the unit cell section. The predominant contribution to D_{yy} is the facing moment of inertia. It is modified to account for the combined Poisson's effect of both the facesheets and the core. Only the facesheets are used in the computation of D_{xy}.

$$D_{xx} = \frac{E(I_c + I_f)}{2p(1-\nu^2)} \quad , \quad D_{yy} = \frac{E \cdot I_f}{2p\left(1 - \frac{\nu^2 I_c}{I_c + I_f}\right)} \quad , \tag{2.9}$$

$$D_{xy} = \frac{E \cdot I_f}{2p(1+\nu)} \quad , \quad D_{Qx} = \frac{Et_c^2}{p(1+\nu)A_c}\left(h - \frac{t_1}{2} - \frac{t_2}{2}\right)^2$$

2.2.4 Numerical Computation of D_{Qy}

The transverse shear stiffness, D_{Qy}, has been derived for numerous specific cases of core geometry including the continuous truss core (Libove and Hubuka, 1951) including a simplified derivation for the truss core (Lok and Cheng, 2000), Z-core (Fung et al., 1994), C-core (Fung et al., 1996). A numerical analysis approach was set described by Cheng et al (2006), which used a shell analysis finite element method to determine all of the elastic constants. Since this method proved to be general virtually any geometry truss core can be analyzed.

Implementation of the frame analysis into the analysis routine is a relatively simple process. Figure 2.16 shows the model that can used for either a continuous or non-continuous truss core. Rigid links are provided between the core and the face sheet between nodes 2 and 10, 3 and 11

etc. In the continuous core case the dimension, w_1, is taken to be zero and the nodes 1 and 9 are removed from the analysis. The cut nodes along the cut edges of the unit cell (1 or 2 and 19, 9 or 8 and 23) are constrained to move the same distance in the vertical direction. In reality the unit cell is under plane strain conditions, therefore, the resulting displacements must be multiplied by the factor $(1-\nu^2)$.

If a single laser stake weld is used only links at 3-11, 7-14 and 17-21 are retained. The model is fixed against rigid body motion at node 5. A total unit vertical shear force is applied at the right and left hand cuts ($Q_1 + Q_2 = 1$). The horizontal forces are such to keep the unit cell in equilibrium ($H_1+H_2 = 2p(Q1+Q2)/h$). By symmetry $H_1 = H_2$.

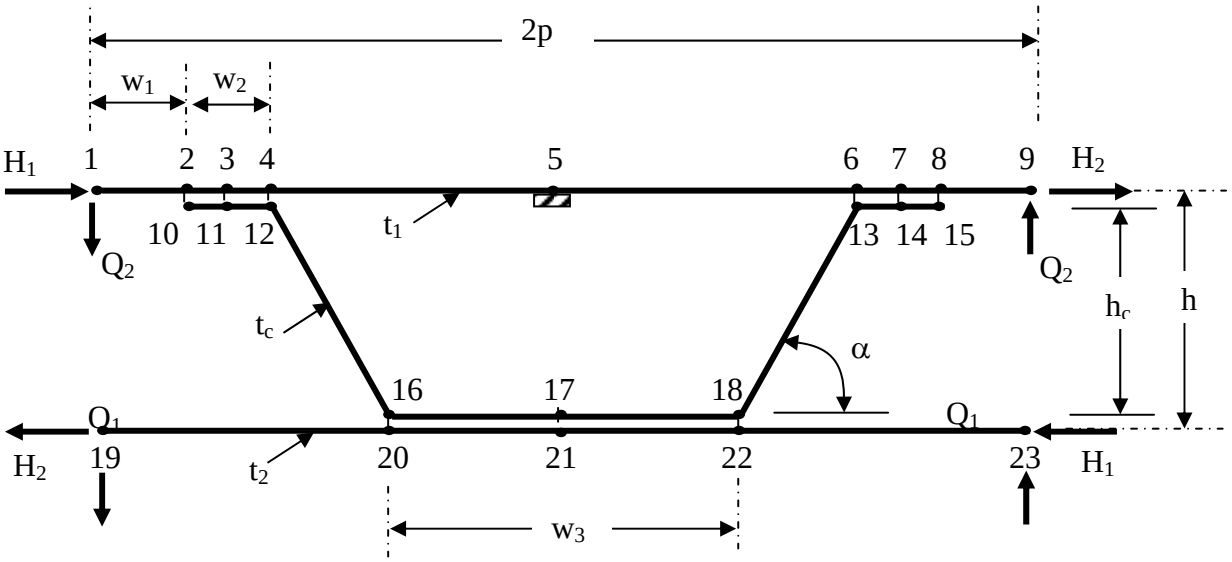

Figure 2.16 Frame FEM for Computation of D_{Qy}

2.2.5 MATLAB Results

The method was coded into the MATLAB computer program, which is an interactive computer program for solving technical computing problems especially powerful with matrix and vector formulations. In the numerical computations, two cases are considered one including and the

other ignoring the Poisson's effect on the computation of D_{QY}. The results are given in Tables 2.3 and 2.4, respectively.

Table 2.3 Poisson's Effect Included.

Weld Placement	Center Defection (mm)	Max(mm)	Mx(N.mm)	My(N.mm)	Mxy(N.mm)
Center	6.7333	10.48	$6.01x10^3$	-576.0655	0
Corner	6.2742	7.1214	$5.62x10^3$	-295.7196	0
Center and Corner	5.9224	6.7713	$5.32x10^3$	-81.5144	0
Tan Current Case	6.467	7.5692	$5.78x10^3$	-413.3901	0

Weld Placement	Dx(N.mm)	Dy(N.mm)	Dxy(N.mm	Dqx(N.mm	Dqy(N.mm)
Center	$4.11x10^6$	$3.23x10^6$	$2.32x10^6$	$2.85x10^7$	$1.66x10^5$
Corner	$4.11 x10^6$	$3.23x10^6$	$2.32x10^6$	$2.85x10^7$	$2.04x10^5$
Center and Corner	$4.11 x10^6$	$3.23x10^6$	$2.32x10^6$	$2.85x10^7$	$2.38x10^5$
Tan Current Case	$4.11 x10^6$	$3.23x10^6$	$2.32x10^6$	$2.85x10^7$	$1.87x10^5$

Table 2.4 Poisson's Effect Excluded.

Weld Placement	Center	Max(mm)	Mx(N.mm)	My(N.mm)	Mxy(N.mm)
Center	7.036	10.7853	$6.23x10^3$	-759.4097	0
Corner	6.5684	7.4144	$5.84x10^3$	-457.2506	0
Center and Corner	6.202	7.0497	$5.53x10^3$	-221.0796	0
Tan Current Case	6.7645	7.8654	$6.00x10^3$	-583.846	0

Weld Placement	Dx (N.mm)	Dy (N.mm)	Dxy(N.mm	Dqx(N.mm	Dqy(N.mm)
Center	$4.11 x10^6$	$3.23x10^6$	$2.32x10^6$	$2.85x10^7$	$1.51x10^5$
Corner	$4.11 x10^6$	$3.23x10^6$	$2.32x10^6$	$2.85x10^7$	$1.86x10^5$
Center and Corner	$4.11 x10^6$	$3.23x10^6$	$2.32x10^6$	$2.85x10^7$	$2.18x10^5$
Tan Current Case	$4.11 x10^6$	$3.23x10^6$	$2.32x10^6$	$2.85x10^7$	$1.71x10^5$

The current finite element analysis result for the centerline deflection in Tan's case is in good agreement with the MATLAB results. Comparison is made on the bottom centerline where local effects on the deformation due to the pressure load do not exist. The discrepancy between the current FEA result and the MATLAB result is reported as 0.7%. The discrepancy between the Tan's experimental study and the MATLAB result is -12%. When the Poisson's effect are excluded in the MATLAB solution the centerline deflection and Tan's experimental result come closer and the disagreement is -8.5%.

2.3 Case Study – Prismatic Sandwich Panel Analysis (IBRC Panel)

The results of the previous study were used to develop the details of a bridge deck replacement case study. The case study performed involved 15-ft span retrofit deck based upon the replacement of a steel bridge located in Gardiner Maine. Static and fatigue numerical finite element analysis performed by ATS indicate the optimal sandwich panel deck to be 7.25 inches deep and weigh 48 pounds per square foot, for this 15 foot long deck panel span. The design philosophy was to ensure that all AASHTO specifications were met, in order to gain acceptance from practicing bridge engineers. This types of bridge deck offers improved lateral and torsional rigidity of the bridge structure as well as offering improved shear resistance and fatigue strength over traditional orthotropic decks.

Figure 2.17 shows a sandwich panel bridge deck designed to meet current AASHTO requirements for a steel orthotropic bridge deck with a 15-foot span illustrated in Figure 2.18. An iterative finite element approach assuming simple supports on the strong axis and a central patch load simulating an AASHTO HS25 truck tire was used to determine the required thickness of the elements as well as the overall deck depth. The global deflection criterion primarily governs the overall height of the sandwich panel and the local deflection criterion strongly influences the top face-sheet thickness.

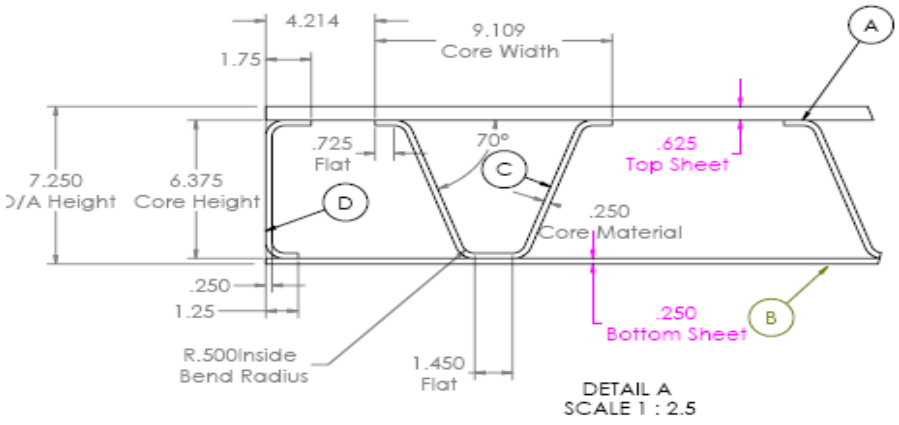

Figure 2.17 Current Sandwich Panel Design With a 15-Foot Span

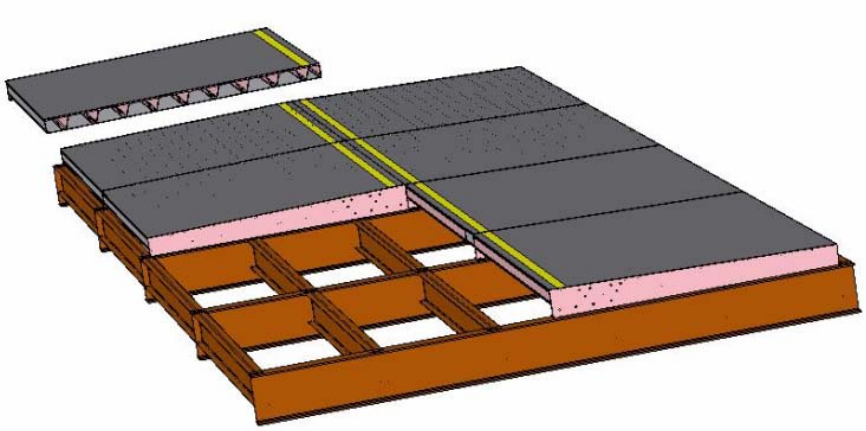

Figure 2.18 Sandwich Panel Layout and Connection to Floor Beam

The case study analyzed is of a symmetric panel subjected to a patch loading. Compared to most sandwich panels, this design has face sheets that are relatively thick. The cross section of the sandwich panel is shown in Figure 2.19. The sandwich panel is designed with discontinuous corrugated cores attached to the top and bottom sheets with laser stake welding as shown in Figure 2.20. The sandwich structure is 144 inches wide by 180 inches long and has a total depth of 7.25 inches. Dimensions are shown in the Figure 2.21 as they are used to create the finite element model and analyze the sandwich panel. The design consists of nine stiffeners, with and overall pitch of 15.717 inches. The panel is closed out from both sides with a boundary plate. Top plate has a thickness of 0.625inch and bottom plate is 0.25inch thick. Stiffeners and the boundary plate have same thickness of 0.25inch.

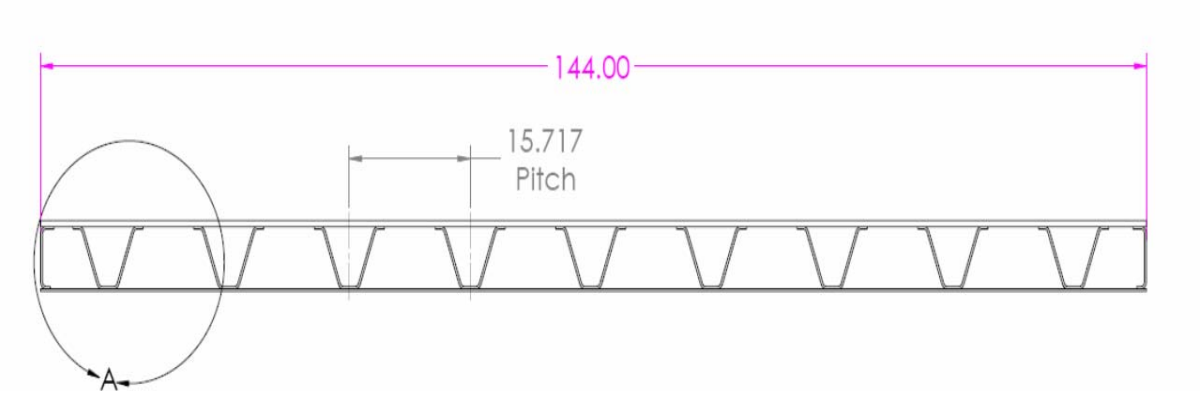

Figure 2.19 Cross Section of Sandwich Panel

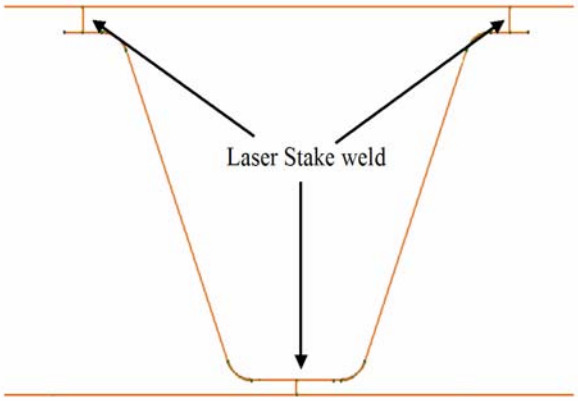

Figure 2.20 - Laser Stake Weld-Actual Cross Section of FEM

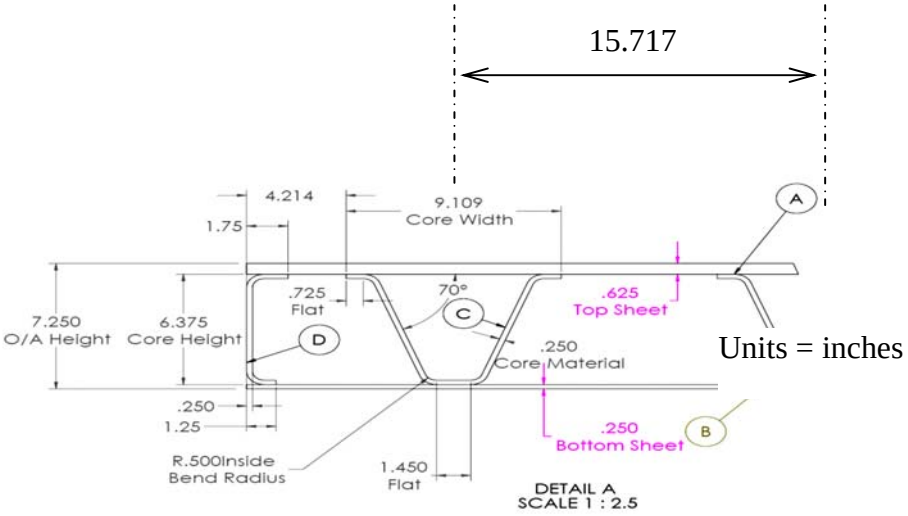

Figure 2.21 - Close Out and Stiffener Detail of Sandwich Panel

2.3.1 Modeling: Boundary Conditions and Loading

The sandwich panel is made of linear elastic steel material with a Young modulus of 29,000ksi and Poisson's ratio of 0.3. In this static analysis a general-purpose conventional stress and displacement element, ABAQUS S8R6 is used. The simply supported boundary conditions for this case are applied in a similar manner as done in Tan's case. Also, the front face and the rear face of the FE model do not include a close out plate, but again constrain the transverse displacements. Boundary conditions are applied to front and rear faces to restrain the rotation. Force consists of a 29,000lbs truck wheel load applied to the top surface of the sandwich panel as a pressure normal to the surface over a 22 inch by 10-inch patch at the center of the panel. Actual patch dimension, which the load is applied, is 11 inch by 5 inch due to quarter symmetry about the longitudinal and the transverse direction. The cross section of the web-core and continuous stake weld configuration of the quarter model symmetry is shown in Figure 2.22 along with the actual model analyzed in ABAQUS in Figure 2.23.

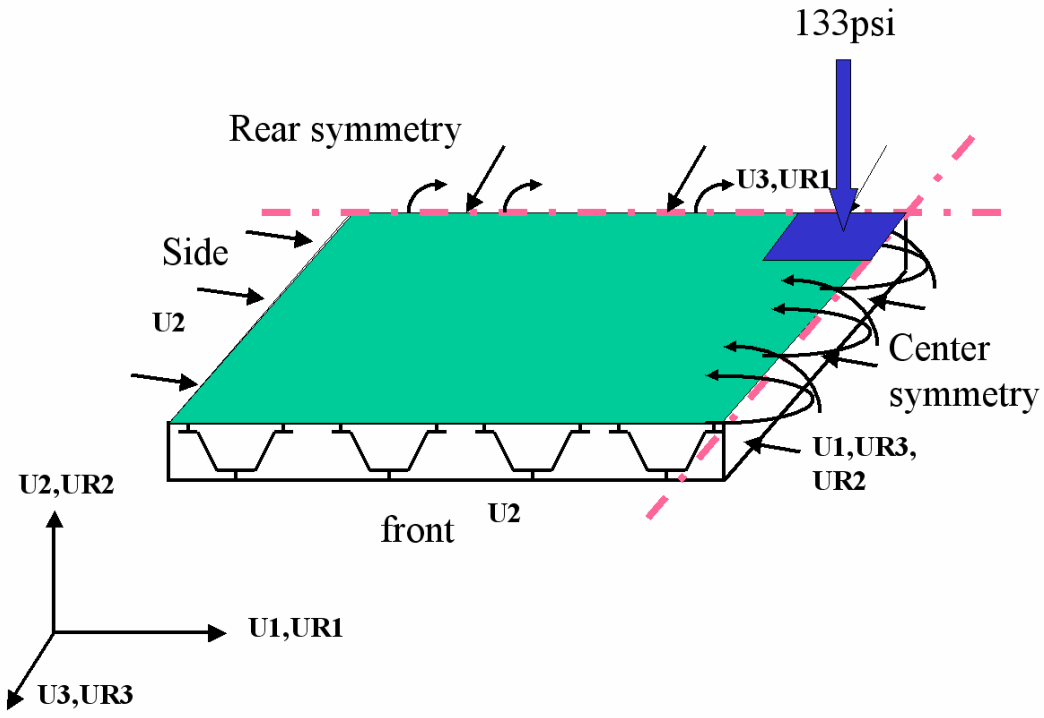

Figure 2.22 Applied Boundary Conditions to the Quarter Model and Patch Load

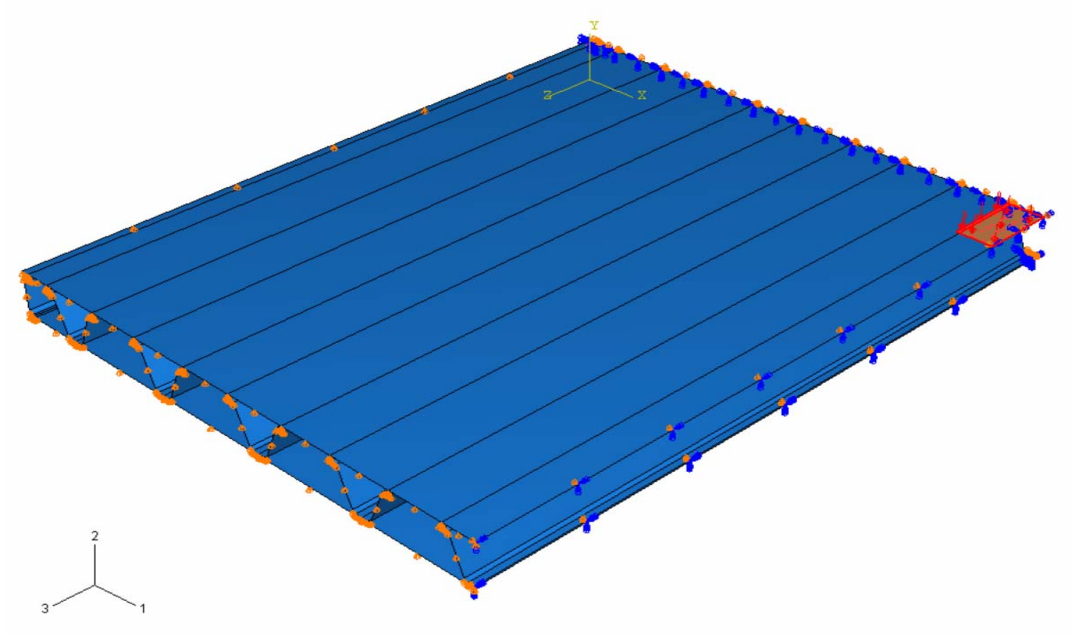

Figure 2.23 Finite Element Model BCs and Patch Load

2.3.2 Mesh Details

After performing the convergence study shown in Figure 2.24 approximately 28,000 S8R6 finite elements as shown in Figure 2.25 are found to be sufficient to have converged results in the analysis of the quarter model.

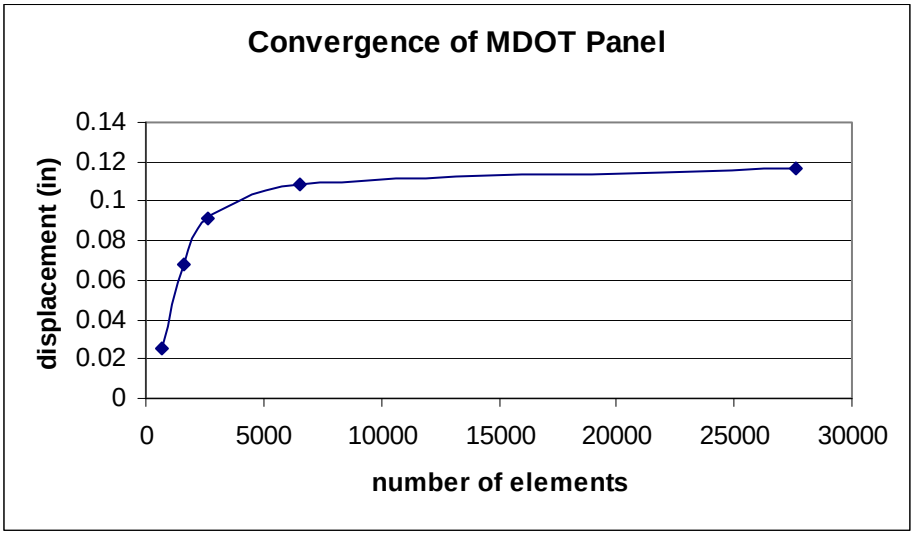

Figure 2.24 Convergence Rate of MDOT Panel

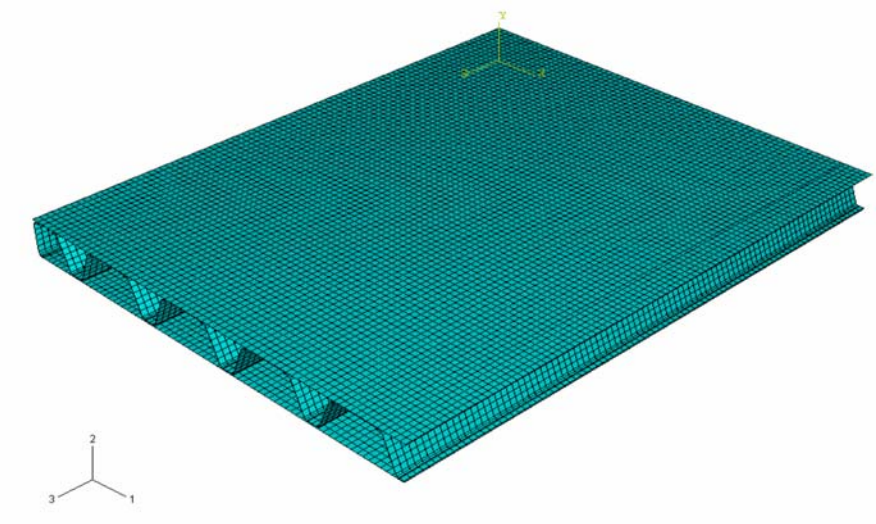

Figure 2.25 Meshed Sandwich Panel

In the meshing process of the corrugations special attention is given to the location where the stiffener changes direction in the transverse orientation. Due to the fillet where the horizontal and the inclined portion of the stiffener meet, a node is placed at the inflection point of the curvature in the fillet as shown in Figure 2.26.

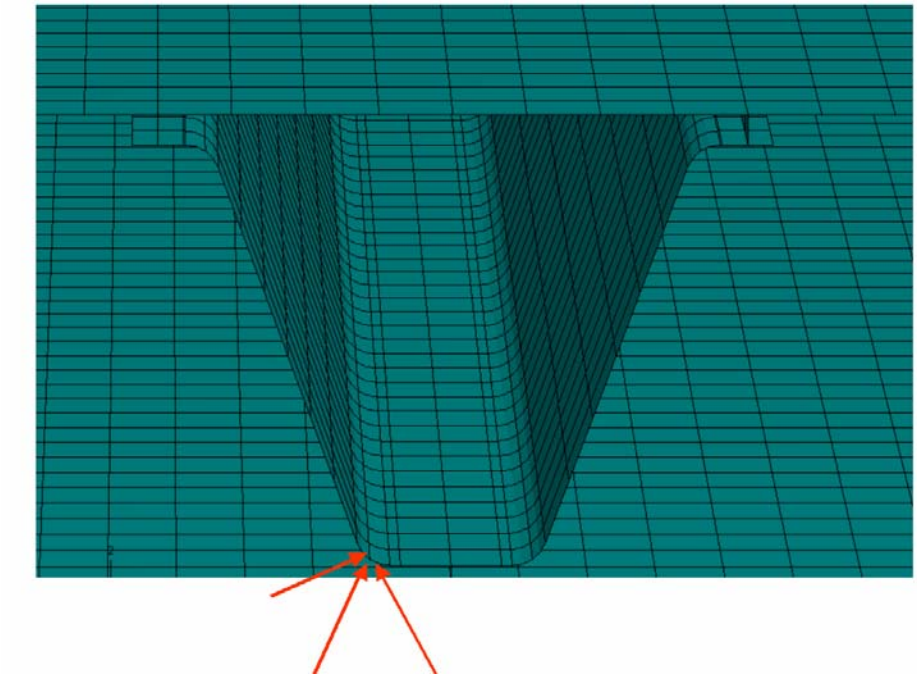

Figure 2.26 Mesh detail of the Stiffener

These nodes assure a smooth transition avoiding excessive stress concentrations in the stiffeners. Same meshing technique is also used in the right hand side of the bottom part as well as top part where the inclined pieces meet the horizontal pieces at the top portion of the stiffener.

2.3.3 Finite Element Displacement Results

The patch load cased examined with the truck wheel load simulated as a patch load over an 11inch by 5inch patch with a total pressure load of 133psi. The goal of this sandwich panel analysis is to verify the theoretical calculations, which are performed to meet the design requirement for the Maine Department of Transportation (MDOT) for bridge decks. Global deflection of the quarter model is shown in Figure 2.27. In this figure local deflections of the top and the bottom plates of the sandwich panel are also shown.

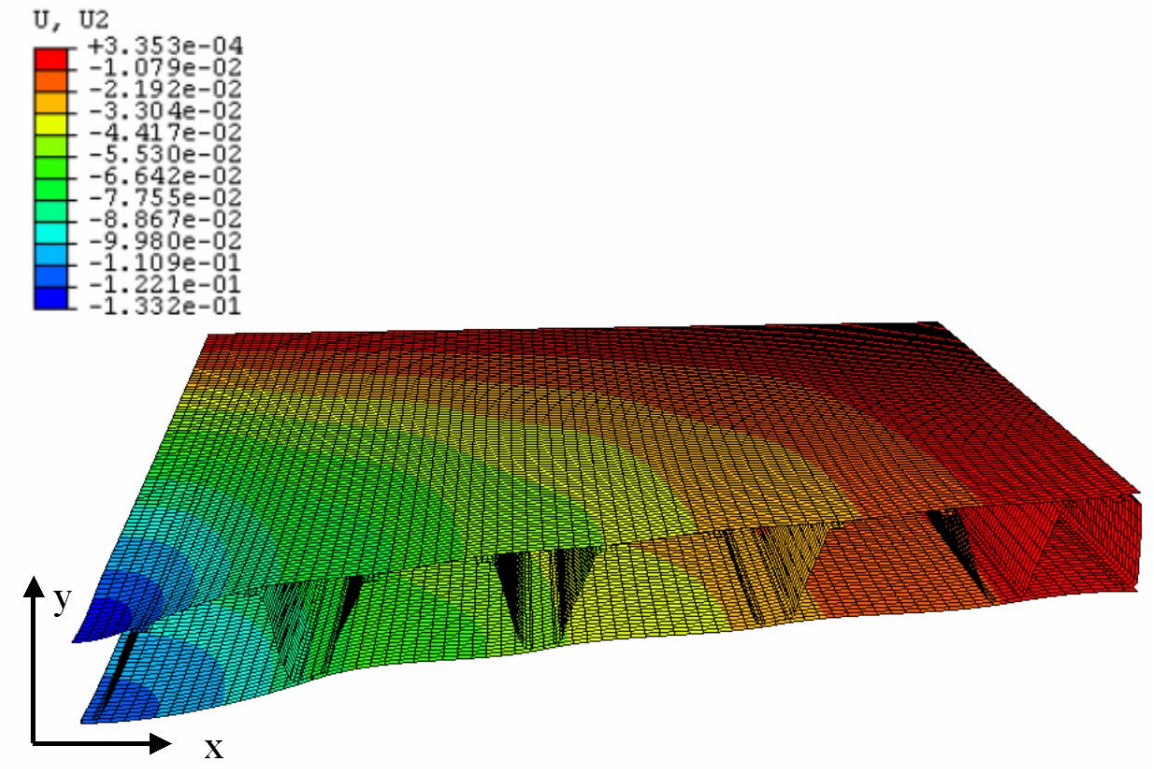

Figure 2.27 Magnified View of Deflected Cross Section of Sandwich Panel

Global deflection result is obtained averaging the local deflection of the top and the bottom plate at the center of the sandwich panel as shown in Figure 2.28. The maximum local deflection of the top plate which is shown in Figure 2.29, at the center of the panel is 0.13 inch and the maximum local deflection for the bottom plate which is shown in Figure 2.30, is 0.11inch. In the global coordinate system the maximum deflection at the center of the panel is 0.12inch. This is at a displacement/span ratio of L/1500.

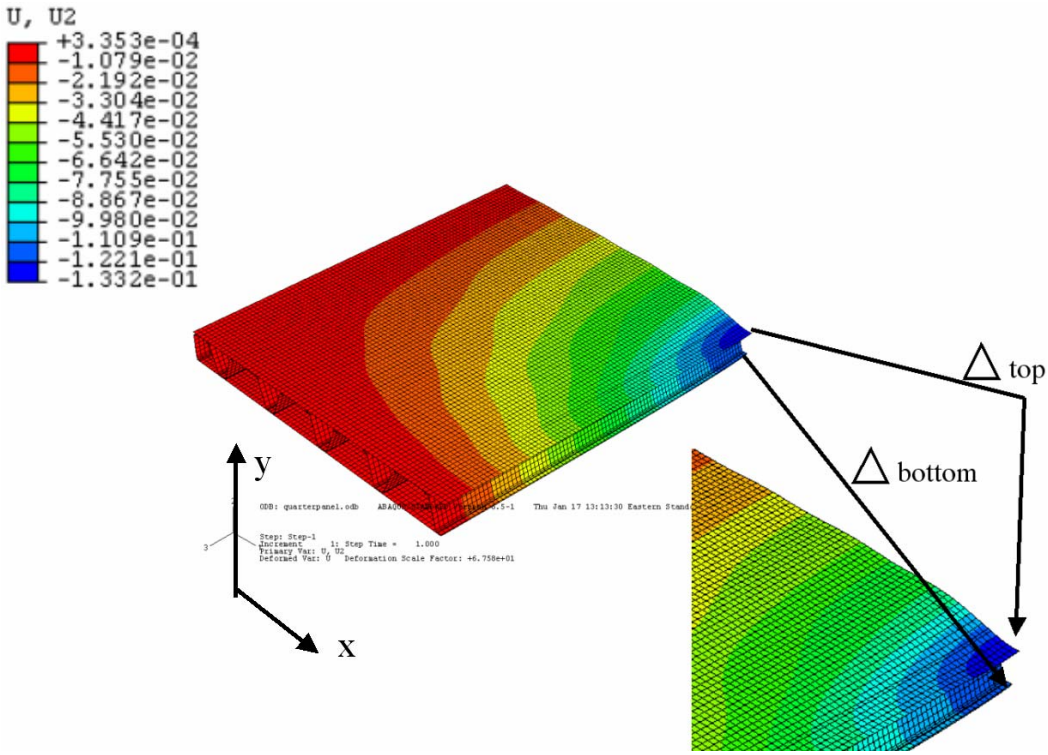

Figure 2.28 Global Deflection

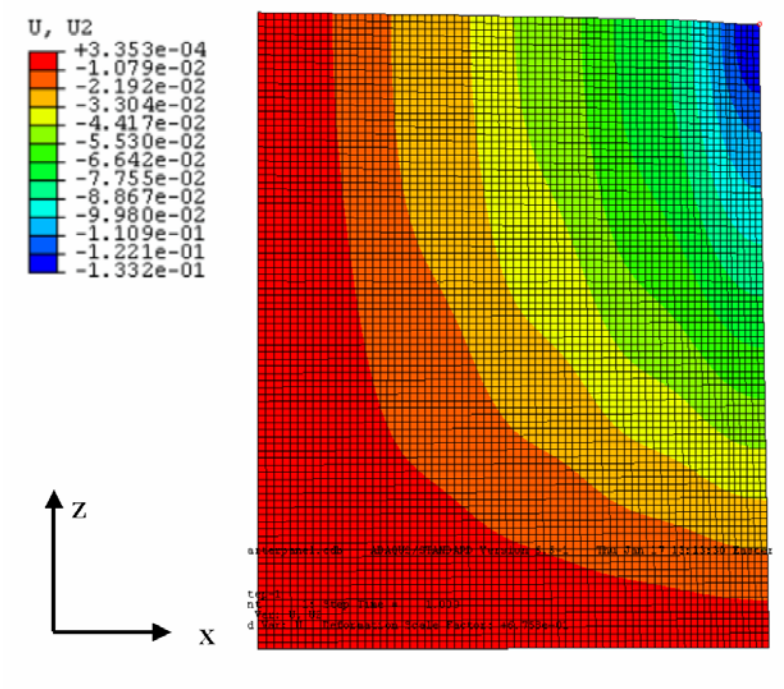

Figure 2.29 Top Plate Surface Deflection

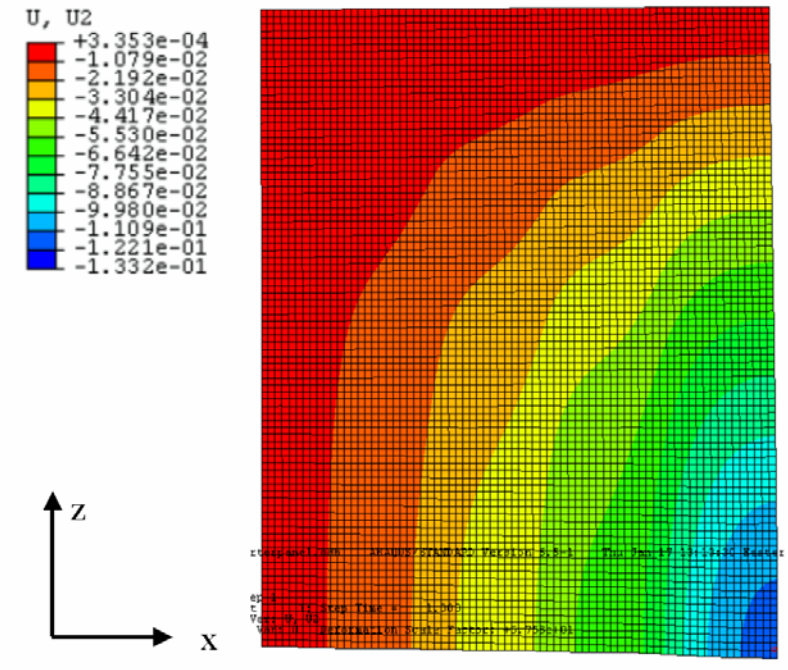

Figure 2.30 Bottom Plate Deflection

2.3.4 Finite Element Stress Results

The maximum in-plane stress occurs at the horizontal portion of the stiffener, which is located at the center of the sandwich panel. The global view is illustrated in Figure 2.31. The maximum in-plane principle stress in x-direction at the center of the top plate is -19010psi is shown in Figure 2.32 and for the bottom plate is +4205psi is shown in Figure 2.33. Stress results at rapidly changing discontinuities need to be treated with caution. Relatively high local values may be indicative of local effects and are possibly due to the modeling techniques.

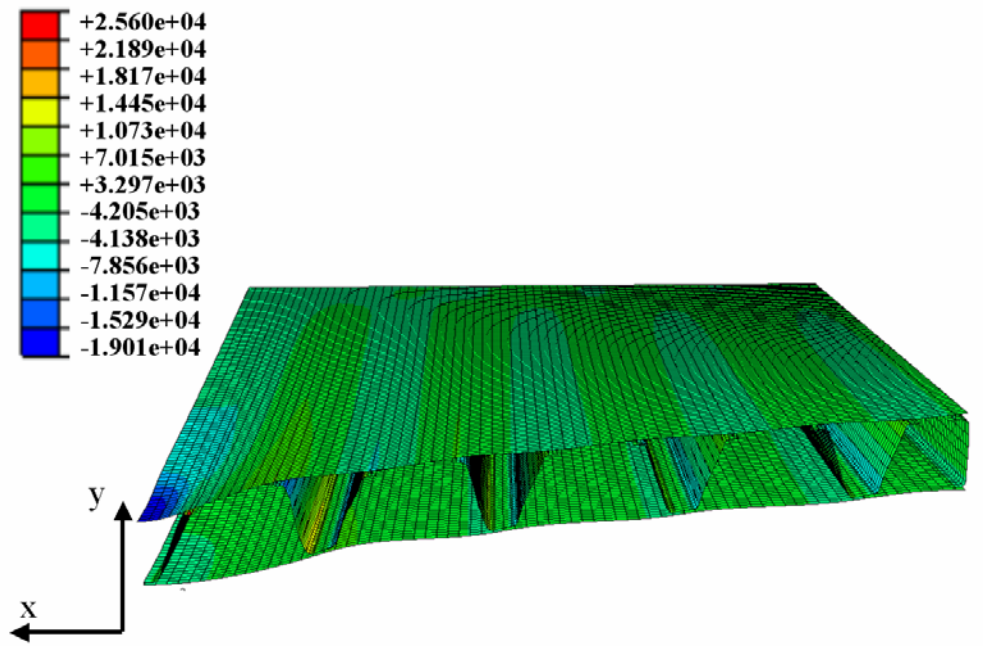

Figure 2.31 Maximum In-Plane Global Principle Stress in x-Direction

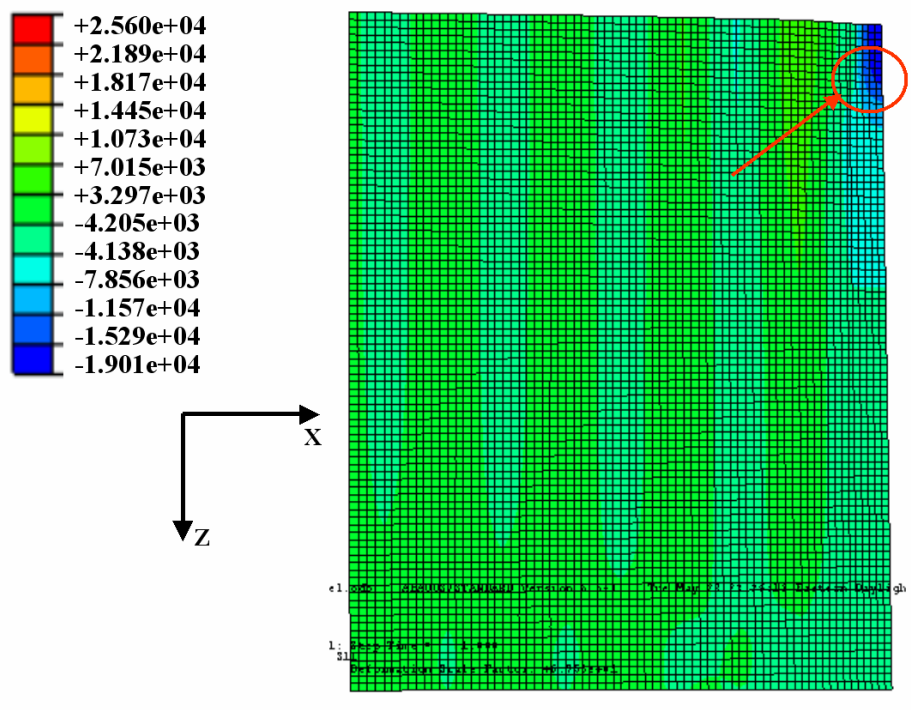

Figure 2.32 Top Plate Maximum In-Plane Stress in x-Direction

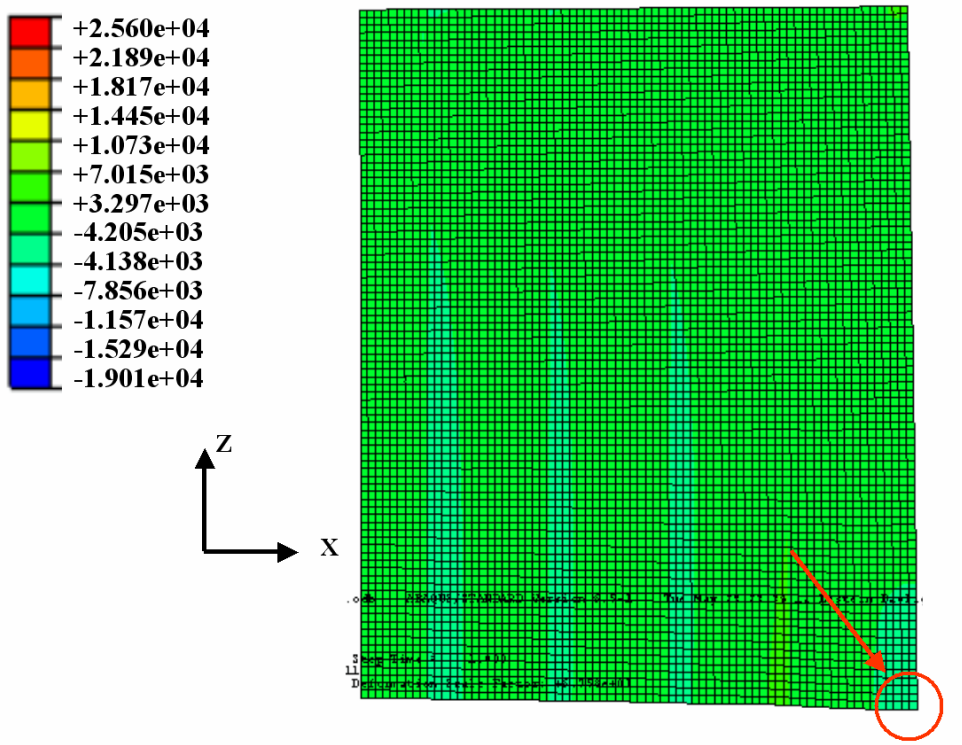

Figure 2.33 Bottom Plate Maximum In-Plane Stress in x-Direction

The maximum in-plane principle stress for the stiffener in x-direction is +25600psi is shown in Figure 2.34.

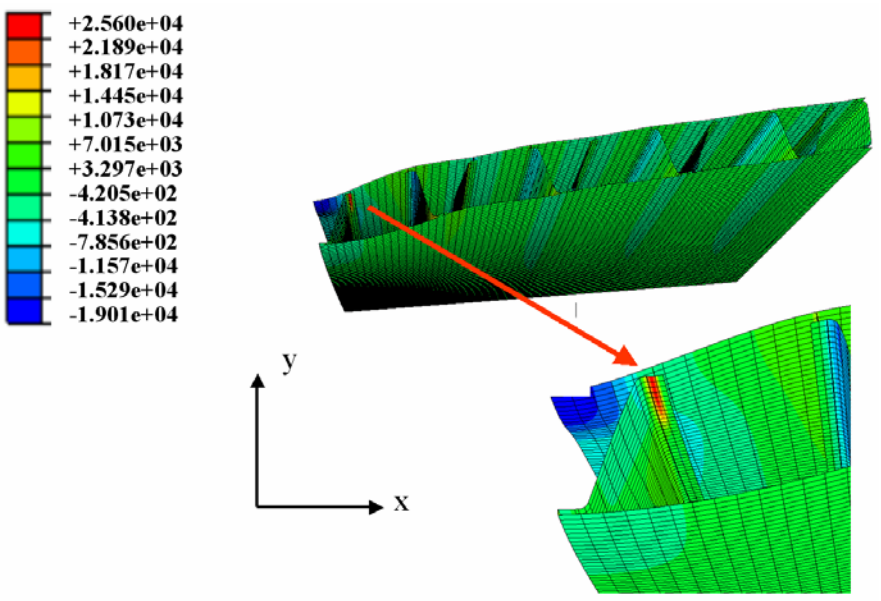

Figure 2.34 Maximum In-Plane Stress for the Stiffener in x-Direction

Global view of the maximum in-plane stress results in z-direction is given in Figure 2.35.
The maximum in-plane stress in z-direction occurs at the center weld. The value is +33960psi and it is shown in Figure 2.36 in detail.

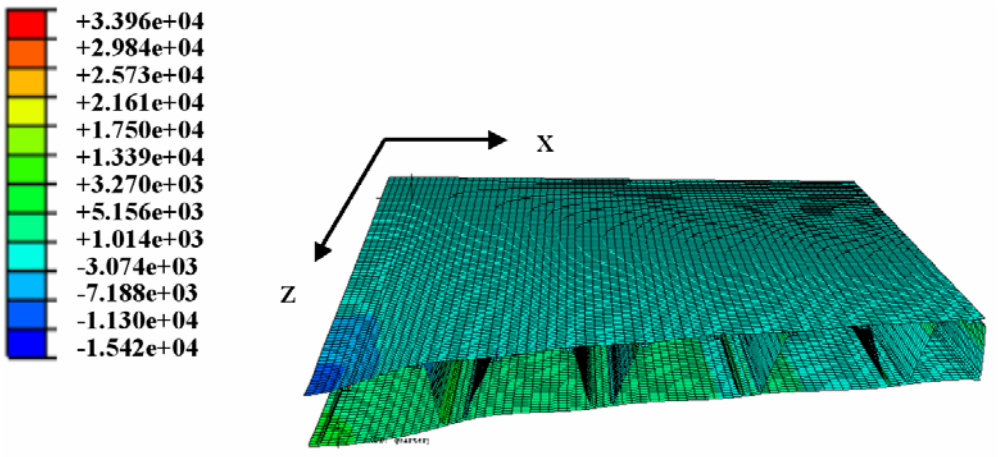

Figure 2.35 Maximum In-Plane Global Principle Stress in z-Direction

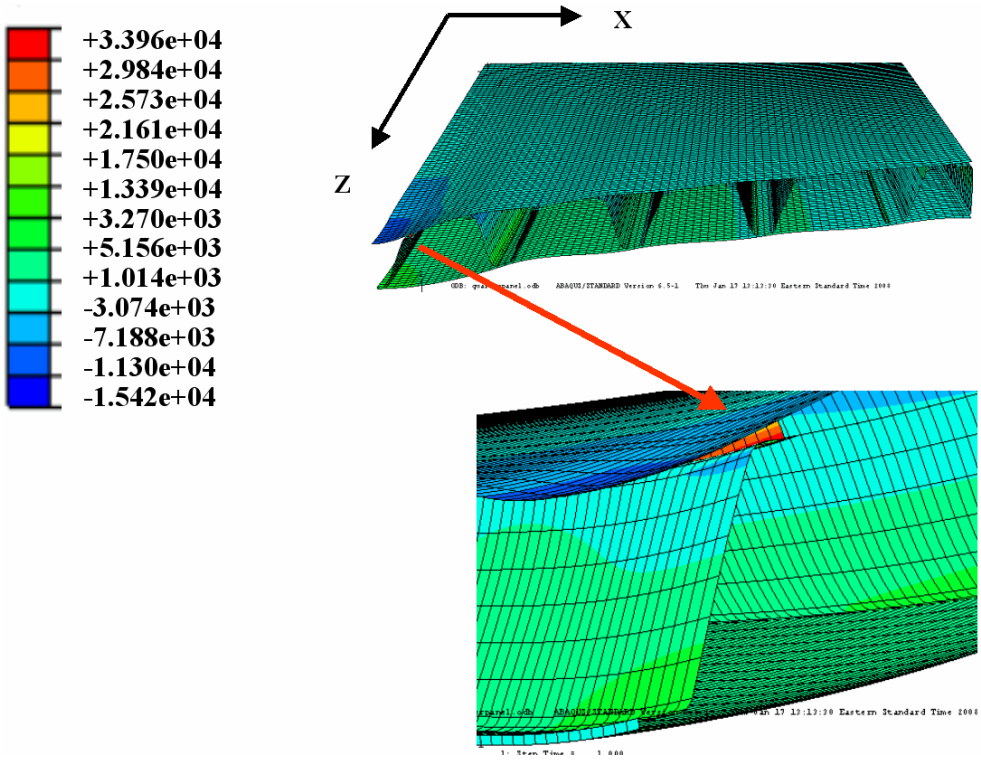

Figure 2.36 Maximum In-Plane Stress in z-Direction for Weld

The maximum in-plane stress for the top plate is –15420psi. The bottom plate maximum stress value is +17500psi. Stress plots are given in Figure 2.37 and Figure 2.38 respectively.

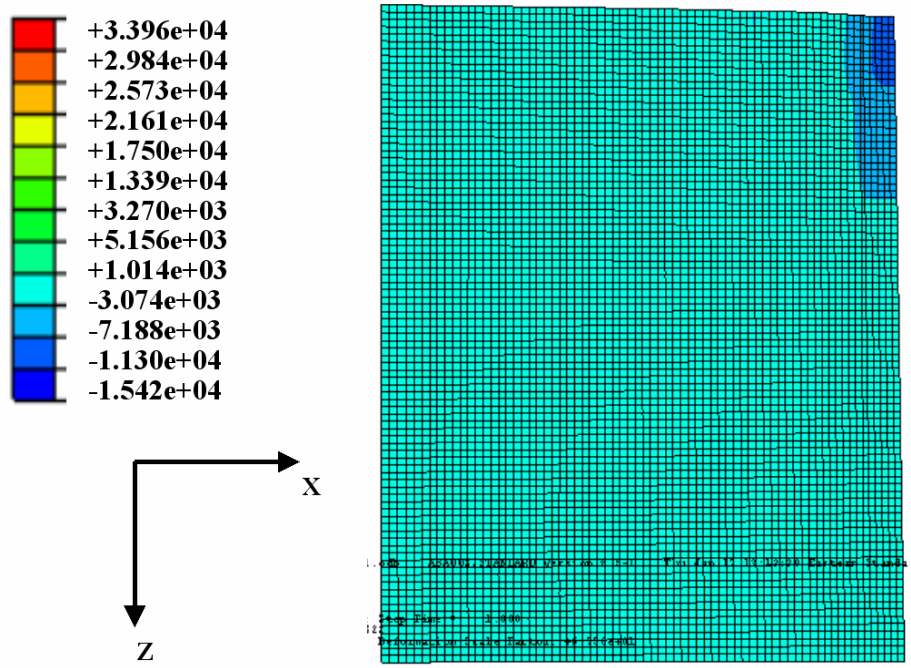

Figure 2.37 Top Plate Maximum In-Plane Stress in z-Direction for Top Plate

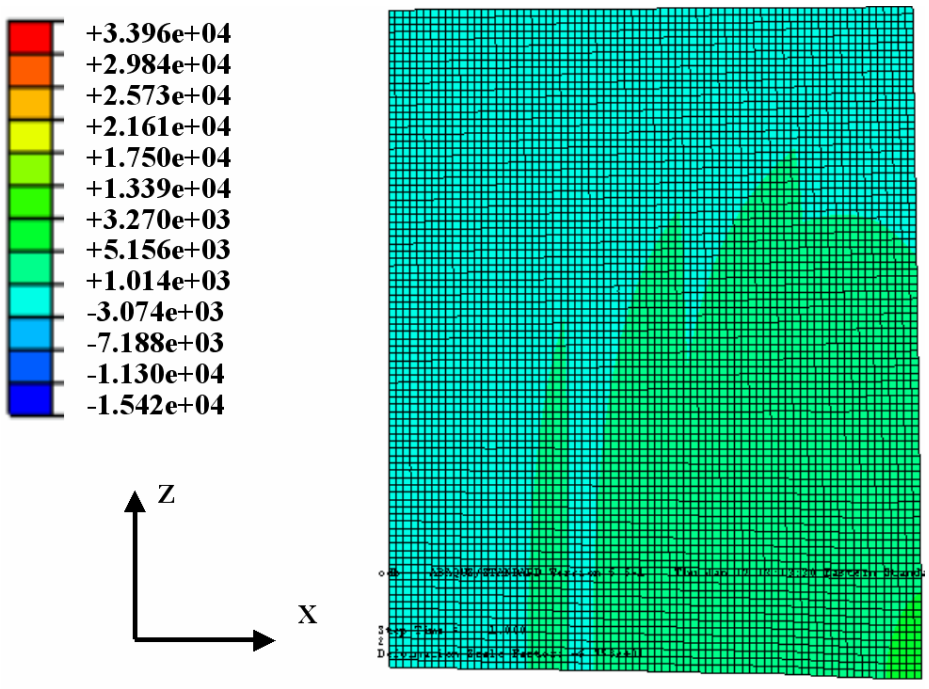

Figure 2.38 Bottom Plate Maximum In-Plane Stress in z-Direction for Bottom Plate

The maximum in-plane stress for the stiffener is +7960psi in Figure 2.39.

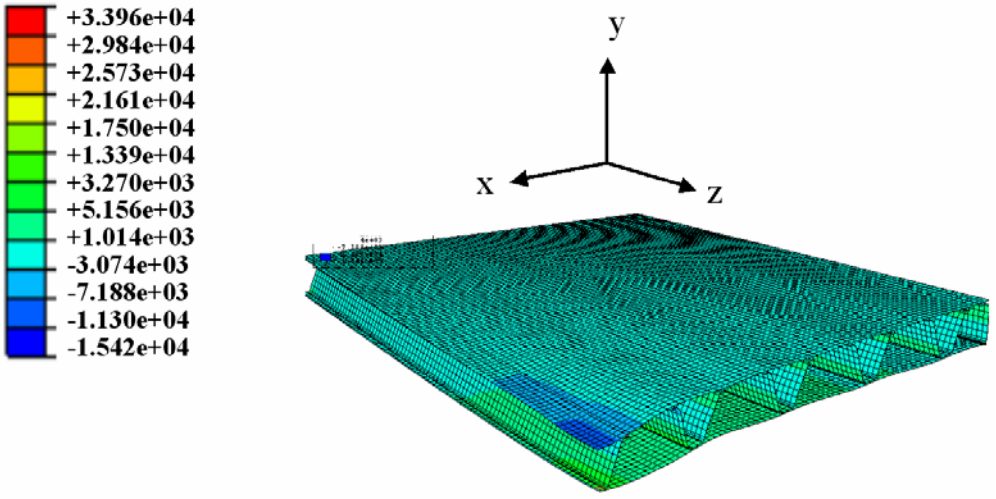

Figure 2.39 Maximum In-Plane Stress for the Stiffener in z-Direction

3. EXPERIMENTAL LAP-SHEAR TESTS OF LASER STAKE WELDS

This section of this report covers the single lap-shear testing of laser stake welds with the purpose to determine weld strength. Test coupons were fabricated by ATS with both longitudinal and transverse welds using HSLA-65 plate material nominally 0.2" thick. Multiple weld passes were used to assess the influence of this parameter on weld capacity.

3.1 Test Objectives

The primary objective of this effort is the performance of laser stake weld strength tests in configurations including longitudinal and transverse single lap shear. Several objectives of this task are summarized as follows:

1. Determine the longitudinal and transverse lap-shear strength of laser stake welds using a readily available base material with good laser welding characteristics.
2. Assess the influence of number of weld passes including dual and quad weld profiles on the shear strength..
3. Determine general guidelines for weld resistance of multiple pass stake welds.

3.2 Transverse Single Lap Shear Test Criteria

A test article with transversely oriented welds can be fabricated by running several stake welds over two wide strips of metal that are the desired thickness. The test articles are then cut to width (W) from the wider piece. The weld test section is separated from the gripped ends by machining a slot of width, A, (see Figure 3.1) through one side of the plate material.

In determining the sizing of the transverse single lap shear test specimens the nominal strength of the plate material, P_y, is related to the yield strength, σ_y, minimum thickness, t_a, and specimen width, W, as given in Equation (3.1).

$$P_y = \sigma_y \cdot t_a \cdot W \tag{3.1}$$

The nominal weld capacity ST_w is estimated as:

$$ST_w = \sigma w_y \cdot w_w \cdot W_L \tag{3.2}$$

where σw_y is the yield strength of the weld material, the dimension w_w is the weld width and W_L is the length of the weld equal to W as shown in the figure below.

For optimal useage of plate material sizing criteria is such to preclude failure in the plate. It is reasonable to assume that the limiting condition will result in weld failure in the heat affected zone and not in the base material due to changes in material properties cuased by welding and stress concentrations. For testing purposes it is desirable to have the failure occur in the weld so that weld strength can be assessed. Failure in the plate material will yield a lower bound only with regard to weld capacity. If the weld strength is assumed equal to the plate strength and the plate material is sized to be as strong as the weld it results in a maximum value for the dimension w_w of:

$$w_w \leq t_a \tag{3.3}$$

Selecting a plate width, W, of 2 inches. The case where the weld width equals the thinnest plate material results in the critical section. Figure 3.2 shows a photograph of a typical transverse test article. Table 3.1 presents a summary of the nominal dimensions for the transverse lap shear test specimens. The table shows the specimen designation which includes an S-T indication a static test with transverse oriented welds. The next set of numbers in the designation indicates the nomimal plate thicknesses in 1000^{th} of an inch. This is followed by a indication of the number of welds used in the test article fabrication. Table 3.2 shows the test matrix indicating 4 samples to be tested in each series. Samples were fabricated from plates as designated in column 2. This number can be traced back to the process control parameters used in fabrication by ATS.

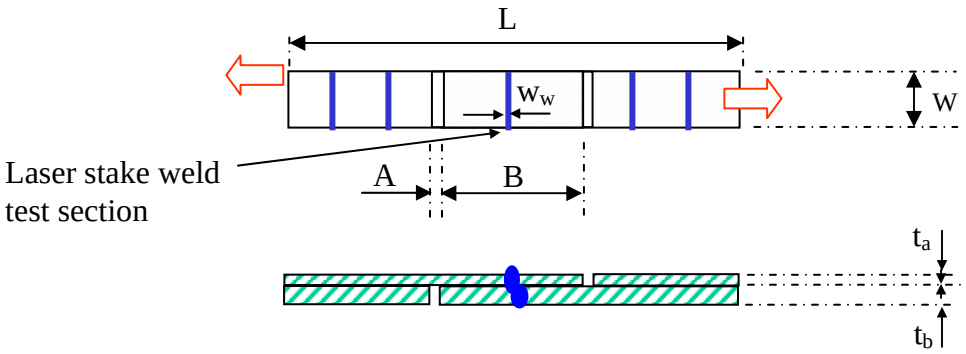

Figure 3.1 - Transverse Single Lap Shear Test Article

Table 3.1 - Transverse Single Lap Shear Specimen Nominal Geometry

Designation	L in.	W in.	A in.	B in.	Plate Thickness in.		Total Welds	Weld Width (nom.)	Ratio
					t_a	t_b		w_w	w_w/t_a
C1-S-T-200x200x4W	11.75±	2	$^5/_{16}$	1-$^5/_8$	0.2	0.2	2	$^3/_{32}$	1
C1-S-T-200x200x2W	11.75±	2	$^5/_{16}$	1-$^5/_8$	0.2	0.2	4	$^3/_{16}$	0.5

Table 3.2 - Transverse Single Lap Shear Test Matrix

Designation	Plate Designation	Number of Samples
C1-S-T-200x200x4W-01 thru 04	3665	4
C1-S-T-200x200x4W-05 thru 08	3666	4
C1-S-T-200x200x2W-09 thru 12	3664	4
C1-S-T-200x200x2W-13 thru 16	3663	4

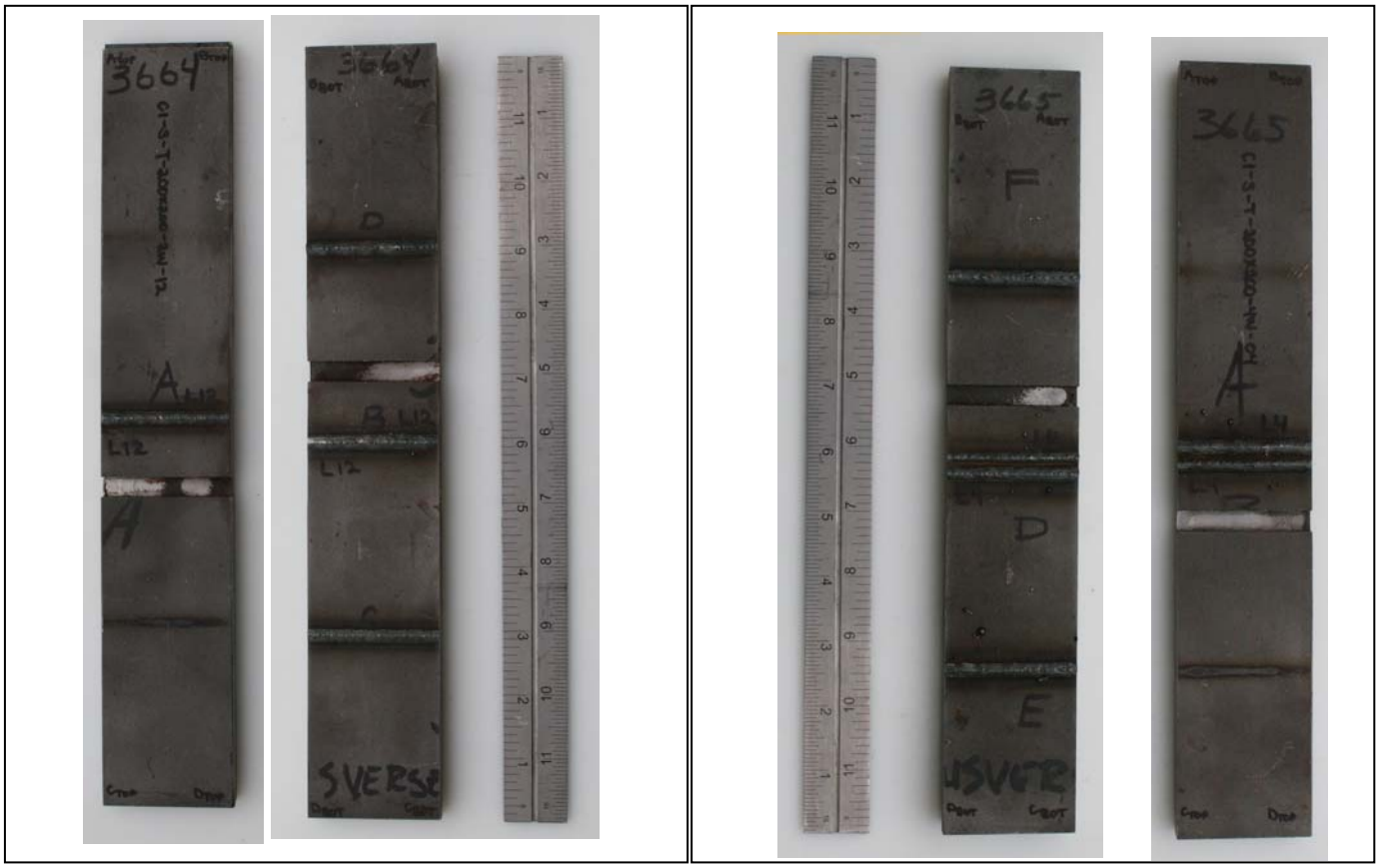

Figure 3.2 – Photographs of a Transverse Sample

3.3 Longitudinal Single Lap Shear Test Criteria

A longitudinal single lap shear test article (see Figure 3.3) is made by running a series of parallel stake welds over two plates of metal which are the desired thickness. The pieces can then be cut to length (L) from the plates. The weld test section is separated from the gripped ends by machining through one side of the plate material. A distance between grips of 6" was used in the longitudinal tests resulting in a grip length of approximately 2-7/8".

In determining the sizing of the longitudinal single lap shear test specimens the nominal strength of the plate material, P_y, is computed as in Equation 3.1. The nominal weld capacity SL_w is estimated as:

$$SL_w = \sigma w_y \cdot w_w \cdot B \tag{3.4}$$

where σw_y is the yield strength of the weld material and the dimension w_w is the weld width and B is the length of the weld as shown in Figure 3.3.

Again, if sizing criteria is such to preclude failure in the plate material and the weld strength is assumed equal to the plate strength and the plate material is sized to be twice as strong as the weld then a maximum length for the dimension B of:

$$B \leq \frac{t_a \cdot W}{2 \cdot w_w} \tag{3.5}$$

Selecting a plate width, W, of 2 inches. The case where the weld width equals the thinnest plate material results in a length B of 1 inch. Figure 3.4 shows a photograph of a typical longitudinal test article.

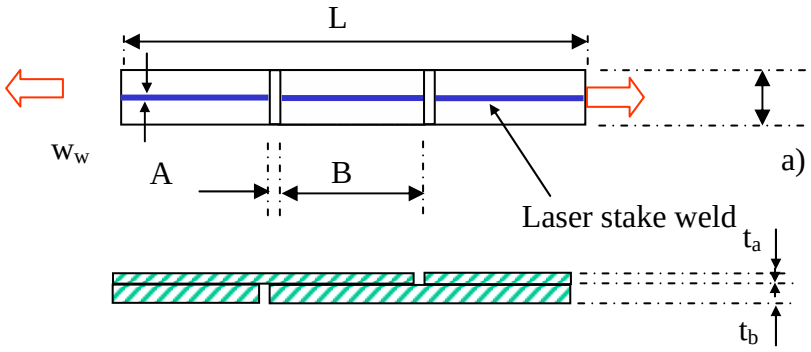

Figure 3.3 - Longitudinal Single Lap Shear Test Article

Table 3.3 presents a summary of the nominal dimensions for the longitudinal lap shear test specimens. The table shows the specimen designation S-L indicating a static test with longitudinal oriented welds. Table 3.4 shows the test matrix indicating 4 samples to be tested in each series. Samples were fabricated from plates as designated in column 2. This number can be traced back to the process control parameters used in fabrication by ATS.

Table 3.3 - Longitudinal Single Lap Shear Specimen Geometry

Designation	**L** in.	**W** in.	**A** in.	**B** in.	**Plate Thickness** in.		**Total Welds**	**Weld Width (nom.)**	**Ratio**
					t_a	t_b	N	w_w	w_w/t_a
C1-S-L-200x200x4W	11.75±	3±	$^5/_{16}$	1	0.2	0.2	2	$^3/_{32}$	0.5
C1-S-L-200x200x2W	11.75±	3±	$^5/_{16}$	1	0.2	0.2	4	$^3/_{16}$	1

Table 3.4 - Longitudinal Single Lap Shear Test Matrix

Designation	**Plate Designation**	**Number of Samples**
C1-S-L-200x200x4W-17 thru 20	3670	4
C1-S-L-200x200x4W-21 thru 24	3668	4
C1-S-L-200x200x2W-25 thru 28	3667	4
C1-S-L-200x200x2W-29 thru 32	3669	4

Figure 3.4 – Photographs of a Longitudinal Sample

3.4 Weld Visualization by Polishing and Etching

The transverse specimens have the weld exposed at the plate end subsequent to cutting and machining the plate to size. This allows for inspection of the weld profile prior to testing. To accomplish this examination the transverse specimens were polished with polishing wheel and then etched with a nitric acid solution. They are then wiped dry with isopropyl alcohol to reduce corrosion. Each weld was photographed with a Nikon 60mm macro lens as shown in Figure 3.5. Weld profiles traced from the specimens are presented in Appendix C.

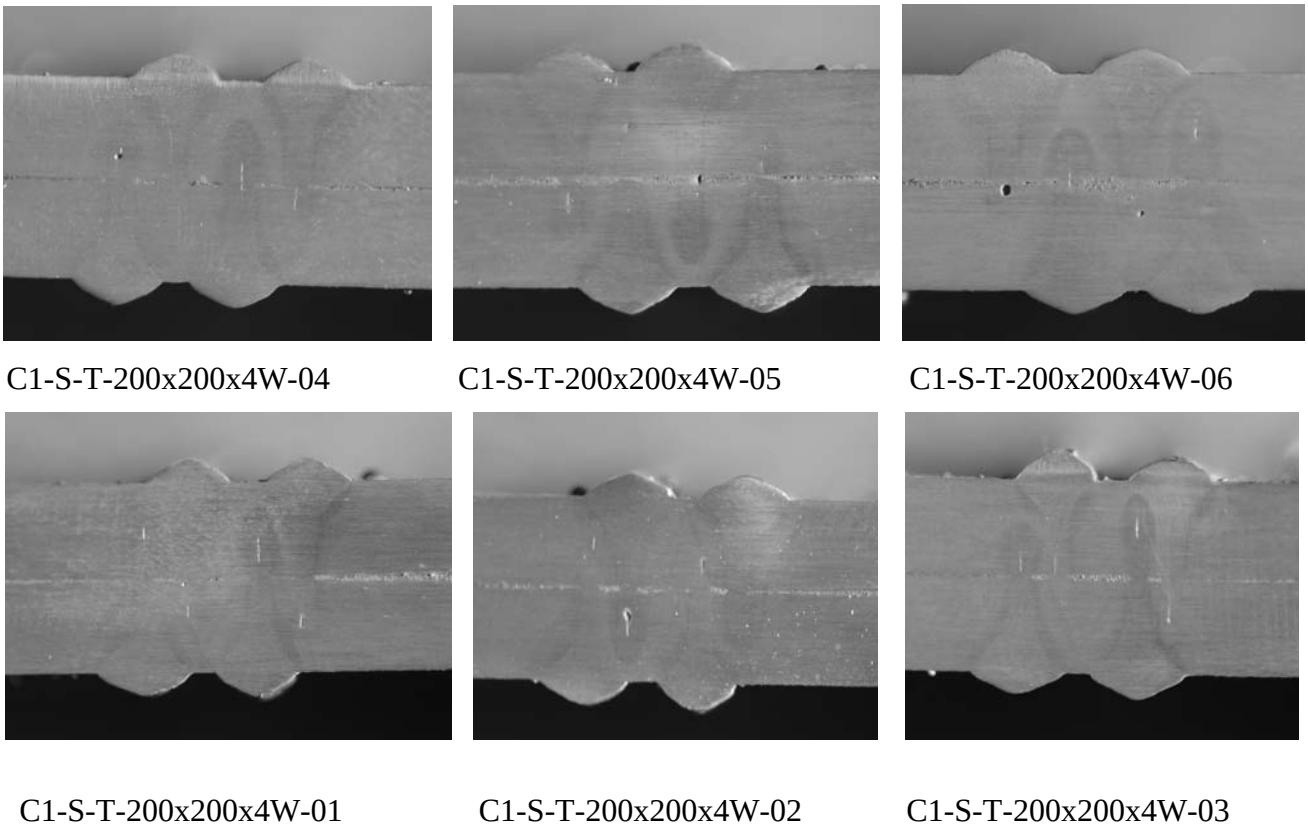

Figure 3.5 – Macro Photographs of the Transverse Stake Welds.

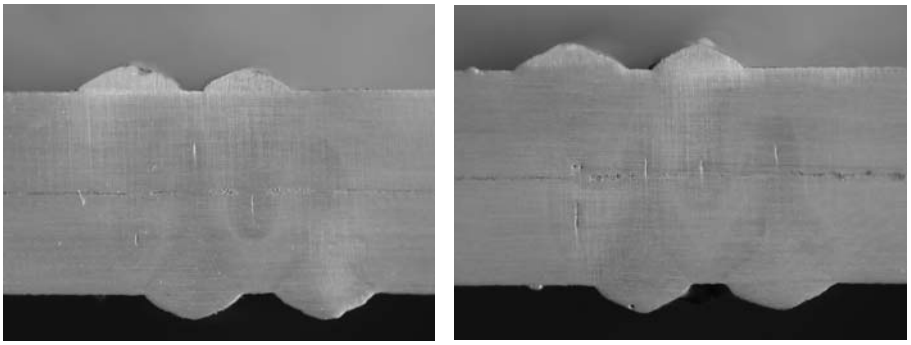

C1-S-T-200x200x4W-07 C1-S-T-200x200x4W-08

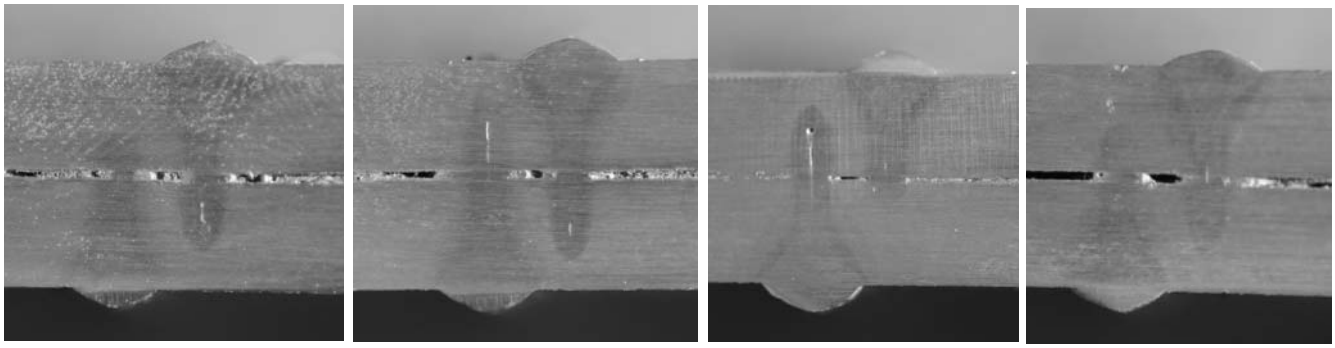

C1-S-T-200x200x2W-9 C1-S-T-200x200x2W-10 C1-S-T-200x200x2W-11 C1-S-T-200x200x2W-12

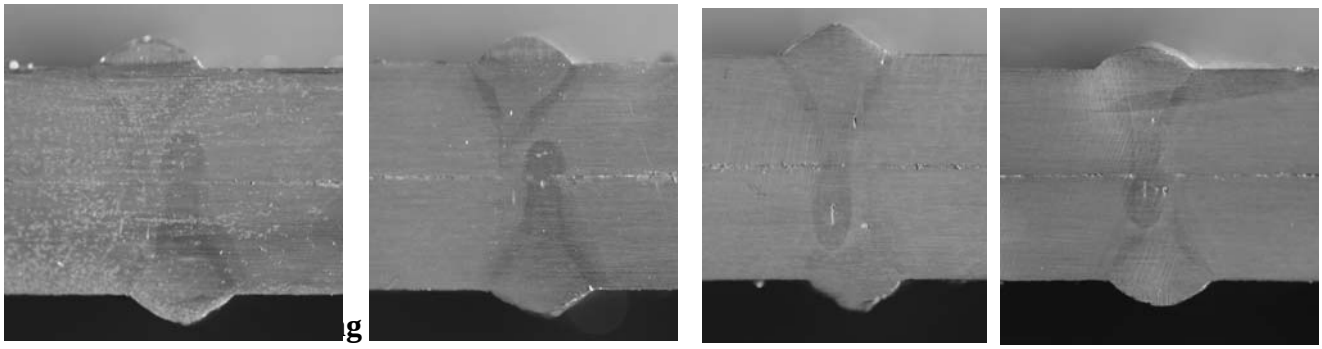

C1-S-T-200x200x2W-13 C1-S-T-200x200x2W-14 C1-S-T-200x200x2W-15 C1-S-T-200x200x2W-16

Figure 3.5 – Macro Photographs of the Transverse Stake Welds (cont'd).

3.4.1 Hardness Testing

Hardenss testing was performed using a specially designed apparatus which faclitates positioning of the hardness testing device at precise locations along the weld. A photograph of the hardness testing device is shown in Figure 3.6a. The device is based upon a Leeb hardness tester Model TH150 manufactured by Time Inc. This hardness tester was selected due to it small ball size and portability which made it easy to incorporate into a position system. It was set to read in a Vickers scale.

Specimens were loaded into the device edgewise and clamped into position. Position along the weld was tracked by a screw mechanism which was attached to a digital caliper readout device. The hardness tester was moved across the weld in 0.025 inch increments and was positioned to start and stop outside the heat affected zone. Figure 3.6b shows the indententation marks created post test. Several tests were also run at 0.05 inch spacing to assess if the spacing influenced the peak hardness values. No discernable differences were observed.

a) b)

Figure 3.6 – Hardness Tester Apparatus

Typical data results in hardness profiles as shown in Figure 3.7. A complete set of hardness test results is presented in Appendix B. Presented are typical cases for both the dual welds (x2) and the quad welds (x4). Each figure includes 2 line tracks, one across each plate. Peak hardenss values recorded for each specimen is presented in Table 3.5 with the average peak hardenss of 296.3 HV. Hardenss of the base metal was estimated by determining the average of the first 5 and last 5 readings. In this manner the base metal hardenss was estimated as 181.4 HV with a standard deviation of 8.4 HV.

Table 3.5 – Summary of Peak Hardness Values

Designation	**Line 1** HV	**Line 2** HV
SW-T-200x200x4W-01	304	303
SW-T-200x200x4W-02	291	289
SW-T-200x200x4W-03	304	305
SW-T-200x200x4W-04	302	303
SW-T-200x200x4W-05	292	316
SW-T-200x200x4W-06	290	280
SW-T-200x200x4W-07	309	305
SW-T-200x200x4W-08	298	289
SW-T-200x200x2W-09	305	299
SW-T-200x200x2W-10	302	297
SW-T-200x200x2W-11	279	309
SW-T-200x200x2W-12	271	303
SW-T-200x200x2W-13	295	281
SW-T-200x200x2W-14	303	281
SW-T-200x200x2W-15	285	295
SW-T-200x200x2W-16	306	290
Average	296.0	296.6
Std. Deviation	10.7	10.7

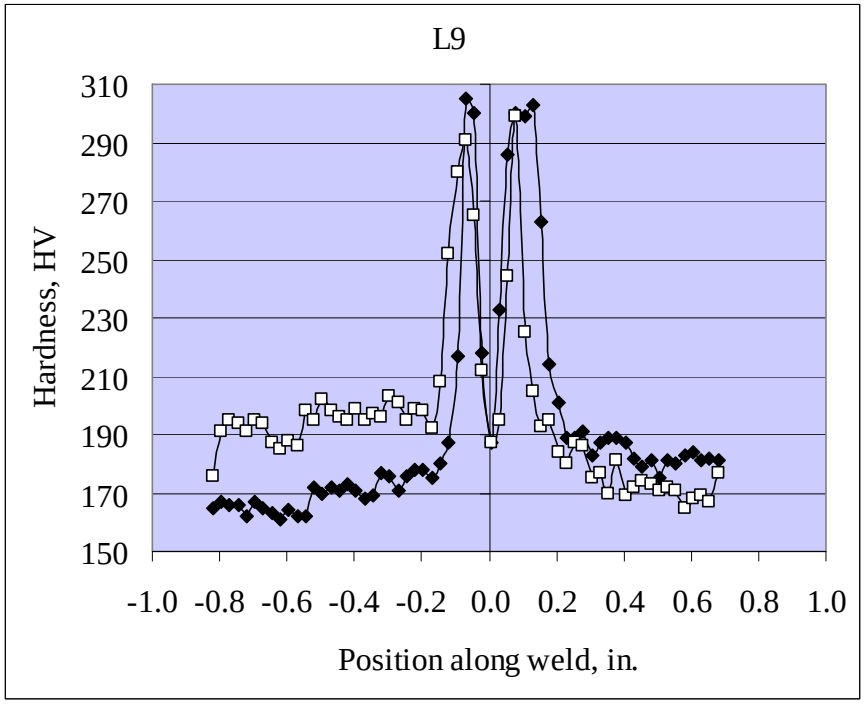

a)

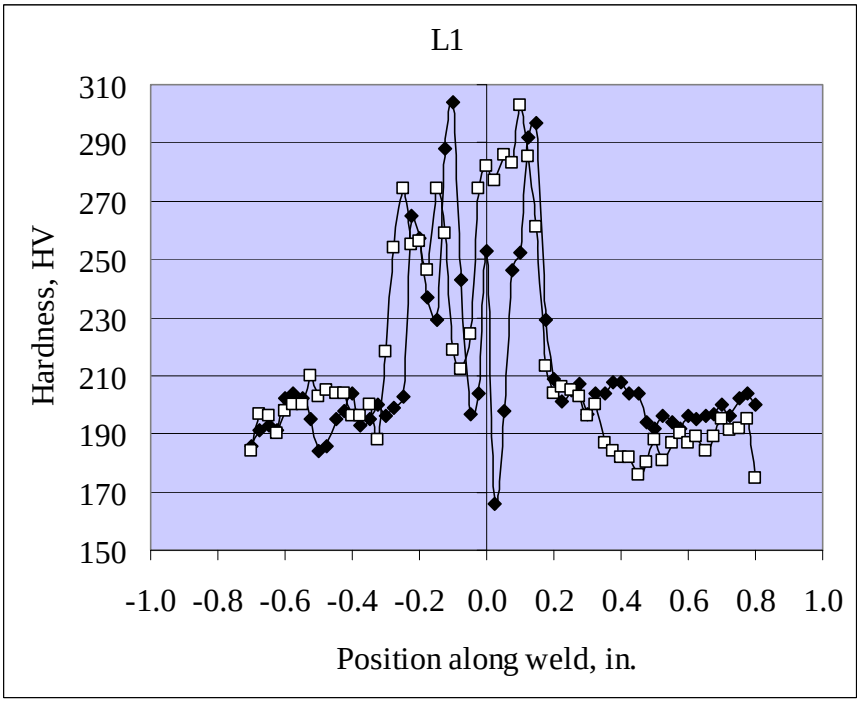

b)

Figure 3.7 – Typical Hardness Test Profiles for a) x2 Weld and b) x4 Weld

3.5 Static Testing

Static tests were performed on 32 laser stake welded single lap shear subcomponents. These tests were conducted monotonically to failure. Test specimens were made using two plates stake welded together as previously described with either longitudinal or transverse welds. Figure 3.8 shows the test coupon layout. Plate material used is HSLA-65 steel. Welds were performed at a speed of 100 in/min with laser power set at 10kW. The hybrid process was used with GMAW voltage set at 24.5 V and mean current varying from 83-172 A. The GMAW wire was fed at 300 in/min.

Lap shear specimens were cut from the nominally 0.2 inch thick plates and a slot of nominally 5/16 in (8-mm) was machined through the plates to isolate the weld in the test section.
Dimensions of the test specimens are summarized in Tables 3.6 and 3.7 including the test section width B, the specimen width, W, and the plate thicknesses, t_1 and t_2. The weld width W_w was estimated post test by measuring the width across the weld root after the two plates were separated. The weld area, Aw, is then estimated as the product of the weld length and the weld width. Accordingly, the weld area is $B*W_w$ and $W*W_w$ for the longitudinal and transverse specimens, respectively.

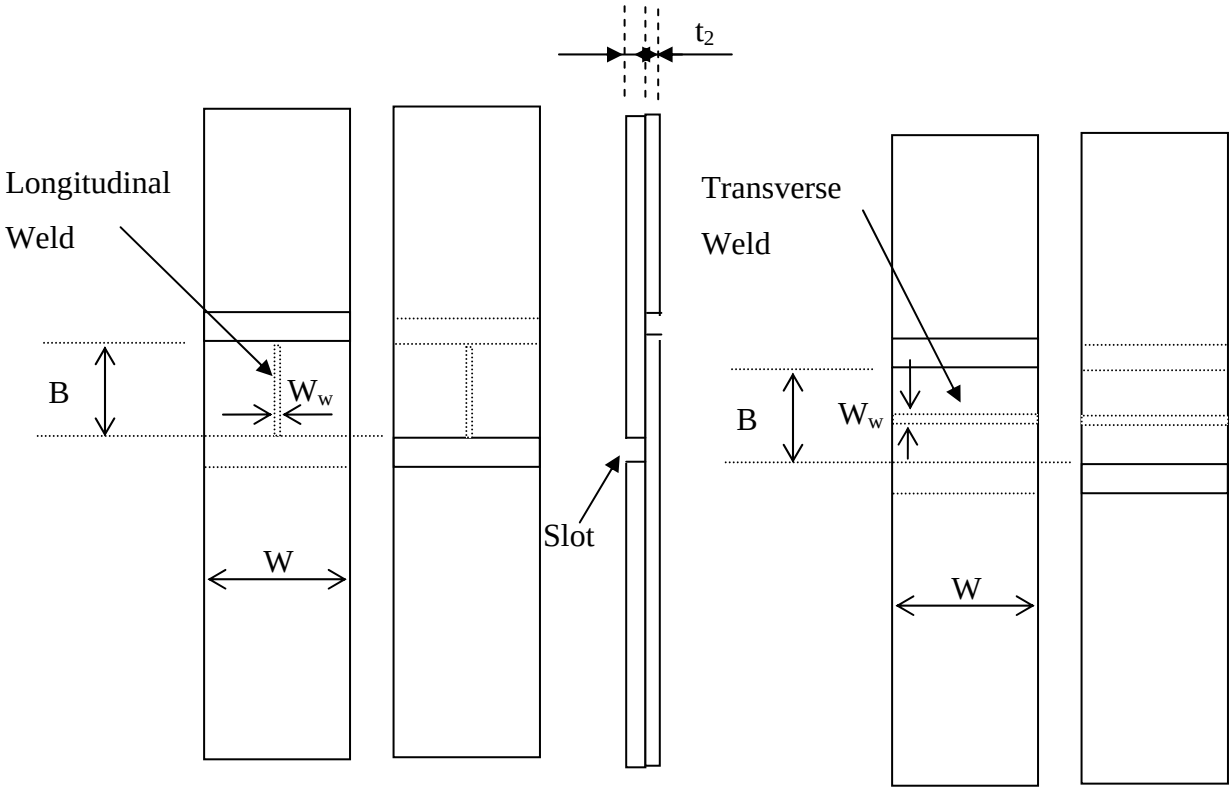

Figure 3.8 – Lap Shear Test Coupon Layout

Table 3.6 - Transverse Single Lap Shear Measured Specimen Geometry

Designation	B in.	W in.	Plate Thickness in.		Total Welds
			t_a	t_b	
SW-T-200x200x4W-01	1.615	1.992	0.2008	0.2000	4
SW-T-200x200x4W-02	1.663	1.975	0.2015	0.1995	4
SW-T-200x200x4W-03	1.634	2.006	0.2023	0.2013	4
SW-T-200x200x4W-04	1.636	2.010	0.2020	0.1998	4
SW-T-200x200x4W-05	1.805	1.994	0.2035	0.2085	4
SW-T-200x200x4W-06	1.835	2.005	0.2050	0.2068	4
SW-T-200x200x4W-07	1.790	1.993	0.2035	0.2030	4
SW-T-200x200x4W-08	1.801	1.998	0.2070	0.2030	4
SW-T-200x200x2W-09	1.760	1.993	0.2065	0.2023	2
SW-T-200x200x2W-10	1.702	1.996	0.2038	0.2055	2
SW-T-200x200x2W-11	1.915	1.976	0.2038	0.2050	2
SW-T-200x200x2W-12	1.685	2.017	0.2028	0.2043	2
SW-T-200x200x2W-13	1.531	1.947	0.2055	0.2025	2
SW-T-200x200x2W-14	1.558	1.975	0.2025	0.2025	2
SW-T-200x200x2W-15	1.558	1.979	0.2018	0.2020	2
SW-T-200x200x2W-16	1.527	2.005	0.2033	0.2020	2

Table 3.7 - Longitudinal Single Lap Shear Measured Specimen Geometry

Designation	B in.	W in.	Plate Thickness in.		Total Welds
			t_a	t_b	
SW-L-200x200x4W-17	1.016	2.967	0.2018	0.2033	4
SW-L-200x200x4W-18	1.002	2.796	0.2013	0.2013	4
SW-L-200x200x4W-19	1.021	2.945	0.2010	0.2010	4
SW-L-200x200x4W-20	1.016	2.821	0.2070	0.2015	4
SW-L-200x200x4W-21	0.994	2.929	0.2023	0.2058	4
SW-L-200x200x4W-22	1.008	2.682	0.1970	0.1983	4
SW-L-200x200x4W-23	1.016	3.069	0.2020	0.2018	4
SW-L-200x200x4W-24	0.976	2.855	0.2023	0.1998	4
SW-L-200x200x2W-25	1.013	2.974	0.2005	0.2013	2
SW-L-200x200x2W-26	1.006	2.955	0.2000	0.2005	2
SW-L-200x200x2W-27	0.976	2.884	0.1998	0.2005	2
SW-L-200x200x2W-28	1.007	2.721	0.2000	0.2013	2
SW-L-200x200x2W-29	0.995	3.169	0.2033	0.2050	2
SW-L-200x200x2W-30	0.995	2.927	0.2040	0.2013	2
SW-L-200x200x2W-31	1.029	2.803	0.2018	0.2005	2
SW-L-200x200x2W-31	0.990	2.831	0.2020	0.2008	2

3.5.1 Test Setup

Tests were conducted using an MTS 810 test machine equipped with a 100-kip load cell. The test setup is shown in Figure 3.9. Tests were performed in displacement control at a rate of 0.005 in/min. Load and displacement data were supplemented with two specially designed gap measurement instruments consisting of an ETI – LCP8P-10 linear motion potentiometer with a peak travel of 0.5 inches. A distance between grips of 6” was used in the longitudinal tests resulting in a grip length of approximately 2-7/8”.

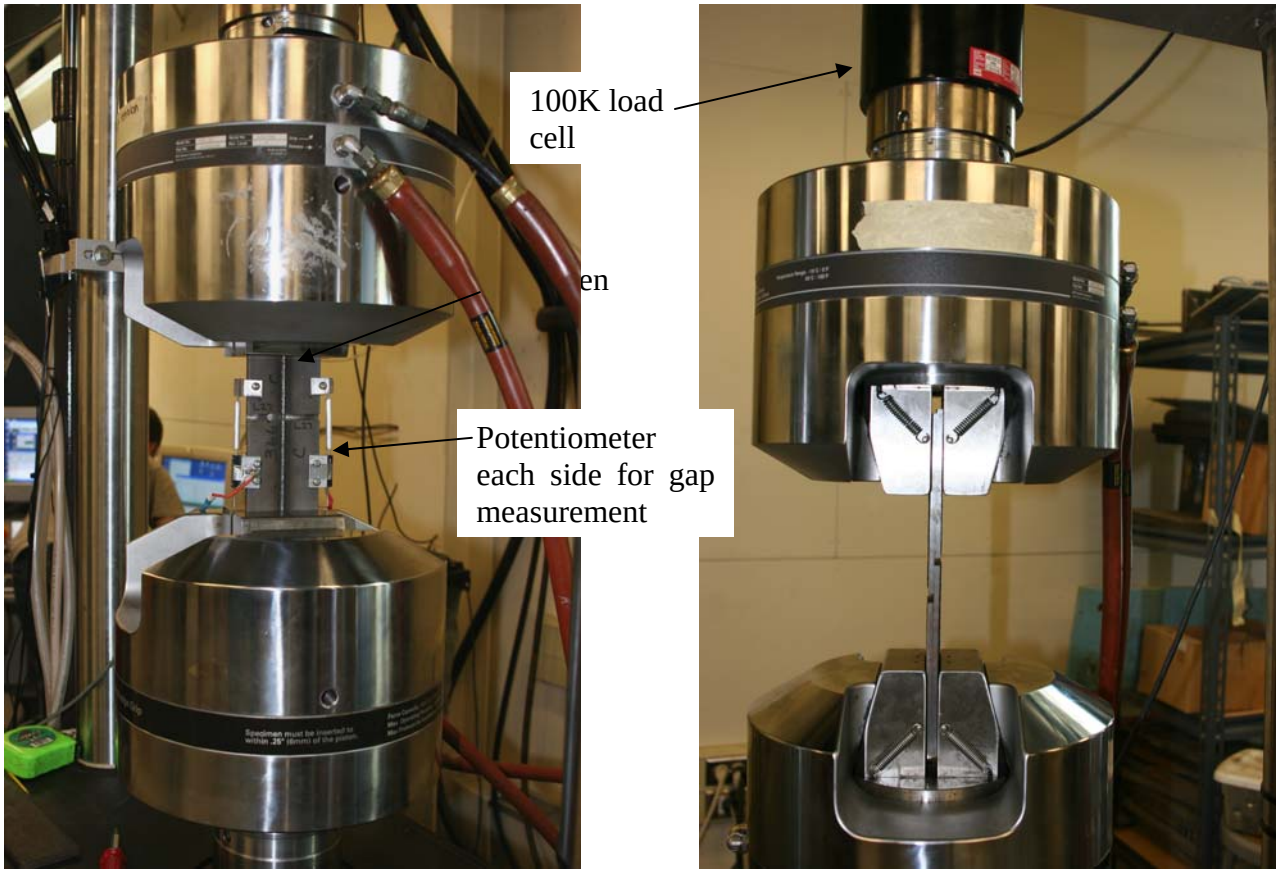

Figure 3.9 – Lap Shear Test Setup in MTS 810

3.5.2 Data Acquisition

Data were gathered from the MTS equipment and gap measurement device through a 16-channel analog data acquisition system (DAS). The heart of the system is a control program DAQFI written at University of Maine. It interfaces a DAQ Board 2000 system from IOTECH. This is a 16 bit +/-10V data acquisition card with 16 single ended analog input and 2 analog output channels per card. Multiple card systems are available if required. This system simultaneously records the data from the MTS controller and was set to read at constant intervals in time. The gap device used an LVDT interface to supply their required direct current (DC) input voltage. The DC output of these units is then read directly by the DAS. Load and displacement output signals from the MTS controller are also sent to the DAS.

3.6 Lap Shear Test Results

Table 3.8 presents a results summary of the transverse and longitudinal lap stake weld tests. A typical load versus displacement plot for the various cases is shown in Figures 3.10 and 3.11, respectively. A complete set of curves is provided in Appendix A. Average weld resistance per

unit length are summarized in Table 3.9. This was computed by dividing the peak load by the measured weld length, which is W in the case of a transverse weld and B in the case of a longitudinal weld. For the transverse weld the average resistance is 14.82 kip/in and 9.25 kip/in for the 4W and 2W cases, respectively. The longitudinal welded cases resulted in an average resistance of 17.14 kip/in and 9.80 kip/in for the 4W and 2W cases, respectively. Ultimate strength was estimated as the load at failure divided by the estimated weld area.

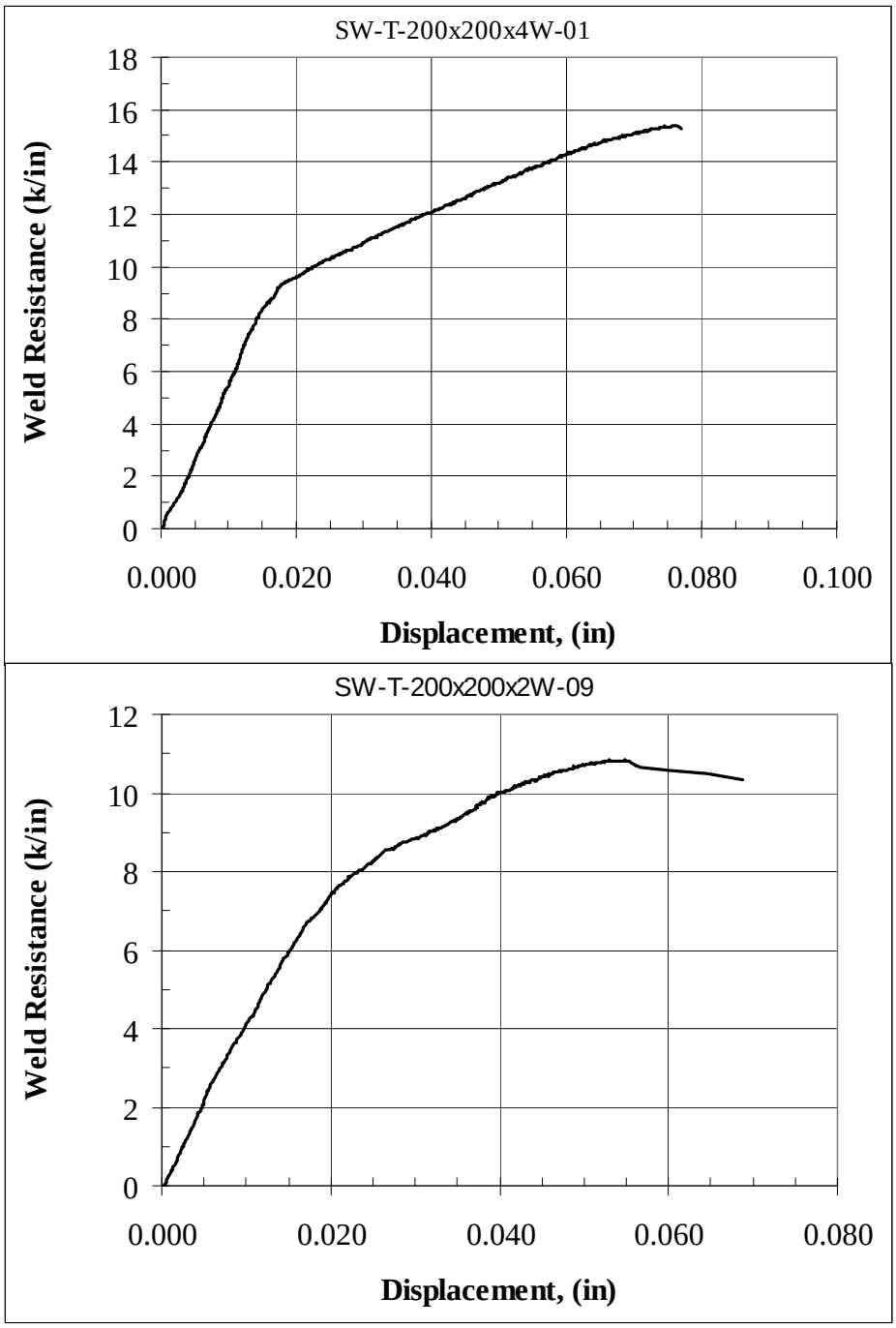

Figure 3.10 – Weld Resistance vs. Displacement, Transverse Case.

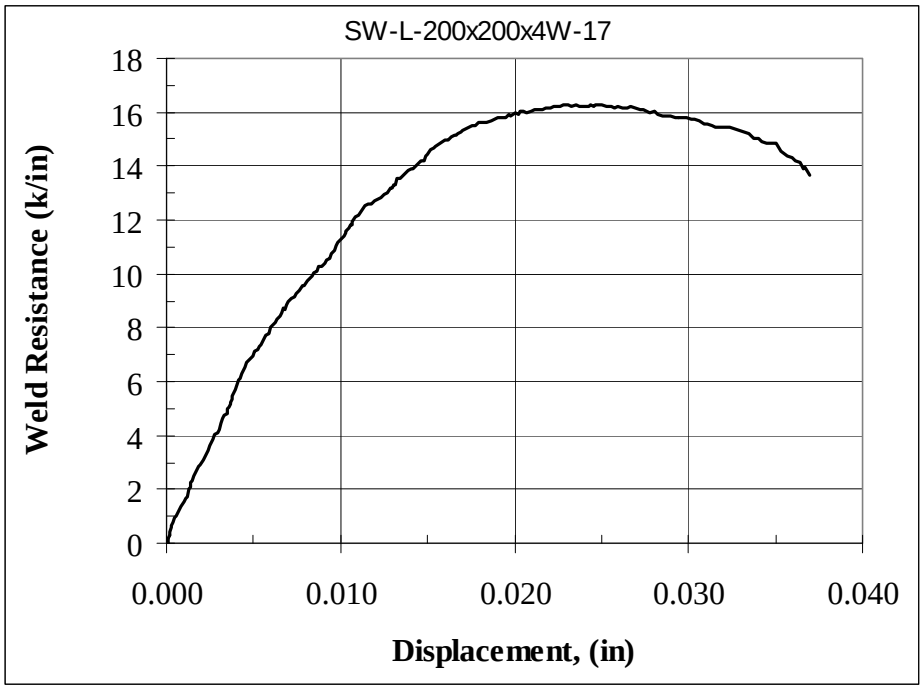

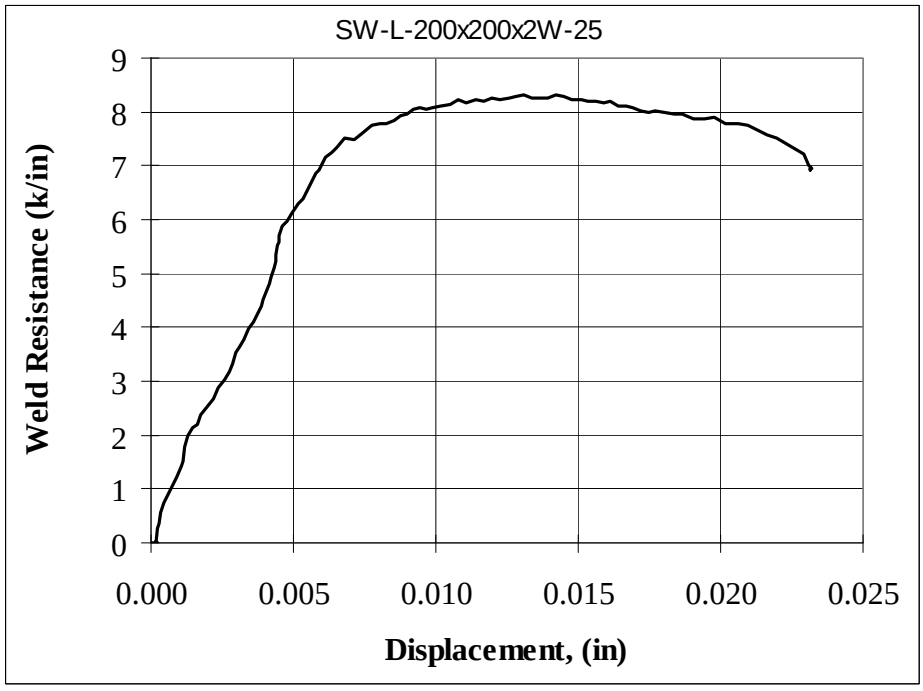

Figure 3.11 – Weld Resistance vs. Displacement, Longitudinal Case.

Table 3.8– Lap Shear Test Results Summary

	Peak Load kip	Weld Length in.	Avg. Weld Width in.	Est. Weld Area in^2.	Weld Resistance kip/in	Weld Strength ksi
Transverse		W	W_w	A_w		
SW-T-200x200x4W-01	30.73	1.992	0.043	0.339	15.43	90.6
SW-T-200x200x4W-02	30.40	1.975	0.044	0.345	15.39	88.2
SW-T-200x200x4W-03	31.03	2.006	0.044	0.355	15.47	87.4
SW-T-200x200x4W-04	30.85	2.003	0.047	0.381	15.40	82.3
SW-T-200x200x4W-05	28.11	1.994	0.051	0.410	14.10	68.6
SW-T-200x200x4W-06	29.04	2.001	0.054	0.434	14.51	67.0
SW-T-200x200x4W-07	29.45	1.993	0.052	0.416	14.78	70.8
SW-T-200x200x4W-08	26.88	1.993	0.053	0.421	13.49	63.9
SW-T-200x200x2W-09	21.60	1.999	0.067	0.268	10.81	80.7
SW-T-200x200x2W-10	20.50	1.996	0.060	0.240	10.27	85.5
SW-T-200x200x2W-11	18.70	1.967	0.058	0.230	9.51	81.4
SW-T-200x200x2W-12	22.69	2.017	0.061	0.246	11.25	92.3
Longitudinal		B	W_w	A_w		
SW-L-200x200x4W-17	16.51	1.016	0.052	0.212	16.25	77.8
SW-L-200x200x4W-18	16.76	1.002	0.053	0.213	16.73	78.7
SW-L-200x200x4W-19	16.24	1.021	0.051	0.208	15.91	78.1
SW-L-200x200x4W-20	14.45	1.016	0.048	0.197	14.22	73.5
SW-L-200x200x4W-21	19.63	0.994	0.056	0.222	19.75	88.6
SW-L-200x200x4W-22	17.23	1.008	0.059	0.238	17.09	72.4
SW-L-200x200x4W-23	19.44	1.016	0.078	0.317	19.13	61.4
SW-L-200x200x4W-24	17.6	0.976	0.068	0.265	18.03	66.4
SW-L-200x200x2W-25	8.43	1.013	0.048	0.096	8.32	87.5
SW-L-200x200x2W-26	9.31	1.006	0.050	0.101	9.25	92.5
SW-L-200x200x2W-27	8.95	0.976	0.043	0.083	9.17	107.9
SW-L-200x200x2W-28	9.53	1.007	0.045	0.091	9.46	104.3
SW-L-200x200x2W-29	9.60	0.995	0.049	0.097	9.65	99.3
SW-L-200x200x2W-30	10.85	0.995	0.053	0.106	10.90	102.0
SW-L-200x200x2W-31	11.63	1.029	0.053	0.109	11.30	106.6
SW-L-200x200x2W-32	10.20	0.990	0.052	0.103	10.30	99.0

Table 3.9– Compiled Test Results Summary

Designation	Average Weld Resistance k/in.	Standard Deviation k/in.	Average Weld Strength ksi	Standard Deviation ksi
SW-T-200x200-4W	14.82	0.74	77.33	10.87
SW-T-200x200-2W	9.25	1.40	86.42	6.16
SW-L-200x200-4W	17.14	1.80	74.60	8.29
SW-L-200x200-2W	9.80	0.98	99.88	6.99

3.7 Failure Modes

Typical failures are shown in Figures 3.12 – 3.15. Both a top view and side view are shown. Longitudinal specimens (Figs. 3.14 and 3.15) presented little bending deformation during the test in comparison to the transverse specimens. The transverse welded specimen with 2 welds (Fig. 3.12) shows a slight amount of permanent bending deformation and the transverse welded specimens with 4 welds (Fig. 3.13) showed a high degree of bending deformation; which accounts for their lower resistance per unit length than the longitudinal specimens as shown in Table 3.9. Failures were all characterized by a shearing of the weld across the plate interface as shown in the Figures.

Figure 3.12 Typical Failure in SWT-2W Specimen

Figure 3.13 Typical Failure in SWT-4W Specimen

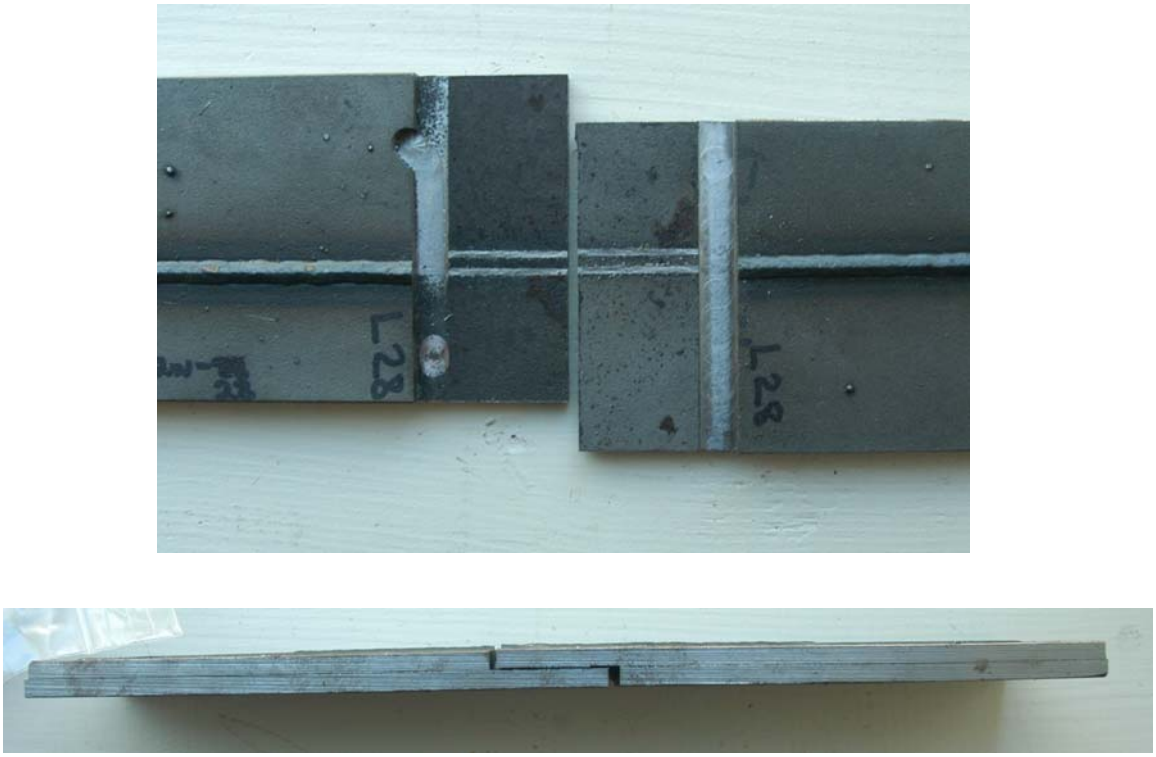

Figure 3.14 Typical Failure in SWL-2W Specimen

Figure 3.15 Typical Failure in SWL-4W Specimen

5. CONCLUSIONS

This report summarizes the analysis of laser welded steel sandwich panels and testing of HLAW single lap shear test coupons in relation to use in bridge deck replacement. As a verification study, an analysis of a steel sandwich panel with spot welded corrugation based on a study performed by Tan et al. (1989) was conducted. An experimental study of a spot welded sandwich panel was used as a baseline for the analysis. The spot weld was modeled with continuous shell elements along the length of the panel due to the difficulties in modeling the intricate details of the spot weld. In this verification effort, finite element analysis and theoretical analysis techniques are used to investigate the mechanical behavior of the steel sandwich panel, Theoretical modeling was performed with the aid of the MATLAB computer program. Finite element analysis techniques are applied using ABAQUS computer program using 8 node 6 degrees of freedom (DOF) elements, S8R6, for modeling the sandwich panel plates and the continuous stake weld. Good agreement was found between the different analytical techniques and the experimental results. The influence of the effect of the weld link thickness on the sandwich panel's mechanical response was studied. It was recommended that a weld link thickness equal to the smaller plate thickness be used. The influence of the weld placement was also studied. Models with welds at the center of each core landing showed a more flexible response than a model with welds, at the corners, as expected. Therefore, there is a design trade-off between the cost of additional welding and the benefit of the additional stiffness.

In addition to the verification study, laser welded steel sandwich panel with discontinuous prismatic stiffeners are analyzed using finite element method for a bridge deck design case study. These analyses were based upon the procedures used in the verification study and included the case of a deck replacement of the bridge in Gardiner Maine. Preliminary design of the bridge was constrained by displacement criteria which were set forth by the Maine Department of Transportation. The design resulted in a center deflection of 1/1500 of the span, which is more than adequate stiffness.

Strength testing of stake welded lap joints was performed in the transverse and longitudinal orientations. Longitudinal specimens presented little bending during the tests and resulted in

higher strength values compared to transverse specimens, especially in the case with 4 welds. For the specimens with 4 welds, average weld resistance was 14.8 k/in and 17.1 k/in for the transverse and longitudinal specimens, respectively. Additionally, for the 2 weld case the average weld resistance was 9.2 k/in and 9.8 k/in for the transverse and longitudinal specimens, respectively. Weld strength was estimated using measurements of the weld area and ranged from 74.6 ksi to 99.9 ksi. Specimens with 4 welds showed lower weld strength likely due to overlap and interaction between the weldments.

REFERENCES

1. Abbott, S.P., Caccese, V., Thompson, L., Blomquist, P.A., Hansen, E.E, 2008, Automated Laser Welded High Performance Steel Sandwich Bridge Deck Development, 17 pages.

2. Allen H.G., 1969, Analysis and Design of Structural Sandwich Panels. Oxford, UK: Pergamon.

3. ASTM A6, Standard Specification for General Requirements for Rolled Structural Steel Bars, Plates, Shapes, and Sheet Piling

4. Bright SR, & Smith JW 2004, 'Fatigue performance of laser-welded steel bridge decks', The Structural Engineer, Nov, pp. 31-39.

5. Chang, W.S., Ventsel, E., Krauthammer, T., John, J., 2005,Bending Behavior of Corrugated-Core Sandwich Plates, Composite Structures, Vol. 70, pp. 81-89.

6. Cheng, Q.H., Lee, H.P., Lu, C., 2006, A Numerical Analysis Approach for Evaluating Elastic Constants of Sandwich Structures with Various Cores, Composite Structures Vol.74, pp.226-236.

7. Fleck, N.A and Deshpande, V.S., 2004 The Resistance of Clamped Sandwich Beams to Shock Loading, Journal of Applied Mechanics, ASME Vol. 71, pp. 386-401.

8. Fung, T.C., Tan, K.H., Lok, T.S., 1996, Shear Stiffness DQy for C-Core Sandwich Panels, Journal of Structural Engineerin., ASCE., Vol. 128, N5, pp.683-689.

9. Fung T.C, Tan K.H, Lok T.S., 1994, Elastic Constants for Z-core Sandwich Panels. Journal of Structural Engineering, ASCE Vol.120, pp.3046-3055.

10. Hutchinson, J.W., Xue, Z., 2005, Metal Sandwich Plates Optimized for Pressure Impulses, International Journal of Mechanical Sciences, Vol. 47, pp. 545-569.

11. Kennedy, S.J., Murray, T.M., 2004, Ultimate Strength of an SPS Bridge-The Shenley Bridge, Quebec, Canada. 2004 Annual Conference of the Transportation Association of Canada Quebec City, Quebec, September 19-20 Session, pp.1-13.

12. Klanac, Alan., Kujala, P., 2004, Optimal Design of Steel Sandwich Panel Applications in Ships, 9th Symposium on Practical Design of Ships and Other Floating Structures, Shiffbautechnische Gesellschaft e.V, 8 pages.

13. Kujala, P., Romanoff, J., Tabri, K., Ehlers, S. 2004, All Steel Sandwich Panels-Design Challenges for Practical Applications on Ships, 9th Symposium on Practical Design of Ships and Other Floating Structures, Shiffbautechnische Gesellschaft e.V, 8 pages.

14. Libove, C., Hubka R.E., 1951, Elastic Constants for Corrugated Core Sandwich Plates. *Technical Note 2289. National Aeronautics and Space Administration (NASA).*

15. Lok, T.S., and Cheng, Q.H., 2000, "Elastic stiffness properties and behavior of truss-core sandwich panel", *ASCE Journal of Structural Engineering*, Vol.126, pp.552-559.

16. Plantema, F., 1966, Sandwich Construction. John Wiley and Sons, Inc., New York, USA.

17. Qiao. P., Yang, M., Mosallam, A.S., Impact Analysis of Composite Sandwich I-Beam System, 9th ASCE Aerospace Division International Conference., March 7-10-2004, Houston, Texas

18. Tan K.H, Montague P, Norris C., 1989, Steel sandwich panels: Finite Element, Closed Solution, and Experimental Comparisons, on a 6 m · 2.1 m Panel. *Structural Engineering* Vol 67, pp.159-166.

19. Vel, S.S., Caccese, V., Zhao.,H, 2005, Elastic coupling effects in tapered sandwich panels with laminated anisotropic composite facings, *Journal of Composite Materials*, Vol. 39, No. 24, pp. 2161-2183.

20. Vinson, J.R. (1999), "The behavior of sandwich structures of isotropic and composite materials",Technomic Publications., Lancaster, PA.

21. Xue, Z., Hutchinson, J.W., 2004, A Comparative study of Impulse-Resistant Metal Sandwich Plates. *International Journal of Mechanical Sciences,* Vol. 30, pp.1283-1305.

22. Yang, M., Qiao, P., 2005, Higher-Order Impact Modeling of Sandwich Structures with Flexible Core. *International Journal of Solids and Structures*, Vol. 42, pp.5460-5490.

23. Zenkert, D., 1995, An Introduction to Sandwich Construction. EMAS Ltd., Solihull, UK.

APPENDIX A – Weld Resistance vs. Displacement Curves

TRANSVERSE SPECIMENS

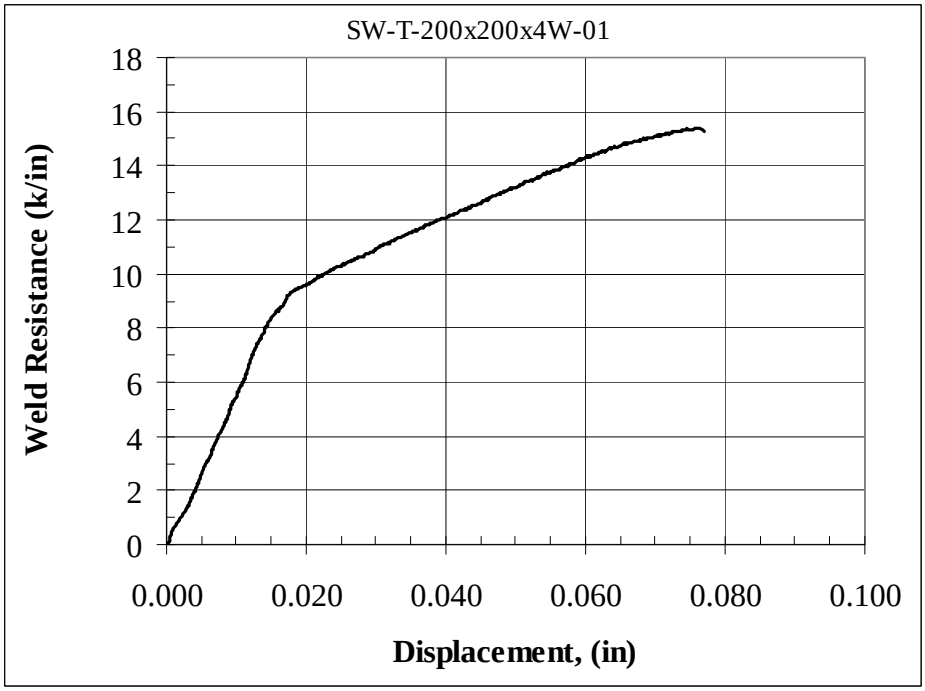

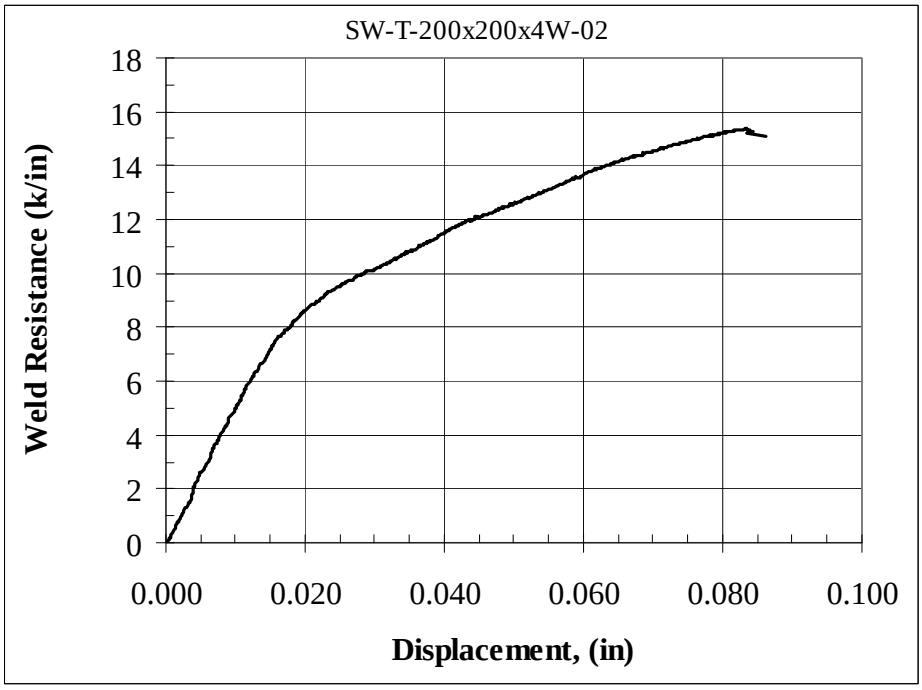

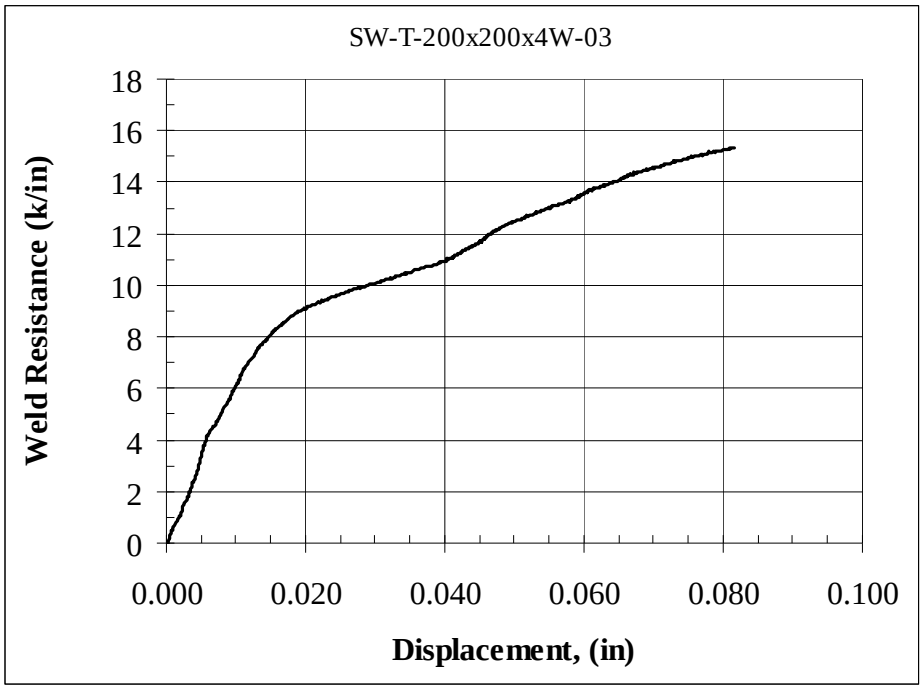
SW-T-200x200x4W-03
Weld Resistance (k/in)
18
16
14
12
10
8
6
4
2
0
0.000
0.020
0.040
0.060
0.080
0.100
Displacement, (in)

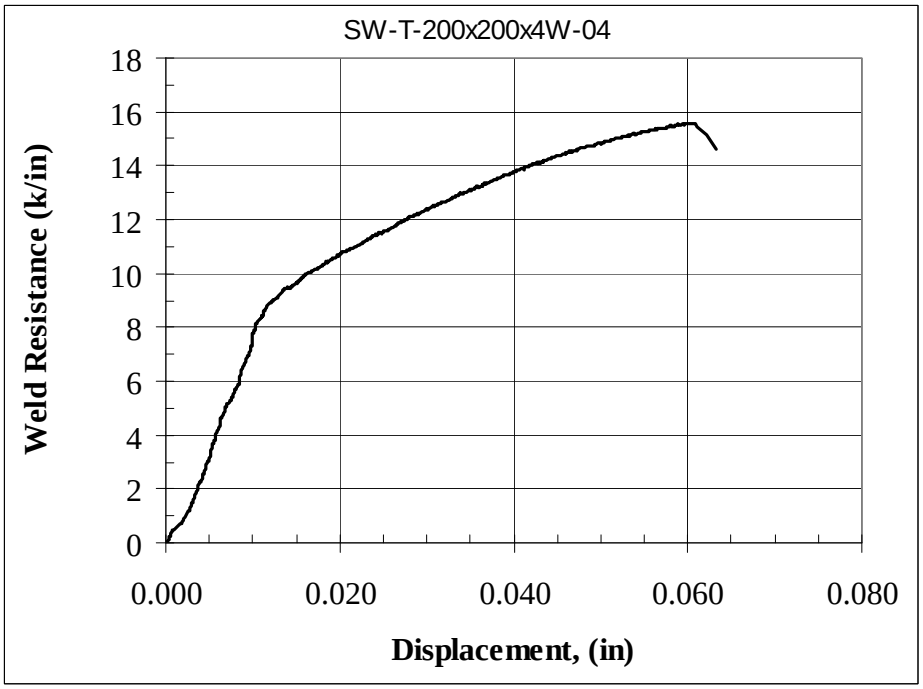
SW-T-200x200x4W-04
Weld Resistance (k/in)
18
16
14
12
10
8
6
4
2
0
0.000
0.020
0.040
0.060
0.080
Displacement, (in)

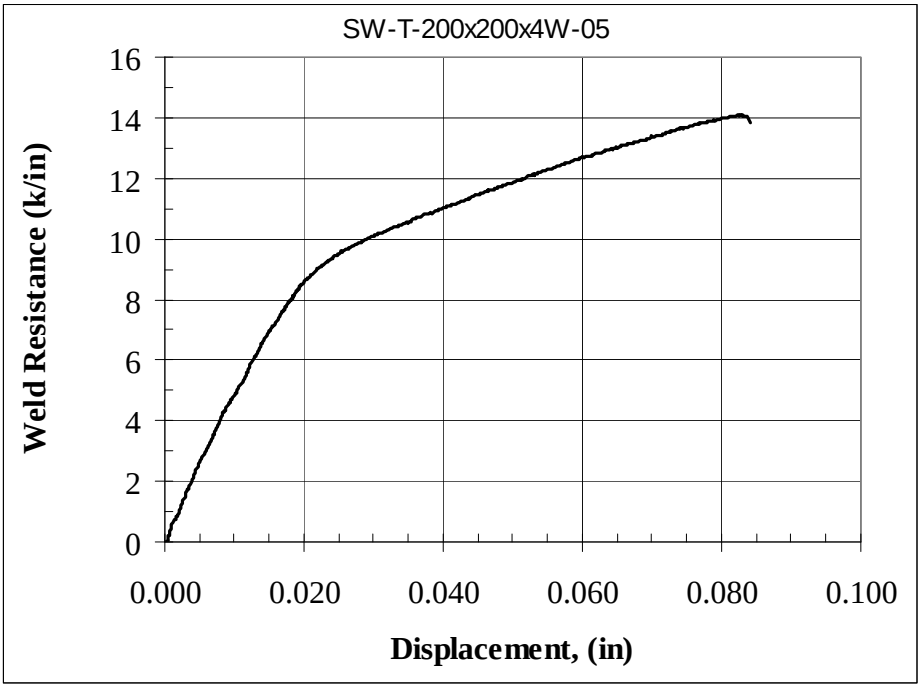
SW-T-200x200x4W-05
Weld Resistance (k/in)
16
14
12
10
8
6
4
2
0
0.000
0.020
0.040
0.060
0.080
0.100
Displacement, (in)

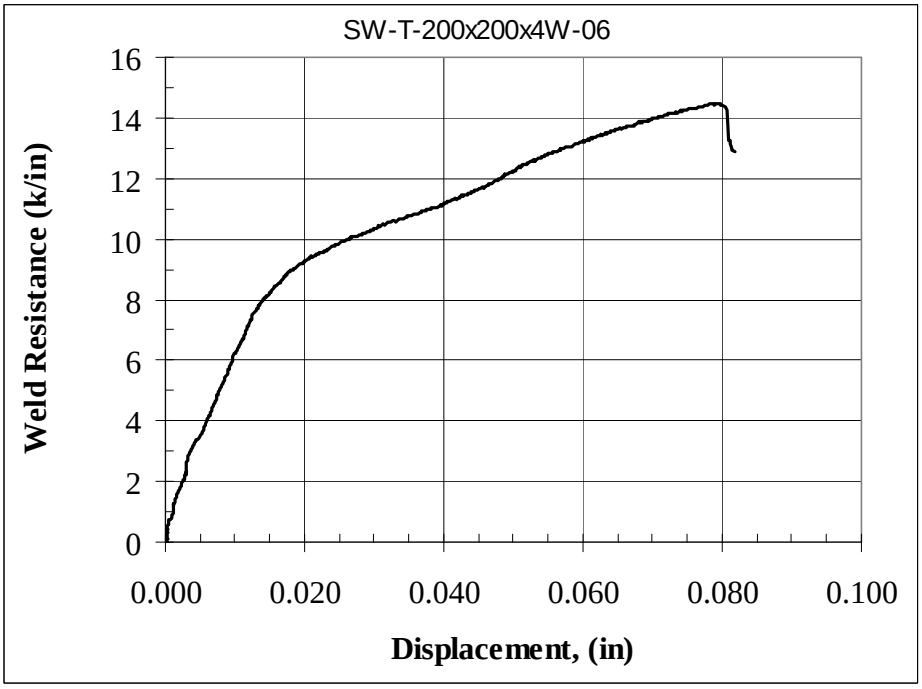
SW-T-200x200x4W-06
Weld Resistance (k/in)
16
14
12
10
8
6
4
2
0
0.000
0.020
0.040
0.060
0.080
0.100
Displacement, (in)

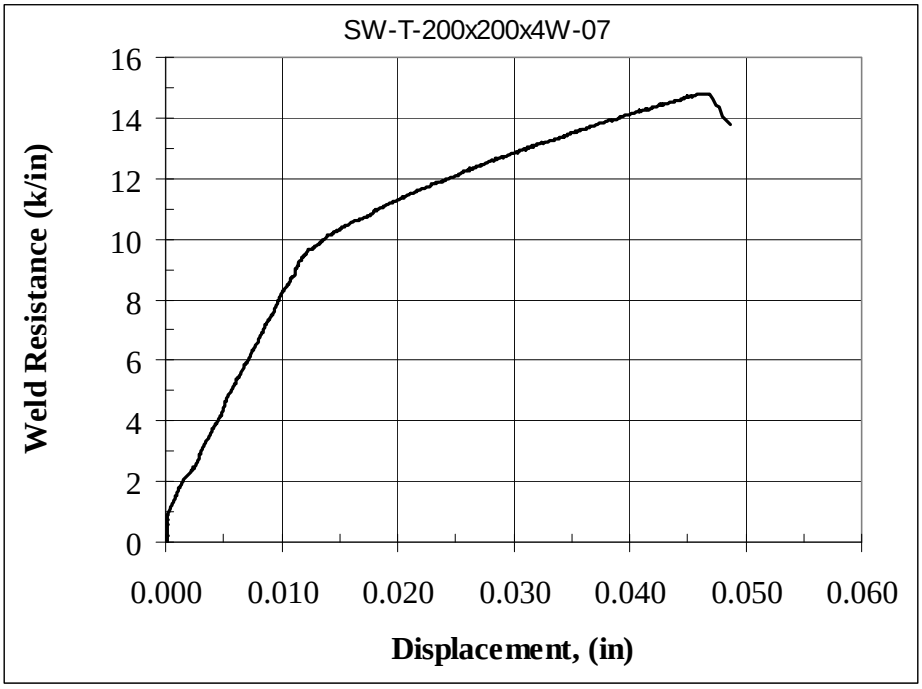
SW-T-200x200x4W-07
Weld Resistance (k/in)
16
14
12
10
8
6
4
2
0
0.000
0.010
0.020
0.030
0.040
0.050
0.060
Displacement, (in)

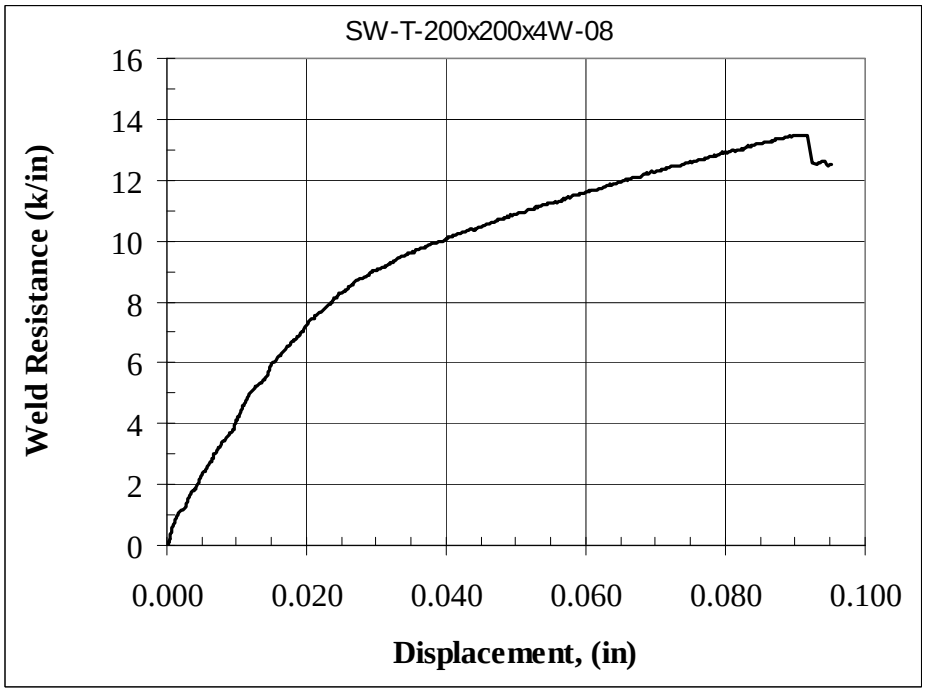
SW-T-200x200x4W-08
Weld Resistance (k/in)
16
14
12
10
8
6
4
2
0
0.000
0.020
0.040
0.060
0.080
0.100
Displacement, (in)

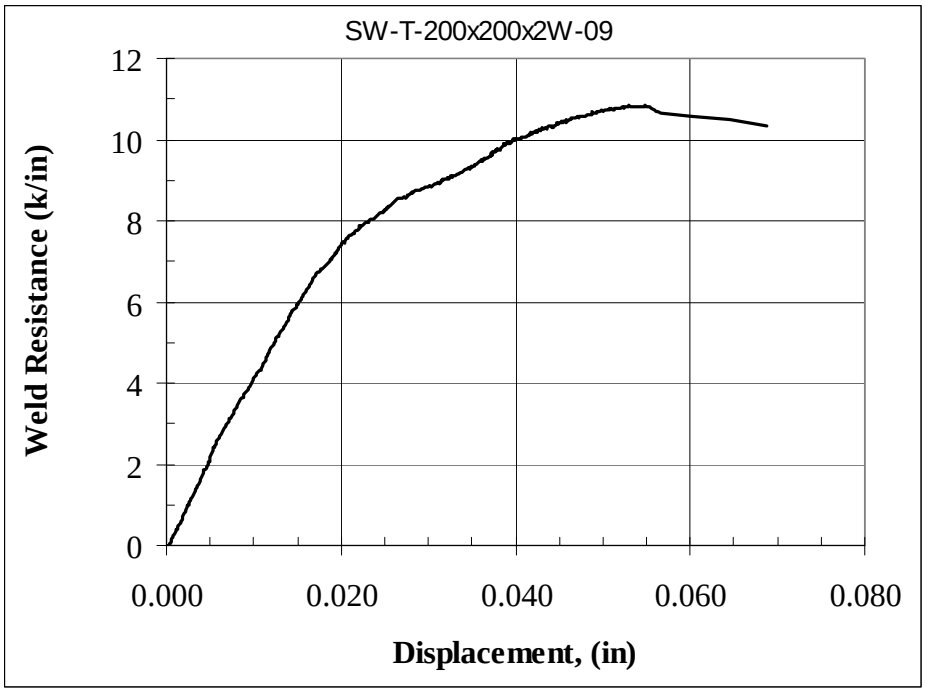
SW-T-200x200x2W-09
Weld Resistance (k/in)
12
10
8
6
4
2
0
0.000
0.020
0.040
0.060
0.080
Displacement, (in)

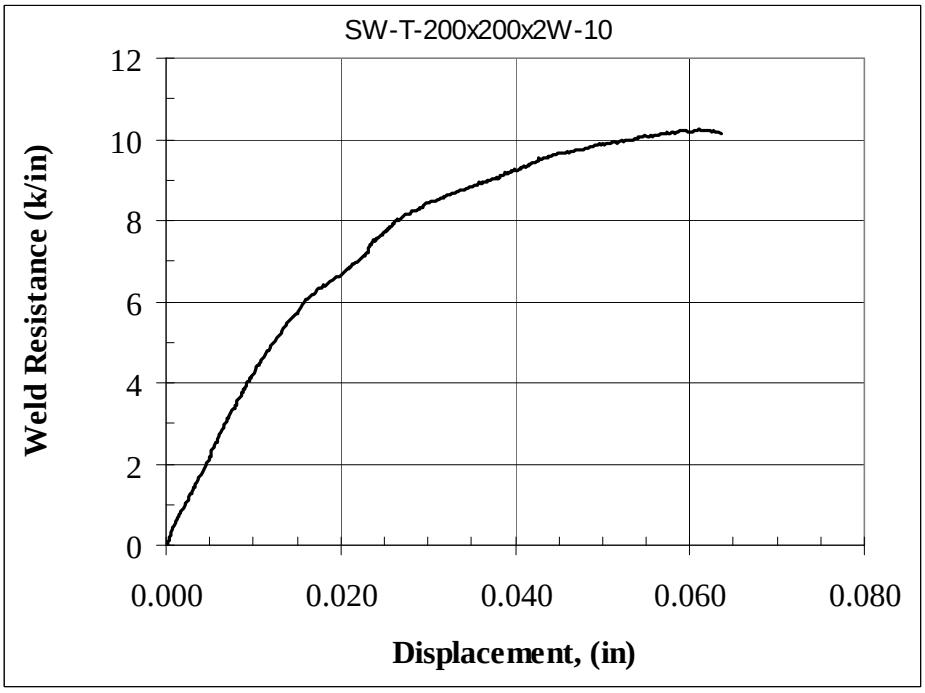
SW-T-200x200x2W-10
Weld Resistance (k/in)
12
10
8
6
4
2
0
0.000
0.020
0.040
0.060
0.080
Displacement, (in)

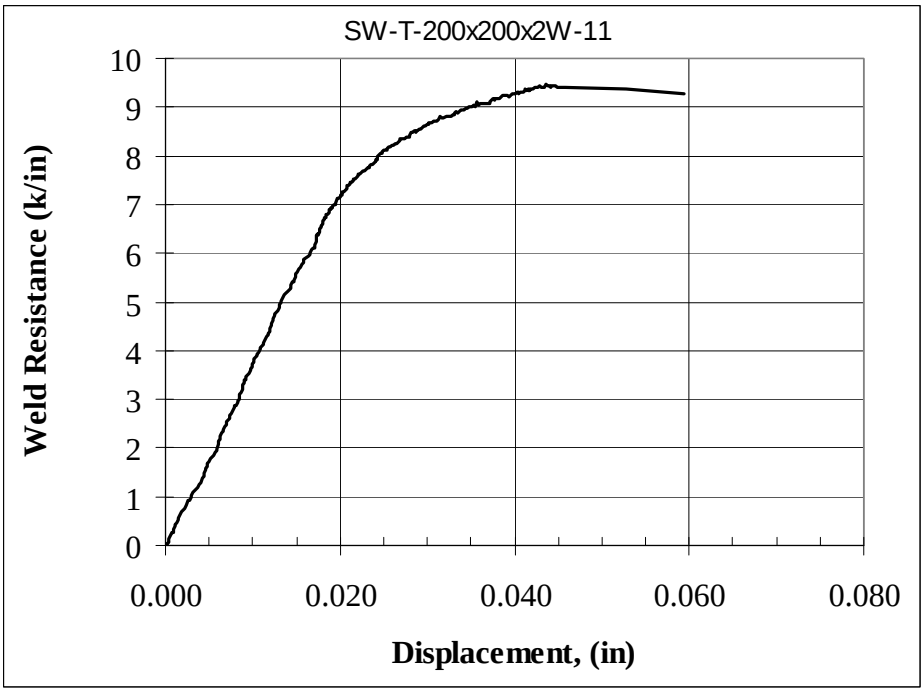
SW-T-200x200x2W-11
Weld Resistance (k/in)
0
1
2
3
4
5
6
7
8
9
10
0.000
0.020
0.040
0.060
0.080
Displacement, (in)

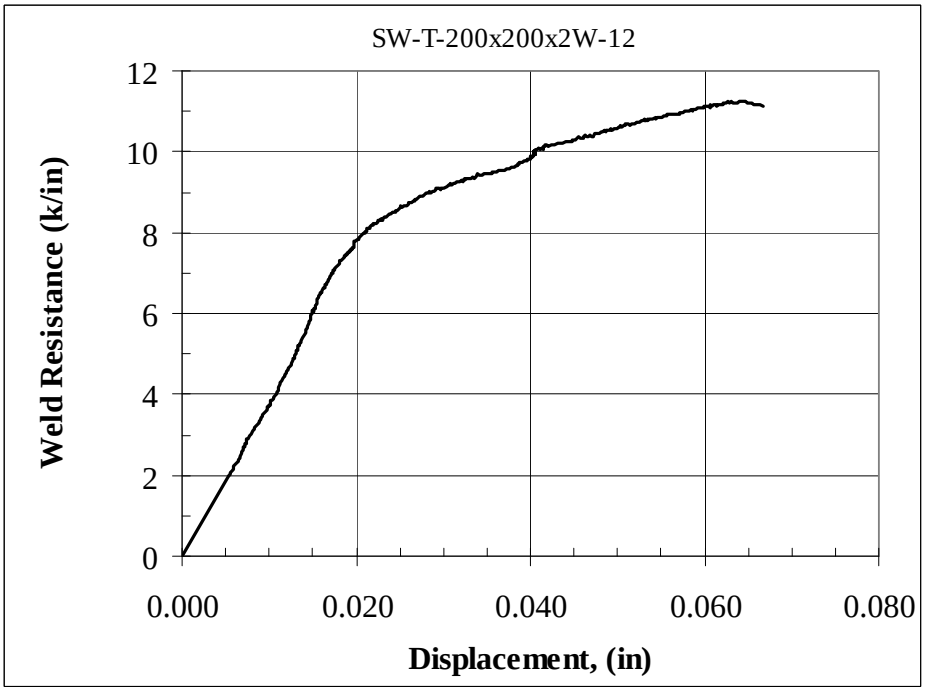
SW-T-200x200x2W-12
Weld Resistance (k/in)
0
2
4
6
8
10
12
0.000
0.020
0.040
0.060
0.080
Displacement, (in)

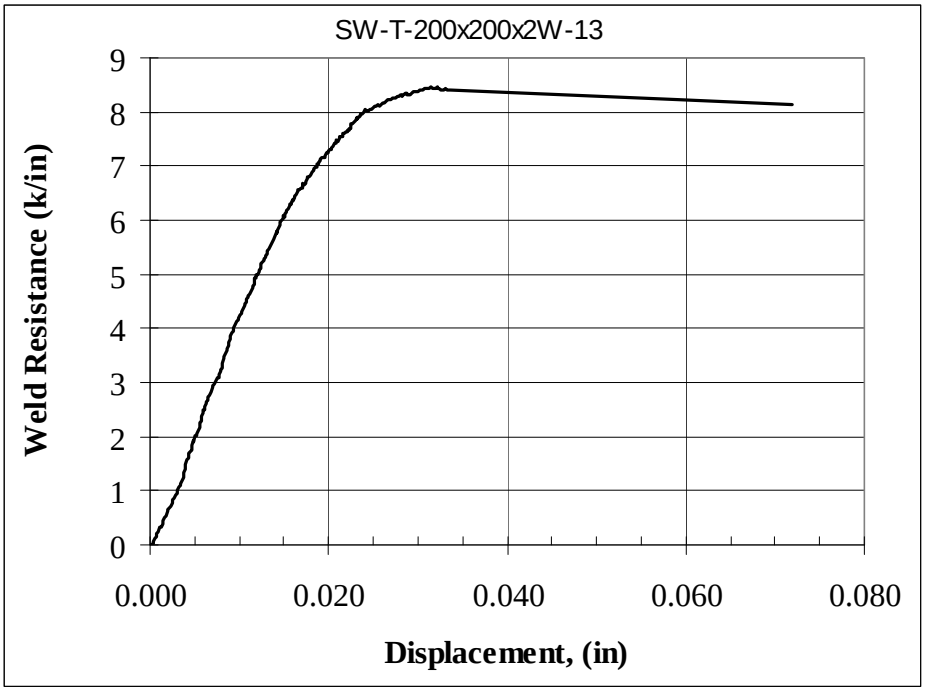
SW-T-200x200x2W-13
Weld Resistance (k/in)
0
1
2
3
4
5
6
7
8
9
0.000
0.020
0.040
0.060
0.080
Displacement, (in)

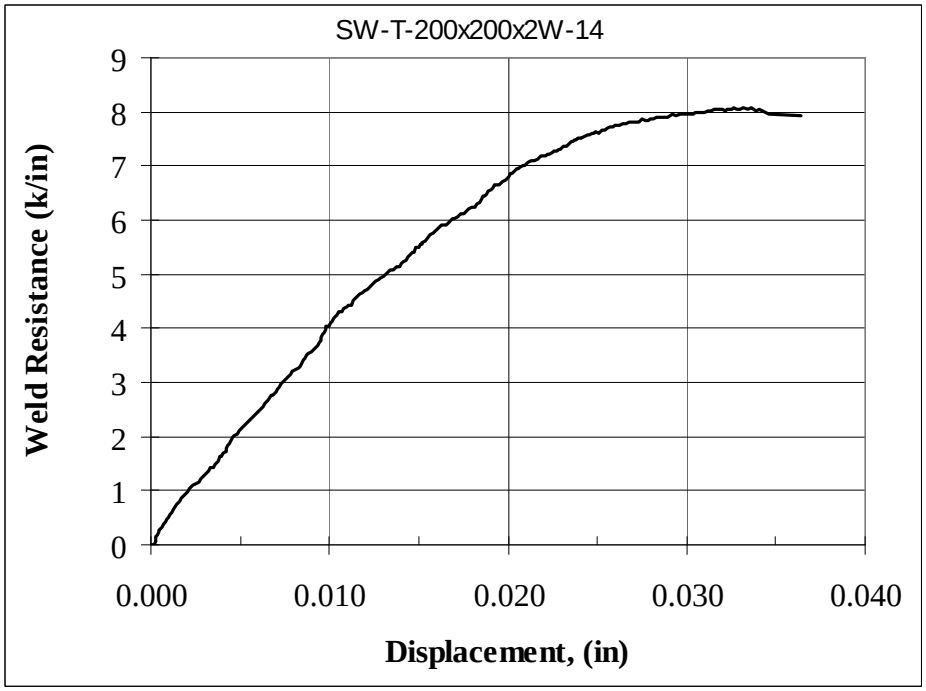
SW-T-200x200x2W-14
Weld Resistance (k/in)
0
1
2
3
4
5
6
7
8
9
0.000
0.010
0.020
0.030
0.040
Displacement, (in)

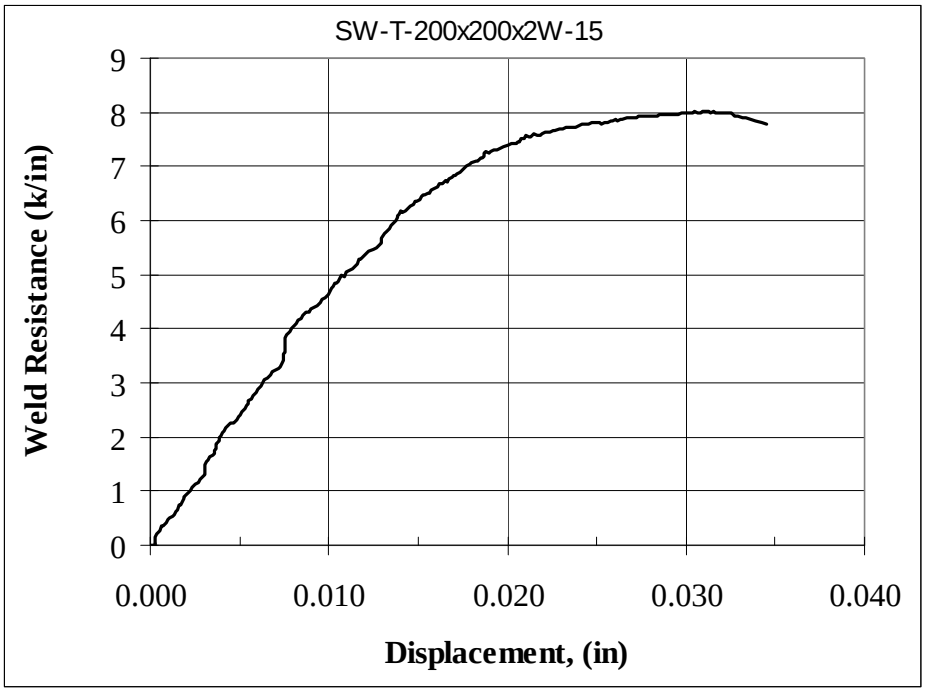
SW-T-200x200x2W-15
Weld Resistance (k/in)
0
1
2
3
4
5
6
7
8
9
0.000
0.010
0.020
0.030
0.040
Displacement, (in)

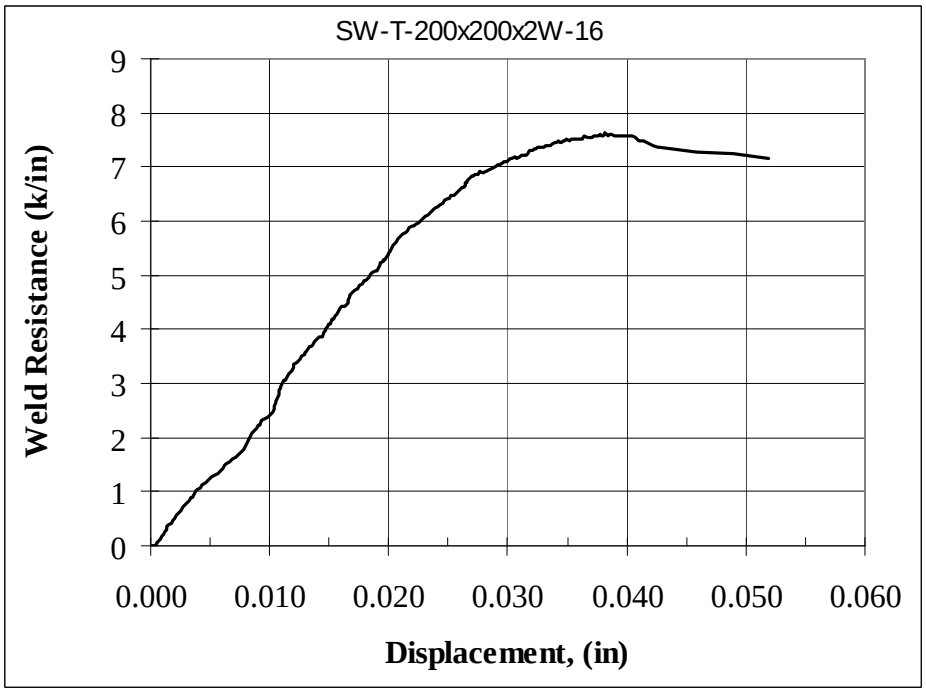
SW-T-200x200x2W-16
Weld Resistance (k/in)
0
1
2
3
4
5
6
7
8
9
0.000
0.010
0.020
0.030
0.040
0.050
0.060
Displacement, (in)

LONGITUDINAL SPECIMENS

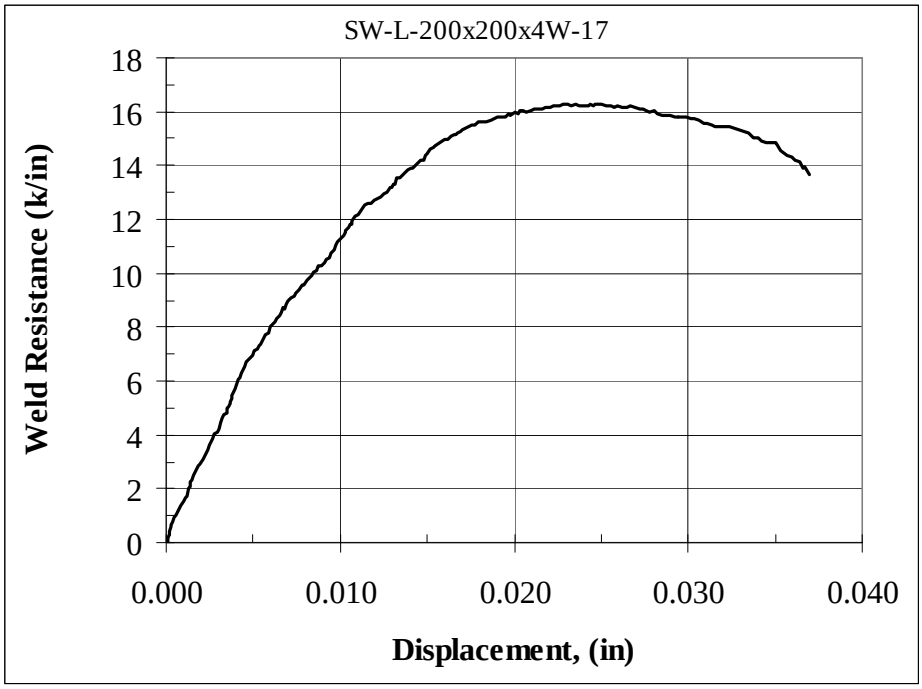

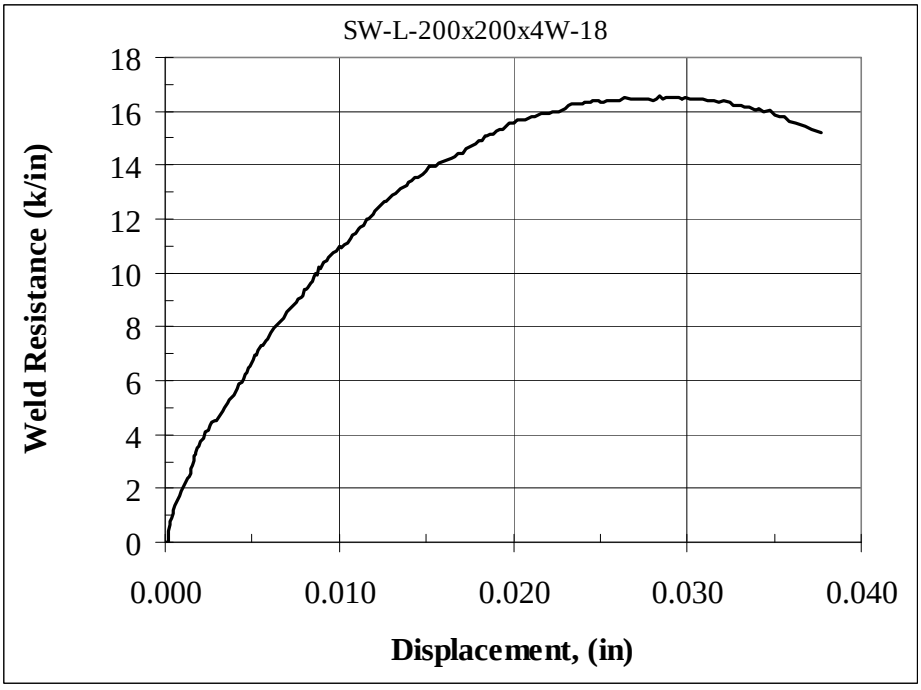

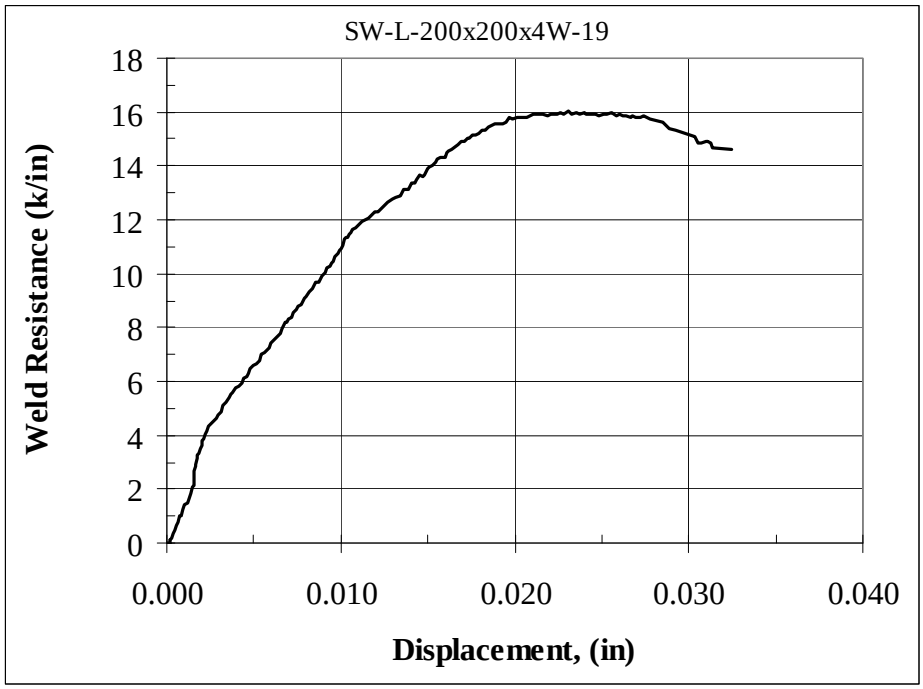
SW-L-200x200x4W-19
Weld Resistance (k/in)
18
16
14
12
10
8
6
4
2
0
0.000
0.010
0.020
0.030
0.040
Displacement, (in)

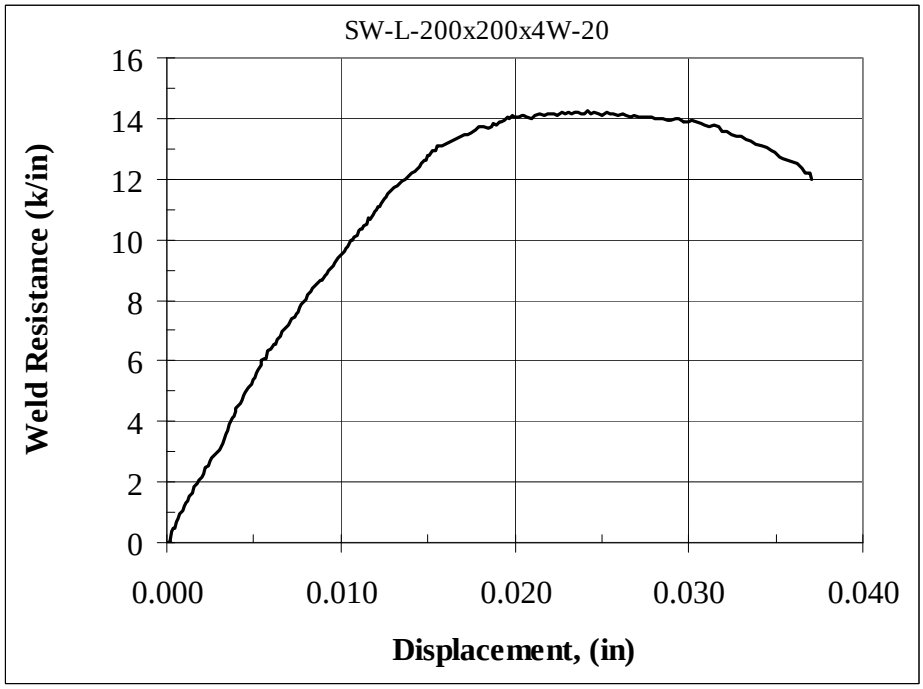
SW-L-200x200x4W-20
Weld Resistance (k/in)
16
14
12
10
8
6
4
2
0
0.000
0.010
0.020
0.030
0.040
Displacement, (in)

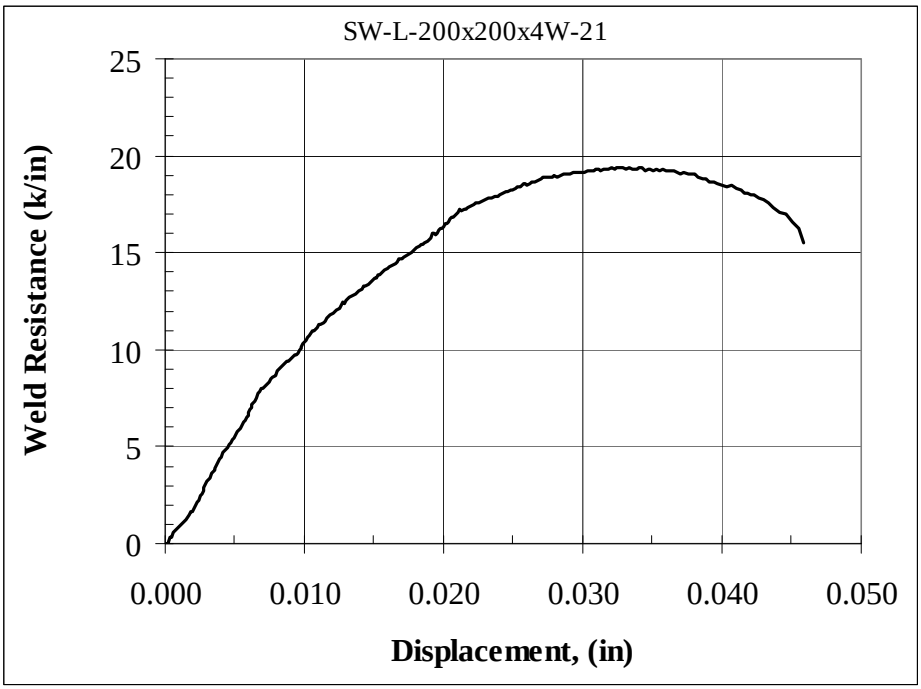
SW-L-200x200x4W-21
Weld Resistance (k/in)
25
20
15
10
5
0
0.000
0.010
0.020
0.030
0.040
0.050
Displacement, (in)

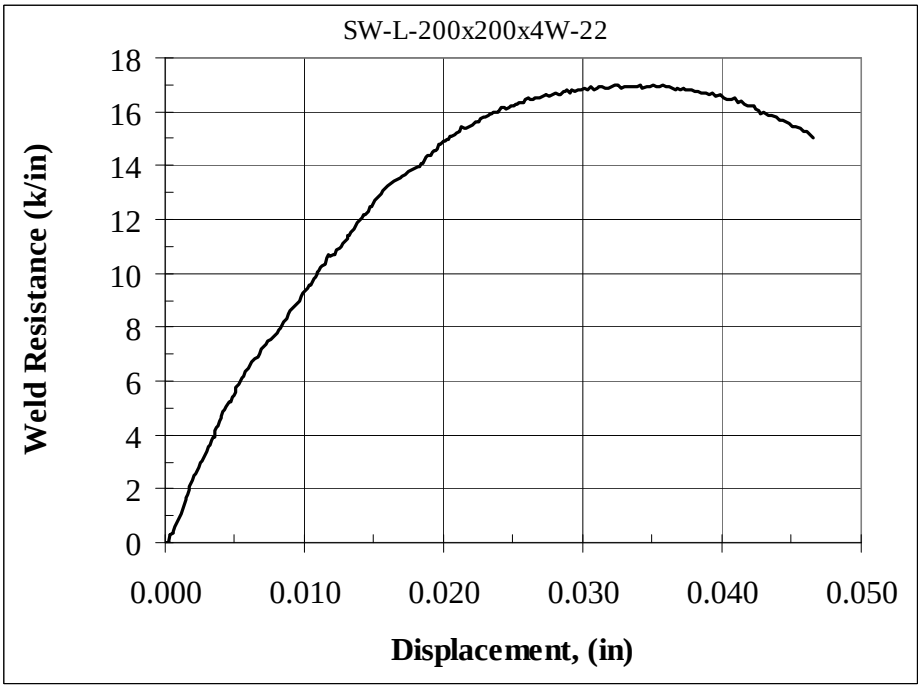
SW-L-200x200x4W-22
Weld Resistance (k/in)
18
16
14
12
10
8
6
4
2
0
0.000
0.010
0.020
0.030
0.040
0.050
Displacement, (in)

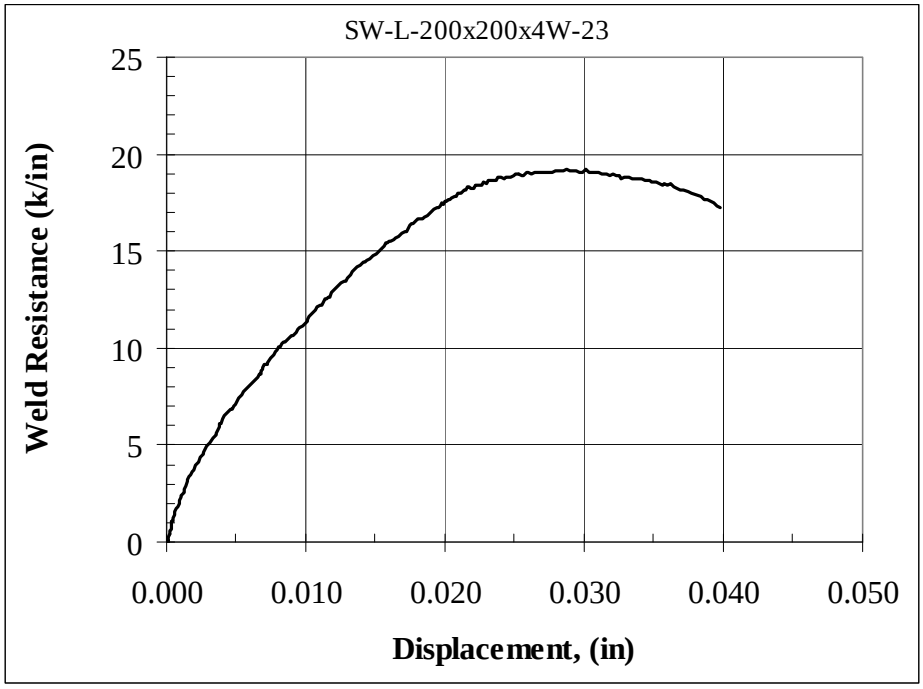
SW-L-200x200x4W-23
Weld Resistance (k/in)
25
20
15
10
5
0
0.000
0.010
0.020
0.030
0.040
0.050
Displacement, (in)

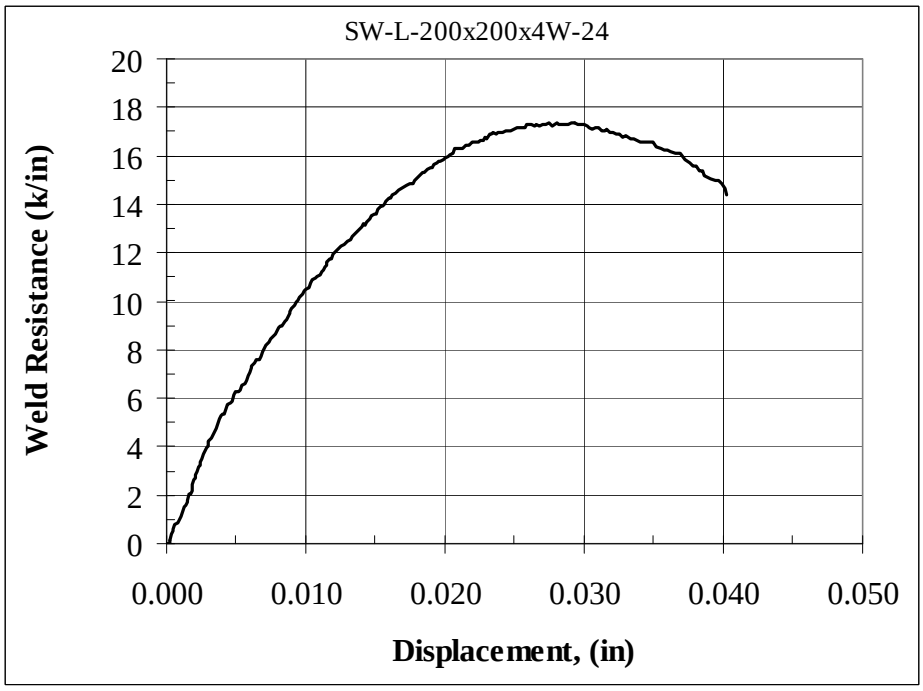
SW-L-200x200x4W-24
Weld Resistance (k/in)
20
18
16
14
12
10
8
6
4
2
0
0.000
0.010
0.020
0.030
0.040
0.050
Displacement, (in)

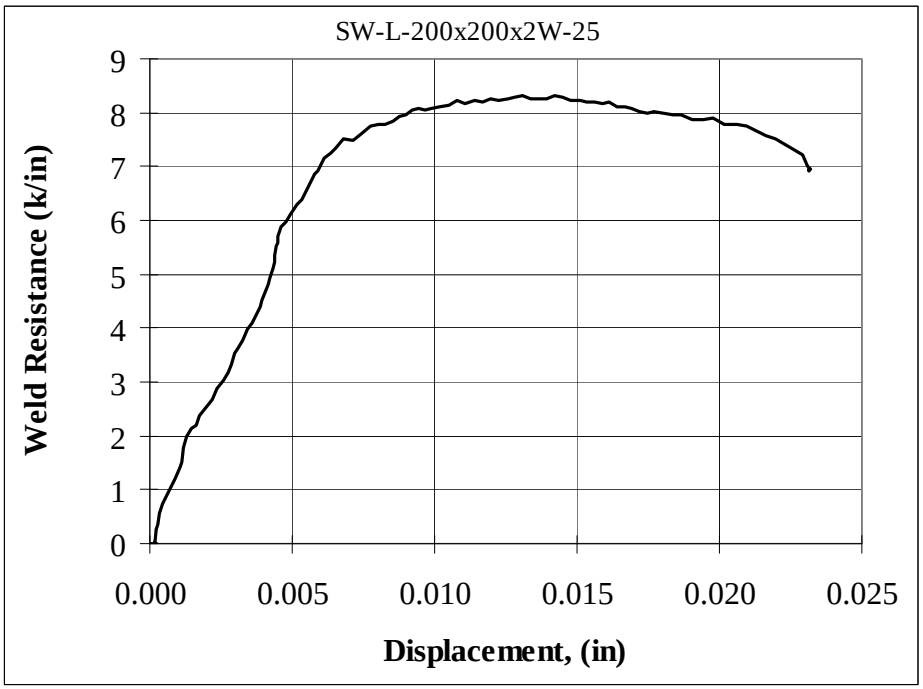
SW-L-200x200x2W-25
Weld Resistance (k/in)
9
8
7
6
5
4
3
2
1
0
0.000
0.005
0.010
0.015
0.020
0.025
Displacement, (in)

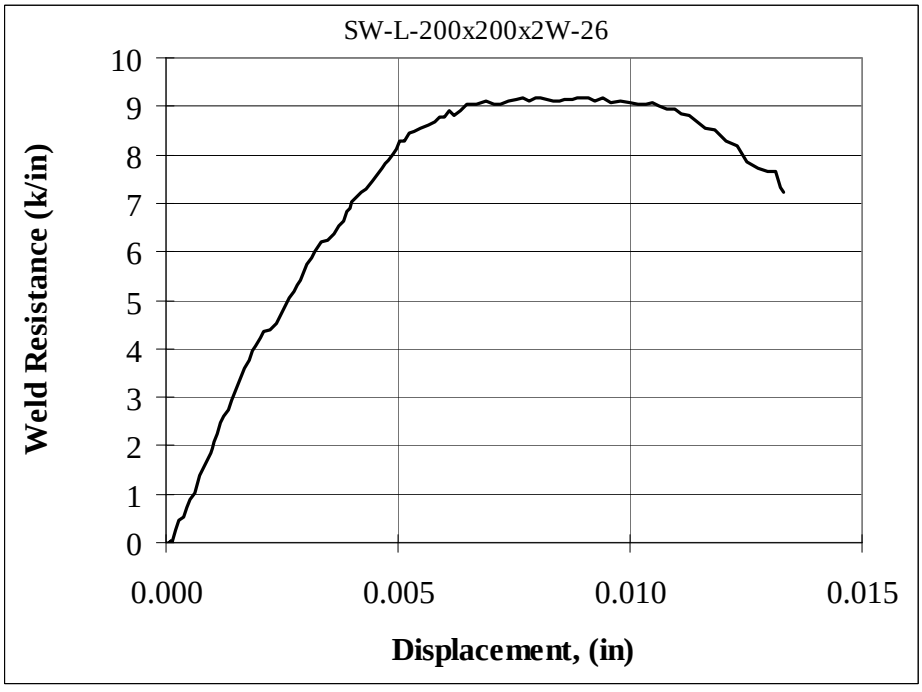
SW-L-200x200x2W-26
Weld Resistance (k/in)
10
9
8
7
6
5
4
3
2
1
0
0.000
0.005
0.010
0.015
Displacement, (in)

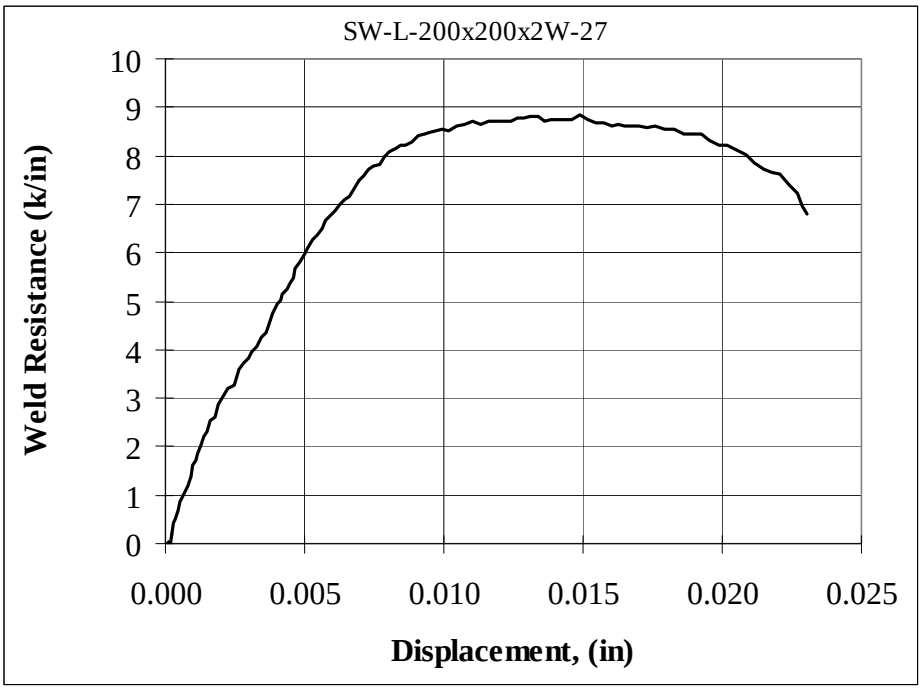
SW-L-200x200x2W-27
Weld Resistance (k/in)
10
9
8
7
6
5
4
3
2
1
0
0.000
0.005
0.010
0.015
0.020
0.025
Displacement, (in)

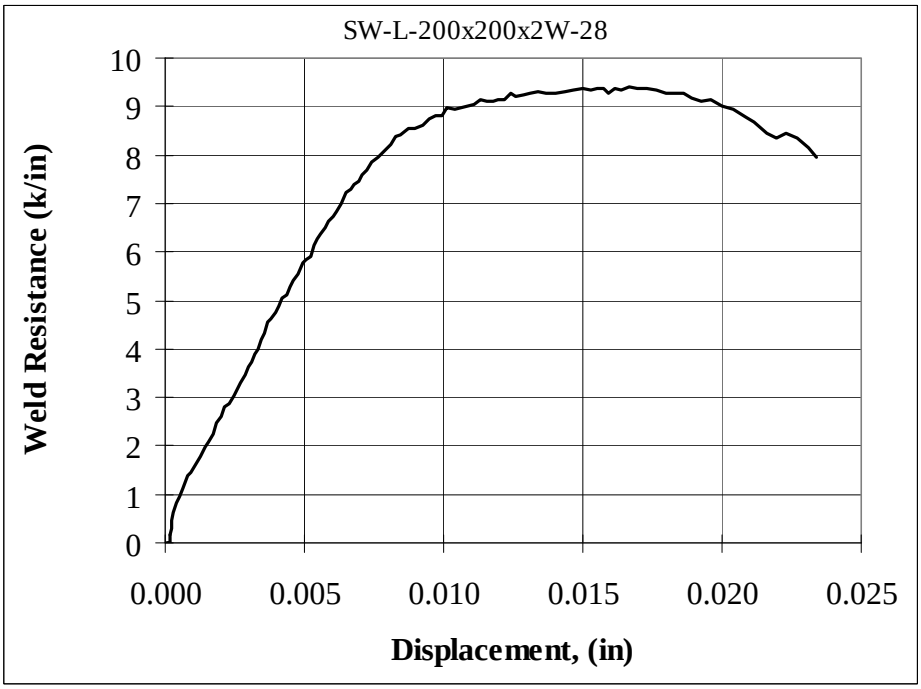
SW-L-200x200x2W-28
Weld Resistance (k/in)
10
9
8
7
6
5
4
3
2
1
0
0.000
0.005
0.010
0.015
0.020
0.025
Displacement, (in)

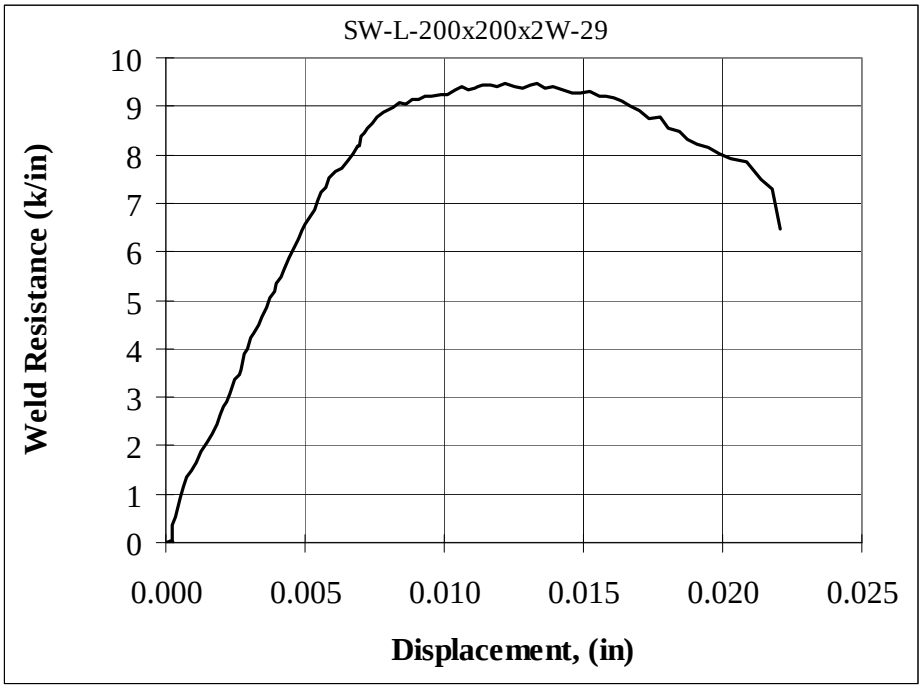
SW-L-200x200x2W-29
Weld Resistance (k/in)
10
9
8
7
6
5
4
3
2
1
0
0.000
0.005
0.010
0.015
0.020
0.025
Displacement, (in)

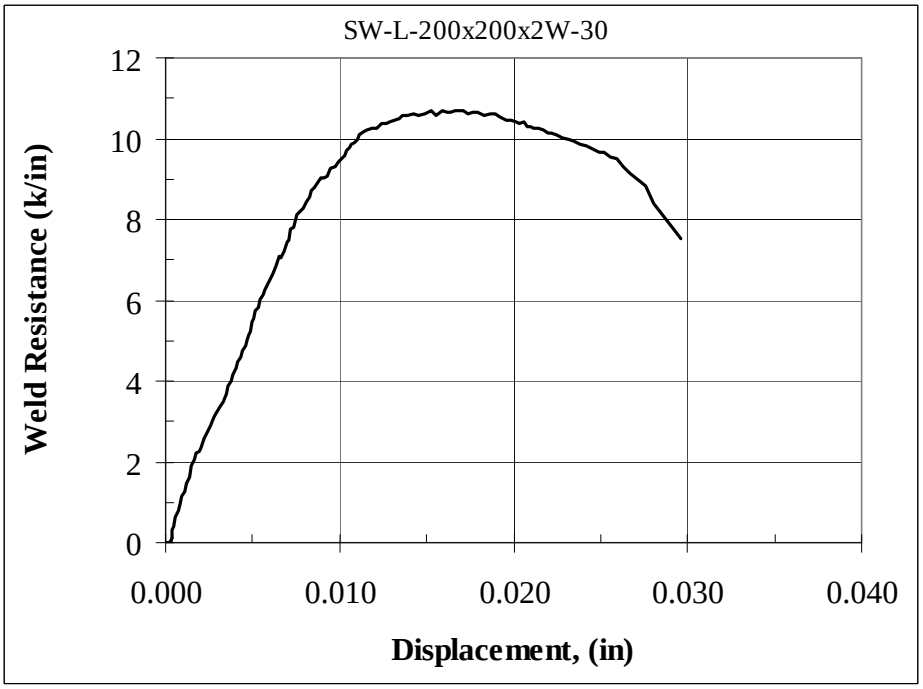
SW-L-200x200x2W-30
Weld Resistance (k/in)
12
10
8
6
4
2
0
0.000
0.010
0.020
0.030
0.040
Displacement, (in)

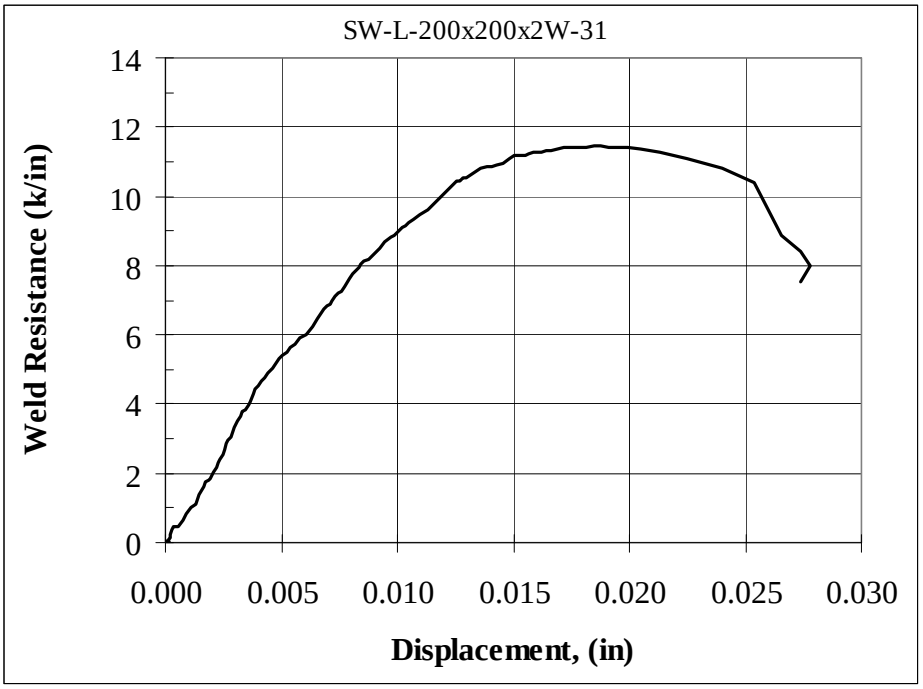
SW-L-200x200x2W-31
Weld Resistance (k/in)
14
12
10
8
6
4
2
0
0.000
0.005
0.010
0.015
0.020
0.025
0.030
Displacement, (in)

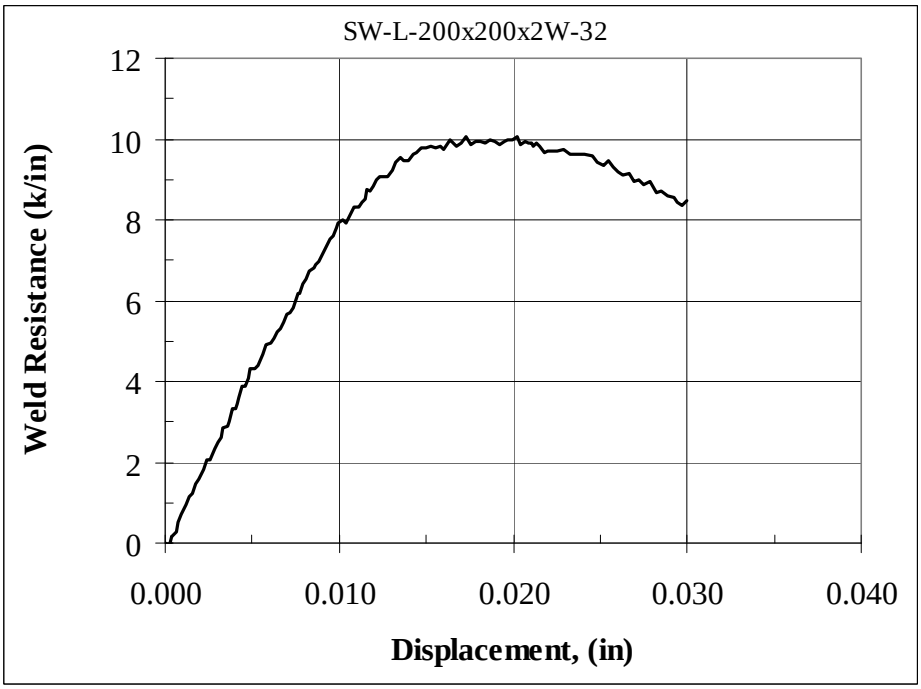
SW-L-200x200x2W-32
Weld Resistance (k/in)
12
10
8
6
4
2
0
0.000
0.010
0.020
0.030
0.040
Displacement, (in)

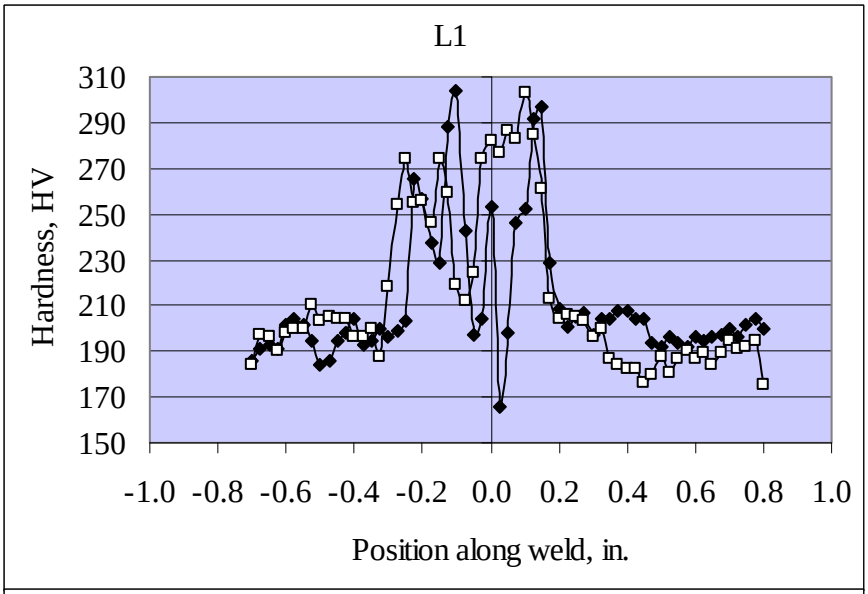
L1
Hardness, HV
310
290
270
250
230
210
190
170
150
-1.0 -0.8 -0.6 -0.4 -0.2 0.0 0.2 0.4 0.6 0.8 1.0
Position along weld, in.

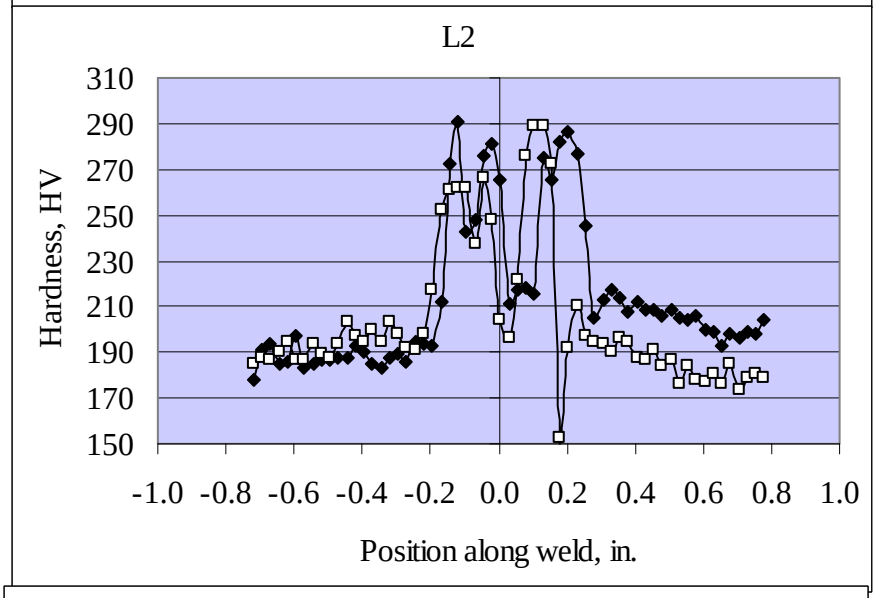
L2
Hardness, HV
310
290
270
250
230
210
190
170
150
-1.0 -0.8 -0.6 -0.4 -0.2 0.0 0.2 0.4 0.6 0.8 1.0
Position along weld, in.

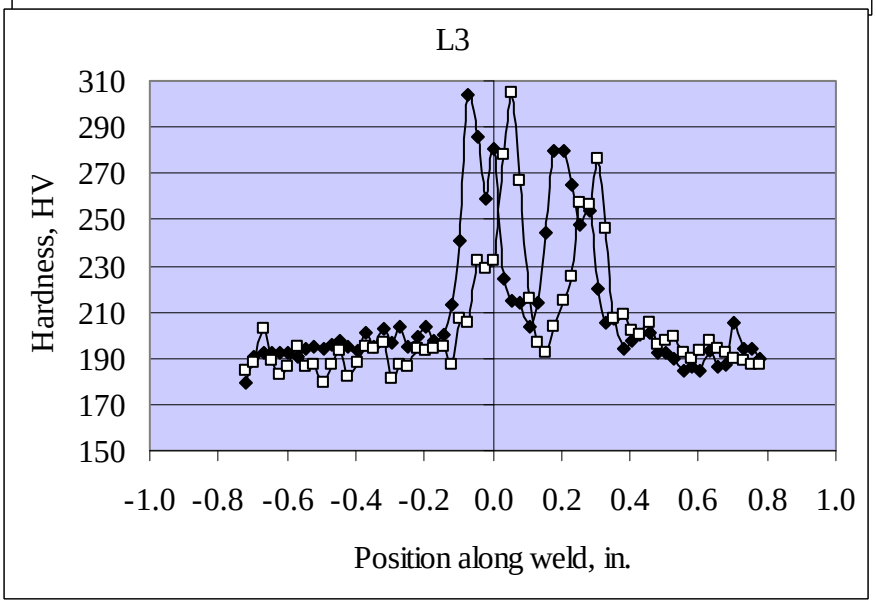
L3
Hardness, HV
310
290
270
250
230
210
190
170
150
-1.0 -0.8 -0.6 -0.4 -0.2 0.0 0.2 0.4 0.6 0.8 1.0
Position along weld, in.

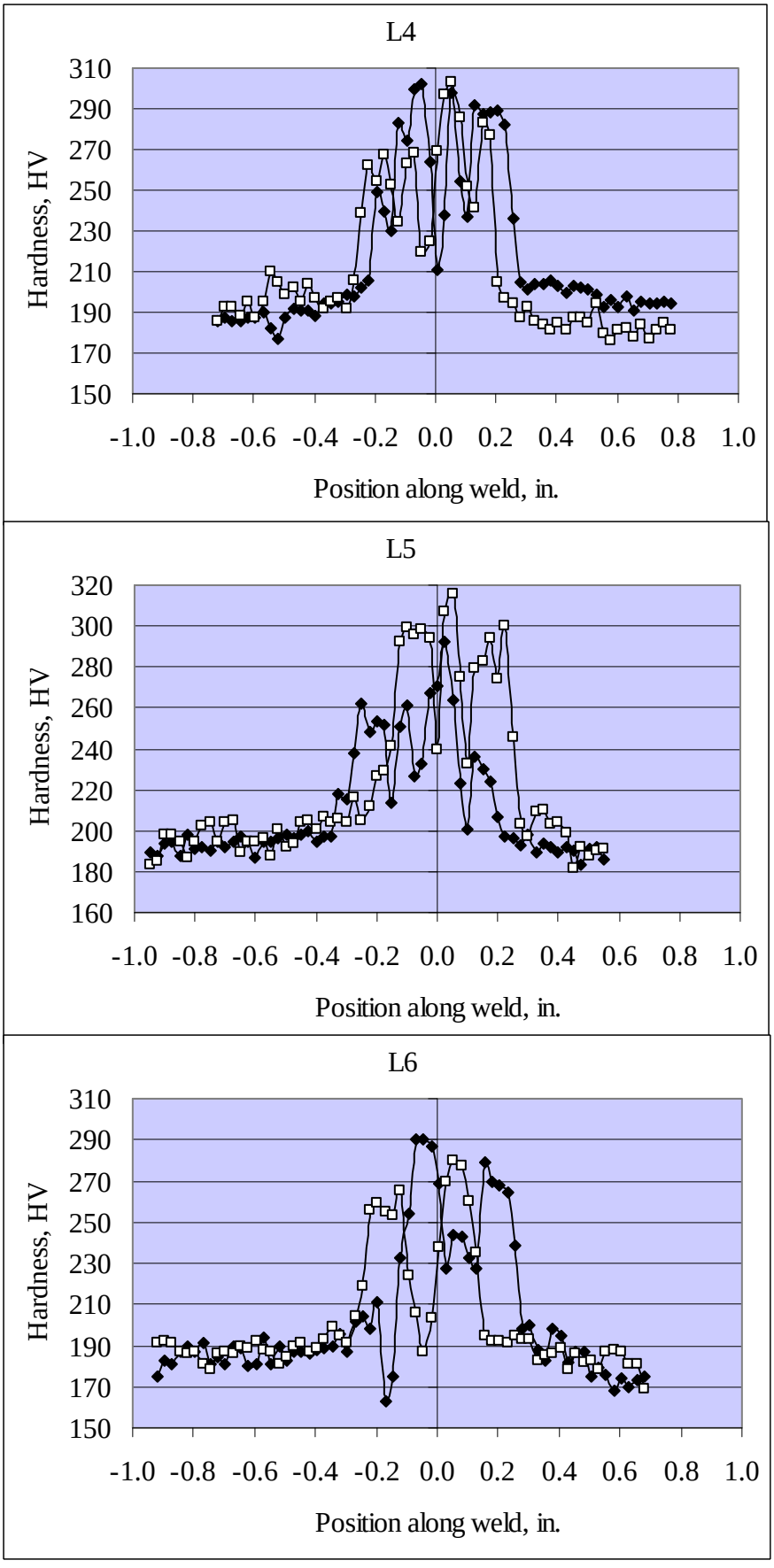
L4
Hardness, HV
310
290
270
250
230
210
190
170
150
-1.0 -0.8 -0.6 -0.4 -0.2 0.0 0.2 0.4 0.6 0.8 1.0
Position along weld, in.
L5
Hardness, HV
320
300
280
260
240
220
200
180
160
-1.0 -0.8 -0.6 -0.4 -0.2 0.0 0.2 0.4 0.6 0.8 1.0
Position along weld, in.
L6
Hardness, HV
310
290
270
250
230
210
190
170
150
-1.0 -0.8 -0.6 -0.4 -0.2 0.0 0.2 0.4 0.6 0.8 1.0
Position along weld, in.

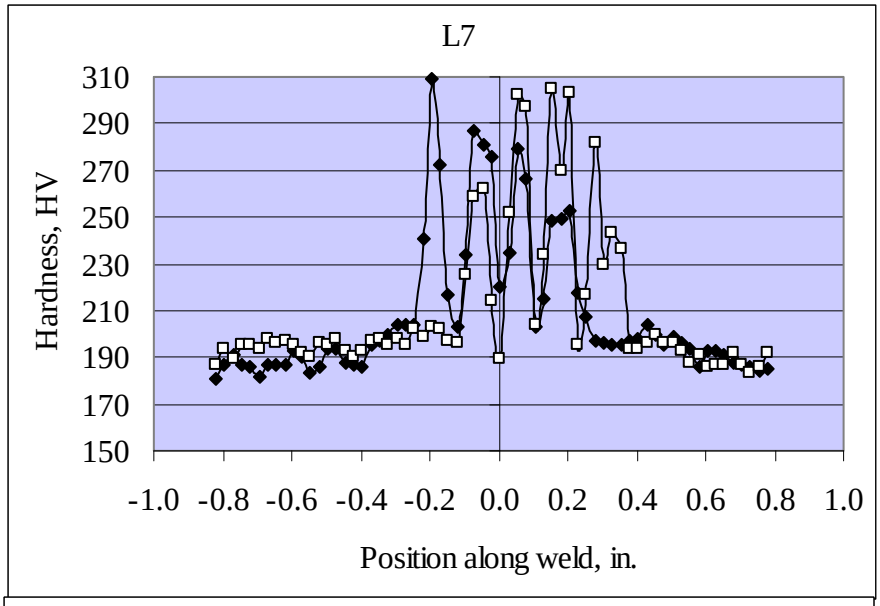
L7
Hardness, HV
310
290
270
250
230
210
190
170
150
-1.0 -0.8 -0.6 -0.4 -0.2 0.0 0.2 0.4 0.6 0.8 1.0
Position along weld, in.

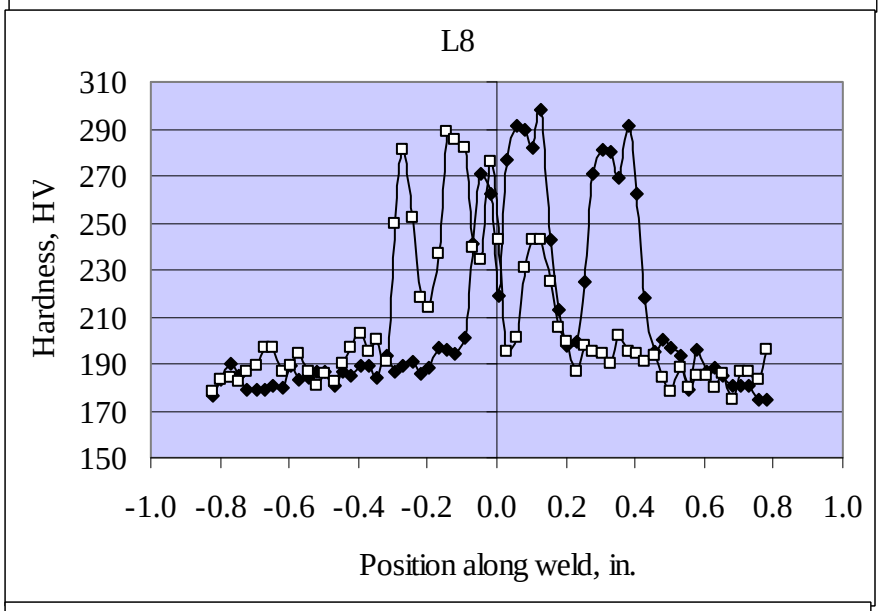
L8
Hardness, HV
310
290
270
250
230
210
190
170
150
-1.0 -0.8 -0.6 -0.4 -0.2 0.0 0.2 0.4 0.6 0.8 1.0
Position along weld, in.

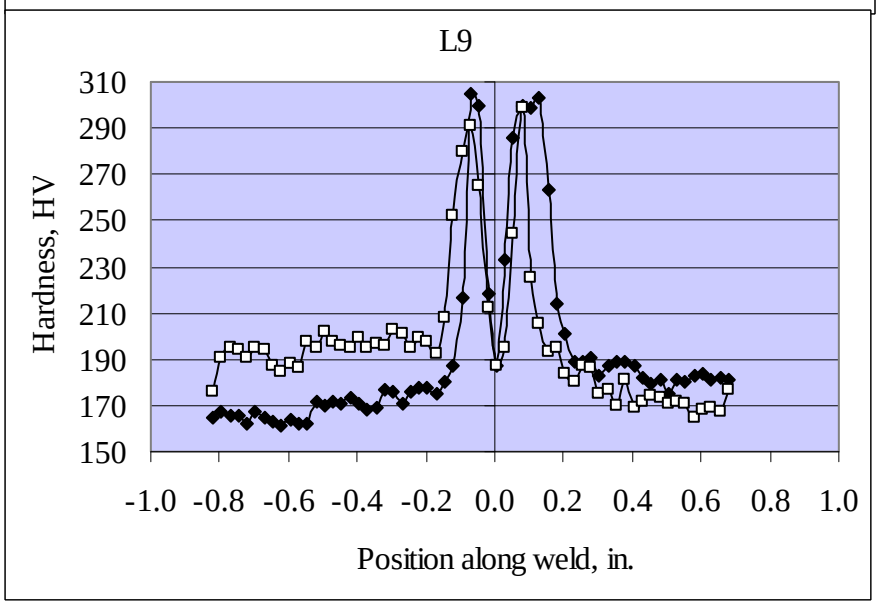
L9
Hardness, HV
310
290
270
250
230
210
190
170
150
-1.0 -0.8 -0.6 -0.4 -0.2 0.0 0.2 0.4 0.6 0.8 1.0
Position along weld, in.

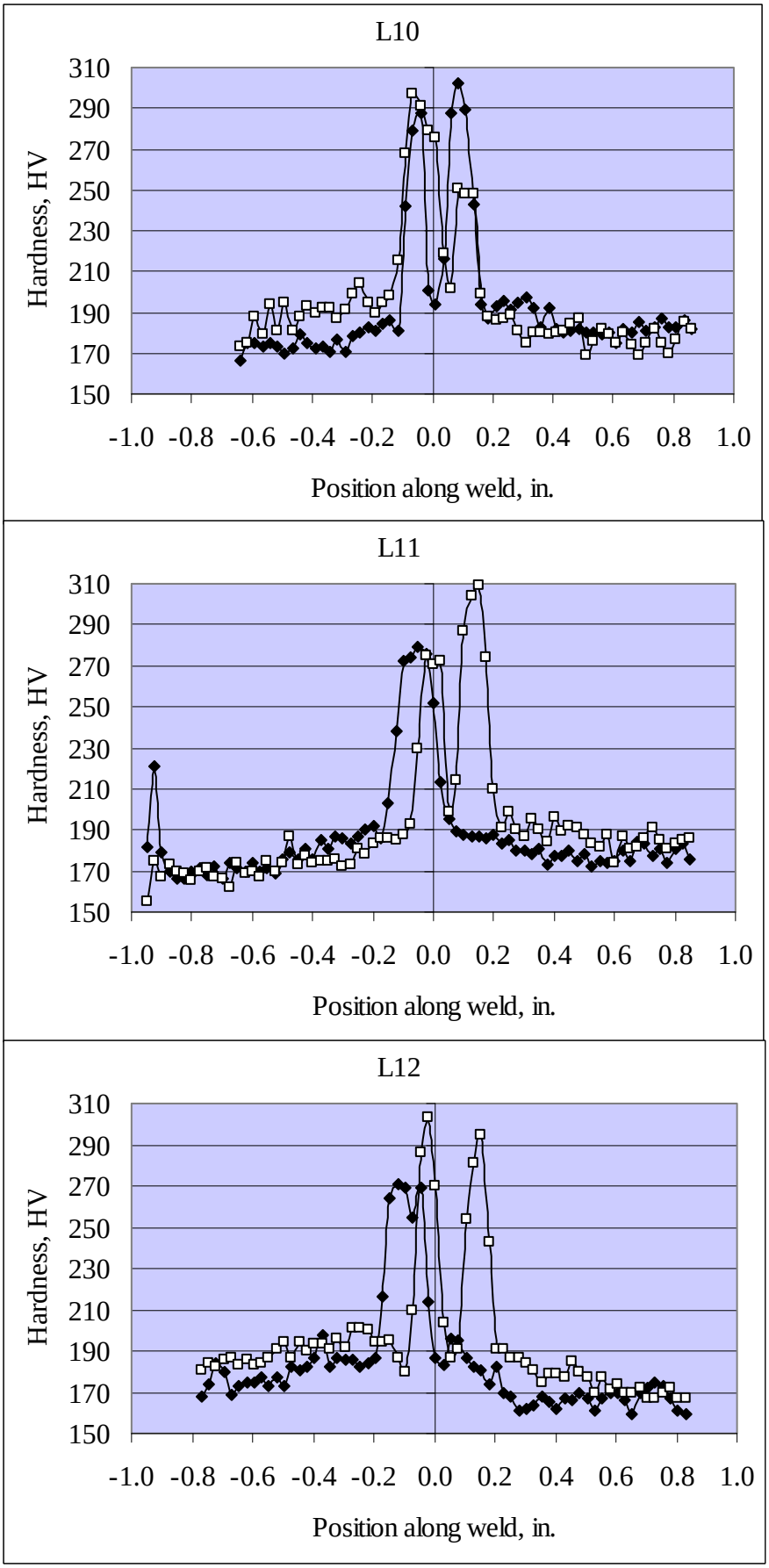
L10
Hardness, HV
310
290
270
250
230
210
190
170
150
-1.0 -0.8 -0.6 -0.4 -0.2 0.0 0.2 0.4 0.6 0.8 1.0
Position along weld, in.
L11
Hardness, HV
310
290
270
250
230
210
190
170
150
-1.0 -0.8 -0.6 -0.4 -0.2 0.0 0.2 0.4 0.6 0.8 1.0
Position along weld, in.
L12
Hardness, HV
310
290
270
250
230
210
190
170
150
-1.0 -0.8 -0.6 -0.4 -0.2 0.0 0.2 0.4 0.6 0.8 1.0
Position along weld, in.

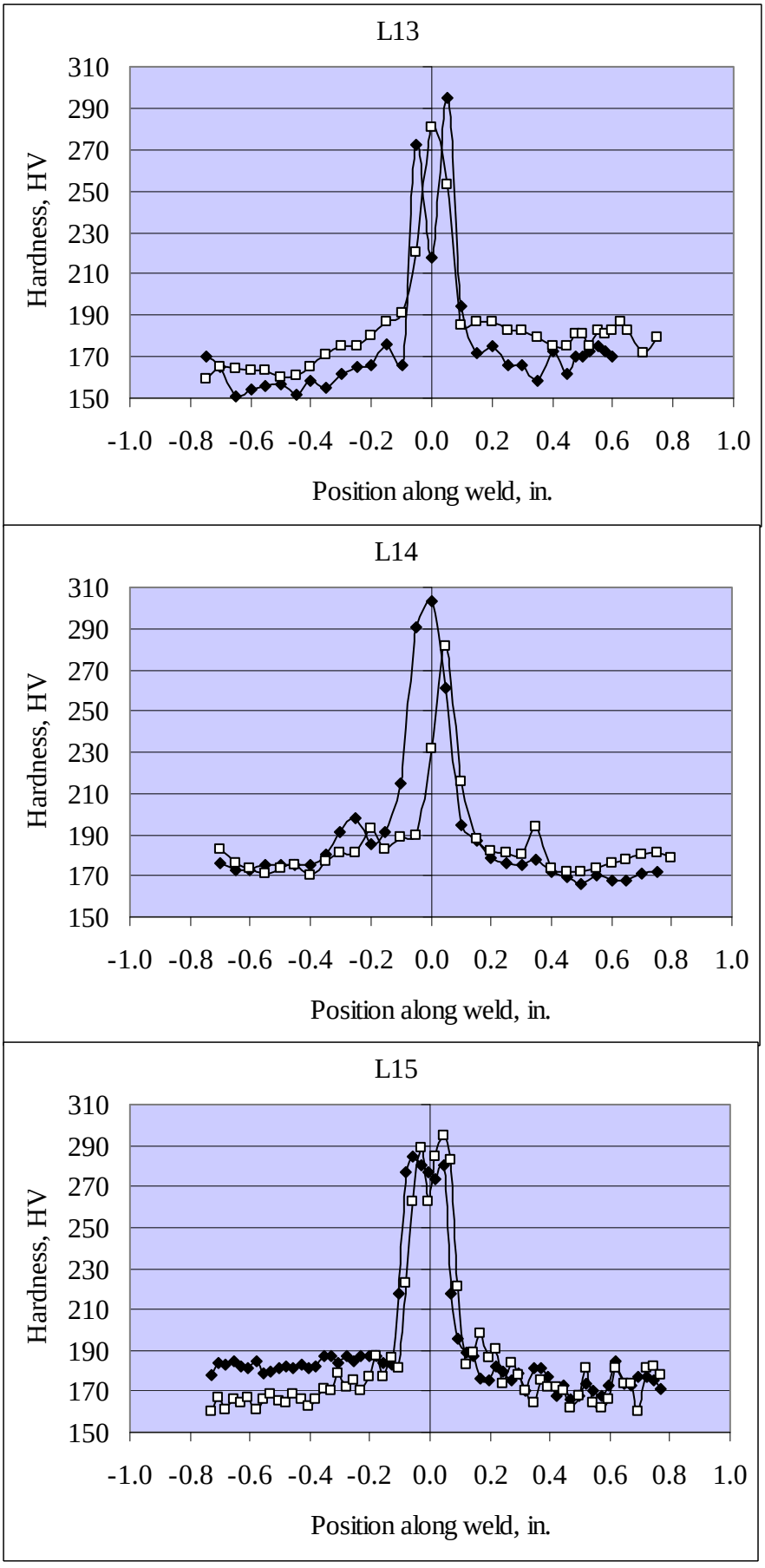
L13
Hardness, HV
310
290
270
250
230
210
190
170
150
-1.0 -0.8 -0.6 -0.4 -0.2 0.0 0.2 0.4 0.6 0.8 1.0
Position along weld, in.
L14
Hardness, HV
310
290
270
250
230
210
190
170
150
-1.0 -0.8 -0.6 -0.4 -0.2 0.0 0.2 0.4 0.6 0.8 1.0
Position along weld, in.
L15
Hardness, HV
310
290
270
250
230
210
190
170
150
-1.0 -0.8 -0.6 -0.4 -0.2 0.0 0.2 0.4 0.6 0.8 1.0
Position along weld, in.

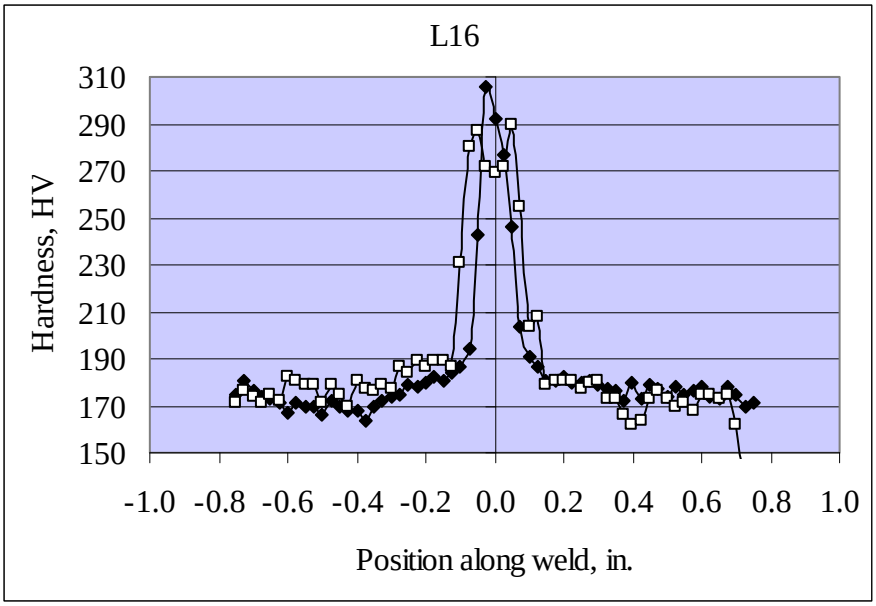
L16
Hardness, HV
310
290
270
250
230
210
190
170
150
-1.0
-0.8
-0.6
-0.4
-0.2
0.0
0.2
0.4
0.6
0.8
1.0
Position along weld, in.

APPENDIX C - Weld Profile Traces

L1:

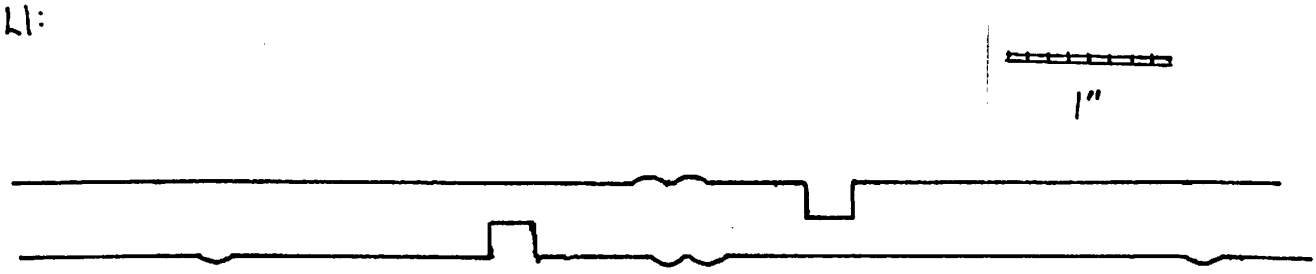

L2:

L3:

L4:

L5:

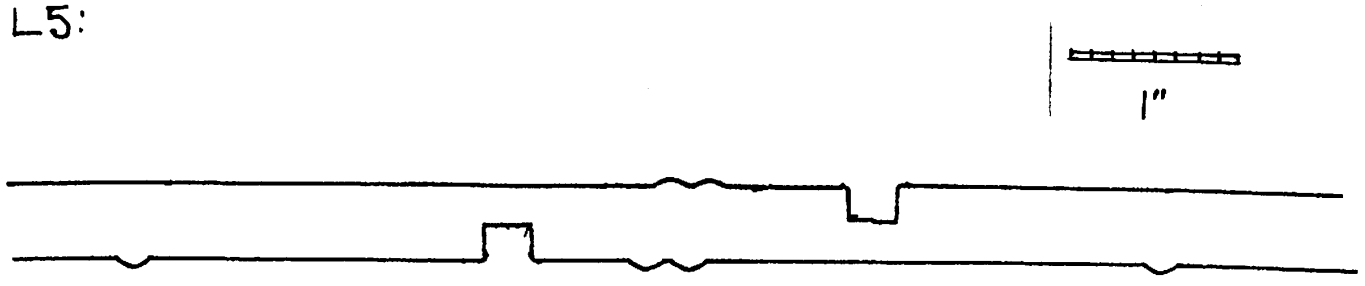

L6:

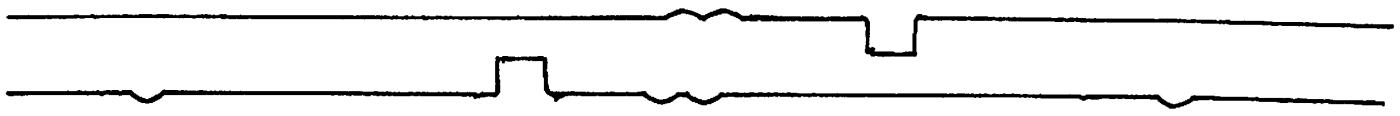

L7:

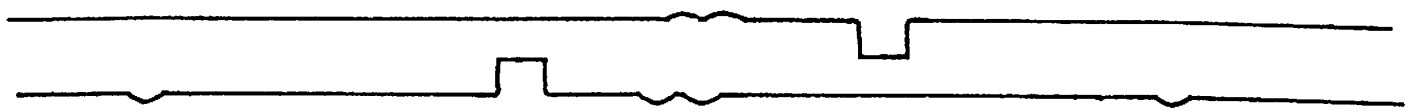

L8:

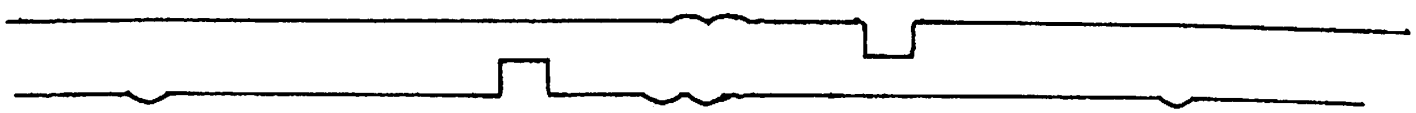

L9:

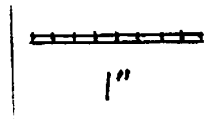

L10:

L11:

L12:

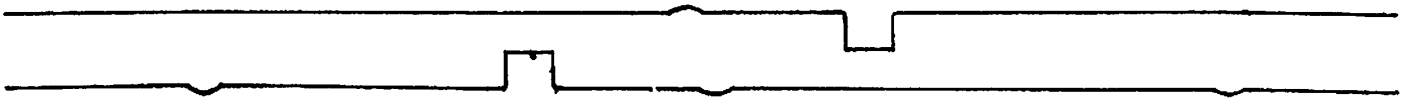

L13:

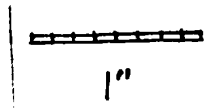

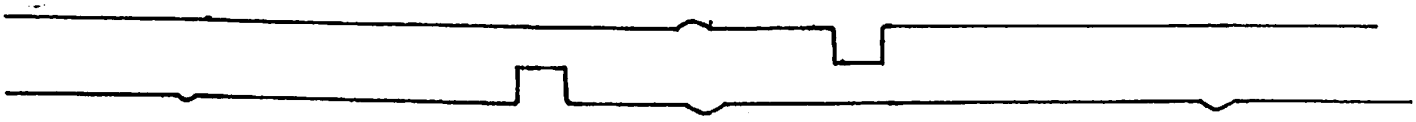

L14:

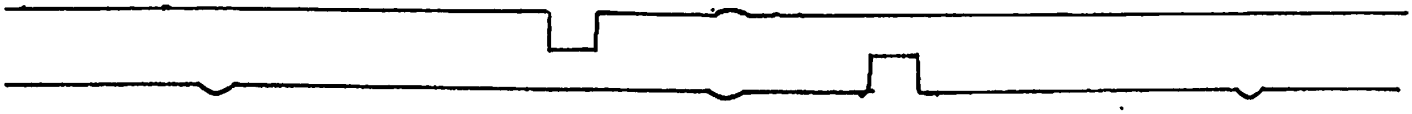

L15:

L16:

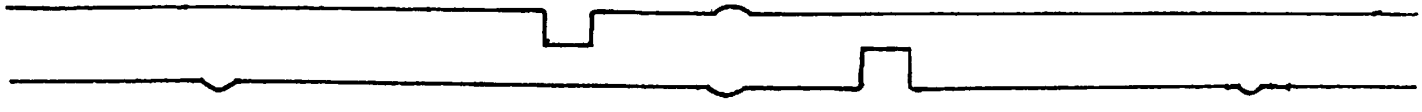

L17: A_{BOT}, B_{BOT} side

L17: D_{BOT}, C_{BOT} side

L17: A_{TOP}, B_{TOP} side

L17: C_{TOP}, D_{TOP} side

L18: A_{BOT}, B_{BOT} side

L18: D_{BOT}, C_{BOT} side

L18: A_{TOP}, B_{TOP} side

L18: C_{TOP}, D_{TOP} side

1"

L19: D_{BOT}, C_{BOT} side

L19: A_{BOT}, B_{BOT} side

L19: D_{TOP}, C_{TOP} side

L19: A_{TOP}, B_{TOP} side

L20: A_{BOT}, B_{BOT}

L20: D_{BOT}, C_{BOT}

L20: C_{TOP}, D_{TOP}

L20: A_{TOP}, B_{TOP}

1"

L21: DBOT, CBOT
L21: ABOT, BBOT
L21: ATOP, BTOP
L21: CTOP, DTOP
L22: DBOT, CBOT
L22: ABOT, BBOT
L22: ATOP, BTOP
L22: CTOP, DTOP
1"

L23: D_{BOT}, C_{BOT}

L23: A_{BOT}, B_{BOT}

L23: A_{TOP}, B_{TOP}

L23: C_{TOP}, D_{TOP}

L24: A_{BOT}, B_{BOT}

L24: D_{BOT}, C_{BOT}

L24: A_{TOP}, B_{TOP}

L24: C_{TOP}, D_{TOP}

1"

L26: A_{BOT}, B_{BOT}

L25: A_{BOT}, B_{BOT}

L25: C_{TOP}, D_{TOP}

L25 - A_{TOP}, B_{TOP}

L25: C_{BOT}, D_{BOT}

L26: A_{TOP}, B_{TOP}

L26: C_{BOT}, D_{BOT}

L26: C_{TOP}, D_{TOP}

L27: Dest, Cest

L27: Amp, Bmp

L27: Cmp, Dmp

L27: Aest, Best

L28: Dest, Cest

L28: Amp, Bmp

L28: Cmp, Dmp

L28: Aest, Best

1"

L29: ABOT, BBOT
L29: DBOT, CBOT
L30: CTOP, DTOP
L30: ATOP, BTOP
L29: CTOP, DTOP
L29: ATOP, BTOP
L30: ABOT, BBOT
L30: DBOT, CBOT
1"

L31: A_{BOT}, B_{BOT}

L31: D_{BOT}, C_{BOT}

L32: A_{BOT}, B_{BOT}

L32: D_{BOT}, C_{BOT}

L31: A_{TOP}, B_{TOP}

L31: C_{TOP}, D_{TOP}

L32: A_{TOP}, B_{TOP}

L32: C_{TOP}, D_{TOP}

1"